NASA TECHNICAL TRANSLATION NASA TT F-16,093

THE EFFECT OF AIR PRECOOLING PRIOR TO COMPRESSION IN AIR-BREATHING ENGINES FOR A SPACE VEHICLE CARRIER. COMPARATIVE ANALYSIS, WITH SPECIAL CONSIDERATION GIVEN TO THE REAL-GAS BEHAVIOR OF FLUIDS

H. Künkler

Translation of "Der Einfluss der Luftvorkühlung vor der Verdichtung bei luftatmenden Antrieben eines Raumfahrzeugträgers. Vergleichende Analyse unter besonderer Berücksichtigung des Realgasverhaltens der Fluide," Technische Hochschule Aachen. Doctoral Dissertation, Nov. 10, 1973, 221 pp.

(NASA-TT-F-16093) THE EFFECT OF AIR PRECOOLING PRIOR TO COMPRESSION IN AIR-BREATHING ENGINES FOR A SPACE VEHICLE CARRIER. COMPARATIVE (Kanner (Leo) Associates) 136 p HC $5.75 CSCL 21E

N75-13864

Unclas
G3/07 05029

NATIONAL AERONAUTICS AND SPACE ADMINISTRATION
WASHINGTON, D.C. 20546 JANUARY 1975

STANDARD TITLE PAGE

1. Report No. NASA TT F-16,093	2. Government Accession No.	3. Recipient's Catalog No.
4. Title and Subtitle THE EFFECT OF AIR PRECOOLING PRIOR TO COMPRESSION IN AIR-BREATHING ENGINES FOR A SPACE VEHICLE CARRIER. COMPARATIVE ANALYSIS, WITH SPECIAL CONSIDERATION GIVEN TO THE REAL-GAS BEHAVIOR OF FLUIDS		5. Report Date January 1975 6. Performing Organization Code
7. Author(s) H. Künkler		8. Performing Organization Report No. 10. Work Unit No.
9. Performing Organization Name and Address Leo Kanner Associates Redwood City, California 94063		11. Contract or Grant No. NASw-2481 13. Type of Report and P- ered
12. Sponsoring Agency Name and Address National Aeronautics and Space Administration, Washington, D.C. 20546		14. Sponsoring Agency Code

15. Supplementary Notes
Translation of "Der Einfluss der Luftvorkühlung vor der Verdichtung bei luftatmenden Antrieben eines Raumfahrzeugträgers. Vergleichende Analyse unter besonderer Berücksichtigung des Realgasverhaltens der Fluide," Technische Hochschule Aachen. Doctoral Dissertation, Nov. 10, 1973, 221 pp.

16. Abstract Air precooling prior to compression is shown to be suitable for considerably extending the flight Mach number range of turbojet engines. It is compared with competing concepts, particularly the turborocket with precooling and combination engines involving the ramjet plus turbojet or turborocket. The turbojet with precocling calls for engineering which does not appreciably exceed the present state of the art, and requires test facilities which are designed for oncoming-flow Mach numbers of 4 to 4.5, in spite of its suitability for flight Mach numbers up to about 7. The system is also to be preferred at lower Mach numbers, e.g. in a methane-fueled SST.

17. Key Words (Selected by Author(s))	18. Distribution Statement
	Unclassified-Unlimited

19. Security Classif. (of this report)	20. Security Classif. (of this page)	21. No. of Pages	22. Price
Unclassified	Unclassified	127	

Foreword

This dissertation was produced during my work as a scientific assistant for the Chair and Institute for Jet Engines and Turbine Power Machinery of the Aachen Engineering College.

I cordially thank Prof. Dr.-Ing. W. Dettmering, who provided the inspiration for this work and made its implementation possible through his generous support. I would like to express my sincere thanks to Prof. Dipl.-Ing. O. David for his interest in my work and for many helpful discussions.

I would also like to thank all of the colleagues who supported me in preparing this dissertation. In particular, my thanks go to Mr. Eller for his excellent execution of the photographic work.

The numerical calculations were made on the CD 6400 computer at the Aachen Technical College computation center.

TABLE OF CONTENTS

		Page
1.	Introduction	1
2.	Air-Breathing Engines for Space Vehicle Carriers	2
	2.1. Requirements	2
	2.2. Engines Based on Conventional Aeronautical Power Plants	5
	2.3. Possibilities for Controlling Thermodynamic Processes Arising from the Peculiarities of the Application	7
	2.31. Turbojet with Upstream Turbine	9
	2.32. Turborocket with Precooling	10
	2.33. Turbojet with Precooling	11
	2.34. Turbofan with Precooling	13
	2.35. Turbofan with Air Liquefaction in Primary Circuit	15
	2.36. Precooling with the Compressed Air	16
	2.37. Liquefaction and Separation of Air into its Components	18
	2.38. Combustion with Excess Fuel	19
3.	Mathematical Principles for Determining the Real-Gas Behavior of the Fluids Involved	20
	3.1. Delimiting the Ranges of States	21
	3.2. Low-Temperature Range	23
	3.21. Thermal Equation of State	24
	3.22. Caloric Equations of State	28
	3.23. Representation of Boundary Curves	31
	3.24. Computing System and Ranges of States Represented	32
	3.3. Medium-Temperature Range	34
	3.4. High-Temperature Range	38
	3.41. Equilibrium Composition	39
	3.42. Combustion Gas Composition in the Case of Incomplete Combustion	47
	3.43. Final Combustion Temperature	49
	3.44. Changes of State in Combustion Gases of "Frozen" Composition or in Labile Chemical Equilibrium	52
4.	Special Requirements Placed on Individual Structural Components and the Computational Methods Used	55
	4.1. Intake	55
	4.11. Special Requirements and Configuration	55
	4.12. Possible Matching Methods, Operating Behavior, Drag	58
	4.13. Wing Precompression	63

Page

4.2. Heat Exchanger 65
4.21. Special Requirements, Configuration and Design 66
4.22. Computational Method 68
4.3. Compressor 77
4.4. Turbine 80
4.5. Mixing Chamber 82
4.6. Combustion Chamber 85
4.7. Nozzle 89

5. Preliminary Design for a Turbojet with Air Precooling Prior to Compression for Propelling a Space Vehicle Carrier 91
5.1. Requirements and Conditions 92
5.2. Engine Configuration and Design of Components 96
5.3. Effect of Precooling on the Thermodynamic Cycle 97
5.4. Analysis of the Engine's Performance 100

6. Comparison between the Turbojet with Precooling and Competing Engine Designs 103
6.1. Performance Data for Turbojet with Precooling, Taking Installation Effects into Consideration 104
6.2. Performance Data for Engine Combinations Involving the Ramjet 108
6.21. Ramjet 108
6.22. Turbojet and Turborocket as Gas Generators 110
6.23. Selected Combination Engines 112
6.3. Performance Data for Turborocket with Precooling 113
6.4. Comparison of Performance 114
6.41. Comparison of Performance Data 114
6.42. Total Weight Comparison for an Example of Application in a Space Vehicle Carrier 118

7. Concluding Remarks 121

References 124

Power Plant Notation

SL	Ramjet engine
TL	Turbojet engine
TR	Turborocket engine
R	Rocket engine
ZTL	Turbofan engine
VK	Precooling (prior to compression)
PC	Afterburning
$\beta > \beta_{st}$	Superstoichiometric fuel input

Frequently Used Symbols

A	m^2	Area
a	m/sec	Sonic velocity
c	m/sec	Velocity
c_p	J/kg/K	Specific heat capacity (p = const)
c_v	J/kg/K	Specific heat capacity (v = const)
D_{Fl}	N	Drag of missile
D_b	N	Bypass drag
D_h	N	Cowling drag
D_z	N	Added drag
$\mathcal{E}$	J/kmol	Chemical potential energy
F	N	Thrust
f	J/kg	Specific free energy
$\mathcal{G}$	J/kmol	Gibbs free energy
H_∞	m	Altitude
h	J/kg	Specific enthalpy
$\mathcal{H}$	J/kmol	Specific enthalpy
k	-	Isentropic exponent
K_n, K_p	-	Equilibrium constants
$\mathcal{M}$	kg/mol	Molar mass
M	-	Mach number
$\dot{m}$	kg/sec	Mass flow
m	kg	Mass, weight
m_A	kg	Takeoff weight of vehicle

m_M	kg	Power plant weight
m_N	kg	Payload
m	-	Number of moles of reactants
n	-	Number of moles of products
n	-	Number of shock waves
N	sec^{-1}	Rotor rpm
N_{Nu}	-	Nusselt number
N_{Pr}	-	Prandtl number
N_{Re}	-	Reynolds number
N_{St}	-	Stanton number
p	N/m^2	Static pressure
p_t	N/m^2	Total pressure
p_h	N/m^2	Static pressure on inlet cowling
Q	J	Heat
q	J/kg	Specific heat
R	J/kg/K	Special gas constant
$\mathcal{R}$	J/kmol/K	General gas constant
s	J/kg/K	Specific entropy
$\mathcal{s}$	J/kmol/K	Specific entropy
T	K	Temperature
u	J/kg	Specific internal energy
V	m^3	Volume
v	m^3/kg	Specific volume
$\mathcal{v}$	$m^3/kmol$	Molar volume
x	-	Vapor content
α	°	Wing angle of attack
α	$W/m^2/K$	Heat transfer coefficient
β	-	Fuel/air ratio
γ	-	Turbine cooling air requirement
δ	°	Angle of deflection, angle of attack
ε	-	Heat exchanger efficiency
η	-	Static/polytropic efficiency
η_{ts}	-	Total isentropic efficiency
κ	-	Ratio of specific heat capacities
λ	-	Bypass ratio

λ	W/m/K	Thermal conductivity
μ	kg/m/sec	Dynamic viscosity
ν	-	Mole fraction
π	-	Pressure ratio
ρ	kg/m^3	Density
σ	°	Shock wave angle
σ_B	N/kg/sec	Thrust over fuel flow
σ_G	-	Thrust over engine weight
σ_L	N/kg/sec	Thrust over air flow
τ	-	Relative mass flow density

Subscripts

A	Outlet
AP	Design point
B	Fuel, on-vehicle weight
C	Combustion
D	Thrust nozzle
E	Intake, inlet
f	Solid
g	Gaseous
ges	Total
H	Intake throat
i,j	Running indices
kin	Kinetic
L	Air
M	Mixing chamber
max	Maximum
min	Minimum
Ox	Oxidizer
PC	Afterburning
st	Stoichiometric
V	Compressor
VK	Precooling
WT	Heat exchanger
∞	Ambient condition, freestream

0	Intake, inlet, freestream
1a	Downstream from first oblique shock wave
1b	Downstream from perpendicular shock wave
1E	Outlet of intake
1	Inlet of compressor
2	Outlet of compressor
3	Outlet of combustion chamber
4	Outlet of turbine
4a	Inlet of afterburner chamber
4b	Outlet of afterburner chamber
5	Outlet of thrust nozzle
I	Primary circuit
II	Secondary circuit
*	Critical
o	Reference point
$\bar{}$	Mean

THE EFFECT OF AIR PRECOOLING PRIOR TO COMPRESSION IN AIR-BREATHING ENGINES FOR A SPACE VEHICLE CARRIER. COMPARATIVE ANALYSIS, WITH SPECIAL CONSIDERATION GIVEN TO THE REAL-GAS BEHAVIOR OF FLUIDS

Hermann Künkler

1. Introduction /1*

A primary task of today's astronautics industry is the development of carrier systems whose utilization considerably reduces the running costs of a mission with an Earth orbit.

In the purely ballistic disposable systems which have been conventional to date, an effective improvement in economy can only be achieved if, in addition to simplification and high-volume production of the first and second stages, which are lost, the valuable last stage can be recovered as a reusable orbiter with an aerodynamic landing. A further improvement can be achieved, moreover, if all stages of the rocket-driven carrier can be used several times after their return (space shuttle system). The advantage in costs relative to the disposable system, which represents the less expensive approach for a short-term estimate period at the present state of the art, also holds when development costs are included if the calculated overall costs are based on a utilization period of more than 5 years with the requirements estimated quite conservatively at present (Fig. 1.1).

The greatest cost reduction can be expected if a booster stage is available for launch and initial acceleration which is suitably equipped with air-breathing jet engines for the entire phase of flight through the dense atmosphere and is consistently employed as an aerodynamic vehicle. Other advantages of such an aerodynamic launch vehicle stage must be considered in addition to a direct increase in economy:

-- great freedom in selecting the launch site and launch direction (inclination), due to the high maneuverability of the launch stage with relatively low fuel consumption, an advantage which may be particularly important in the long run for European space travel; /2

-- unproblematical return of the booster stage to the launch site;

---

* Numbers in the margin indicate pagination in the foreign text.

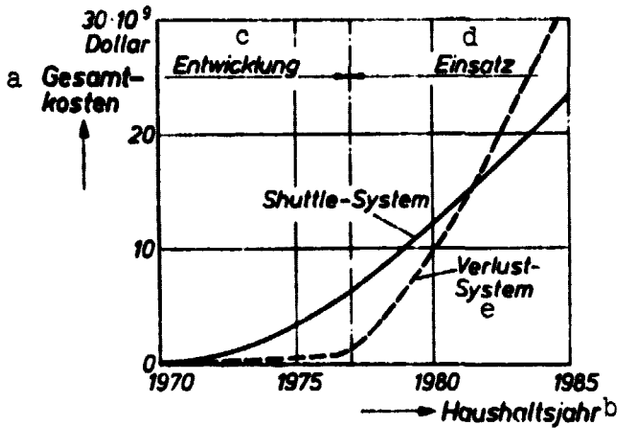

Fig. 1.1. Comparison of total costs for the U.S. space flight program [1].

Key: a. Total costs; b. Fiscal year; c. Development; d. Operation; e. Disposable system

-- the reliability necessary for "passenger travel" and limitation of the accelerations which occur.

In the following material, after the requirements which are placed on the necessary air-breathing power plants are determined, the possibilities and requirements for controlling thermodynamic processes that result from the peculiarities of their utilization in a space vehicle carrier are pointed out and evaluated. In particular, the effect of air precooling prior to compression on the performance of air-breathing turbojets will be studied and presented using the example of the project design for a turbojet engine. Finally, a concluding quantitative comparison with the important competing power plant concepts will determine the suitability of this engine in an aerodynamic booster stage for a practical application. /3

2. Air-Breathing Engines for Space Vehicle Carriers /4

2.1. Requirements

We can assume that it is desirable for a completely reusable aerodynamic space vehicle that is to place a payload in low Earth orbit to be designed with two stages. Fig. 2.1 shows an artist's conception of such a system. It consists of an aerodynamic booster which takes off horizontally and is driven by air-breathing power plants, plus a -- normally smaller -- rocket-driven orbiter which is designed for reentry and landing as a glider. If the orbiter were replaced with a purely ballistic disposable system, the ratio of payload to launch weight could be distinctly improved by distributing the remaining acceleration between two rocket stages. For a completely reusable aerodynamic system, on the other hand, it is to be expected that the introduction of an intermediate stage which makes additional flight equipment necessary, including a crew, produces a poorer payload ratio $\nu = m_N/m_A$. /5

In order to reduce the burden on a single-stage rocket-propelled orbiter, it is therefore desirable that the booster stage,

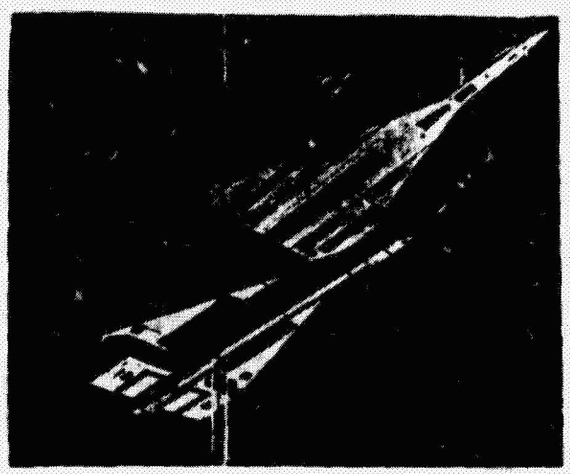

Fig. 2.1. Aerodynamic space shuttle after separation of stages [2].

equipped with air-breathing engines, which are better in terms of consumption, produce acceleration to high flight Mach numbers, beyond $M_\infty = 10$ if possible. Only a ramjet engine with supersonic combustion appears suitable for this Mach number range. The high boundary layer temperatures (Fig. 2.2), which can also increase rapidly to values greater than T = 4000 K above $M_\infty = 10$ for this type of power plant and can be considerably higher than actual combustion gas temperatures, call for a considerable outlay for cooling, however. /6

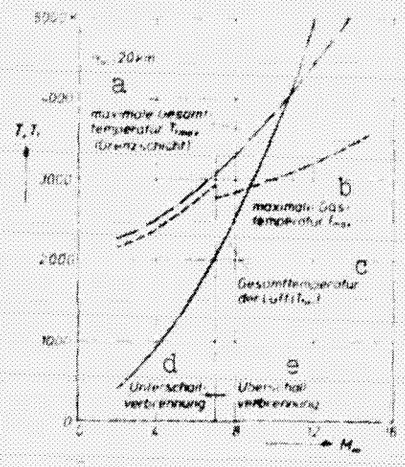

Fig. 2.2. Temperature level in a ramjet engine with supersonic combustion (from [3]).

Key: a. Maximum total temperature (boundary layer); b. Maximum gas temperature; c. Total air temperature; d. Subsonic combustion; e. Supersonic combustion

The relatively larger power plant dimensions -- due to the low energy input per kg of airflow, specific thrust $\sigma_L = F/\dot{m}_L$ only reaches low values in supersonic combustion -- in conjunction with the high temperature level which occurs produce a coolant flow whose magnitude can be several times as high as the fuel flow actually needed, even if liquid hydrogen (LH_2) is used as fuel. Although conditions are somewhat more favorable if it proves possible to stabilize external combustion in the supersonic flow on the underside of the vehicle, the reasonable range of application of ramjet engines with supersonic combustion remains restricted to flight Mach numbers between about $M_\infty = 7$ and $M_\infty = 11$, because of the above-mentioned circumstances. If we also take the thermal problems of the vehicle itself into consideration, the maximum flight Mach number to which aerodynamic booster stages with air-breathing power plants should be accelerated shifts to significantly lower values at the present state of the art.

The decisive advantage for air-breathing engines relative to the rocket engine only comes into play if it proves possible to develop a power plant design which, starting from takeoff, covers the entire range of flight Mach numbers to be flown in the atmosphere and in the process is not appreciably heavier than a conventional turbojet with afterburning that produces comparable thrust in the lower flight Mach number range. Specific fuel consumption should be lower here than that of the afterburner power plant or, in the upper flight Mach number range (up to about $M_\infty = 7$), lower than that of a corresponding ramjet power plant. /7

The ratios $\sigma_B = F/\dot{m}_B$ of thrust to on-vehicle mass flow (fuel flow) which are obtained by conventional air-breathing jet engines in the associated ranges of flight Mach numbers are compared with the corresponding values for a rocket engine in Fig. 2.3. The curve for a ramjet engine with supersonic combustion, as obtained if the cooling problems are not considered, is also included in the graph. The thrusts divided by fuel consumption have been calculated for kerosene as the fuel. If hydrogen is used, values about 2.5 times higher can be achieved with the same types of power plants, due to its higher energy content, as the upper limiting curve indicates. /8

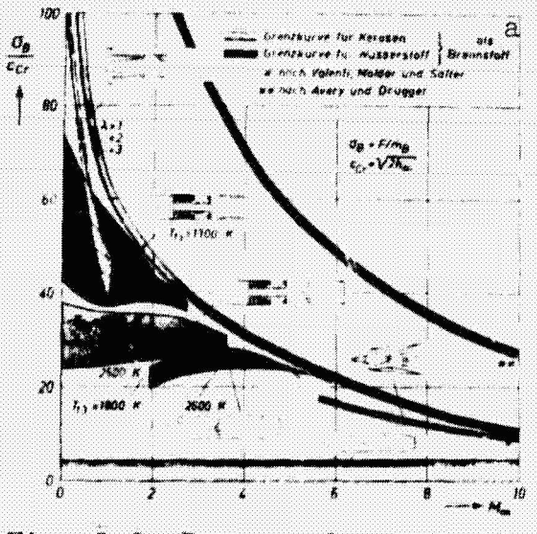

Fig. 2.3. Ranges of application and dimensionless specific thrusts $\sigma_B = F/\dot{m}_B$ for air-breathing jet engines (from [2]).

Key: a. Limiting curves for kerosene and hydrogen, respectively, used as fuels; * from Valenti, Molder and Salter; ** from Avery and Drugger.

It can be seen from Fig. 2.3 that it is always necessary to change to another type of engine for the individual ranges of flight Mach number in accelerated flight if we always wish to provide the necessary thrust with the lowest on-vehicle weight consumption (fuel flow). The total cost for the propulsion requirements in a given mission, consisting of the total weight of fuel required plus power plant weight, will then certainly not assume a minimum value, however. It could be seen from Fig. 2.3, moreover, that although the ramjet engine is suitable for the highest flight Mach numbers among conventional jet engines, it produces insufficient thrust, if any for takeoff and the transonic flight range. From

takeoff on up, the turbojet with afterburning covers the widest range of flight.

The necessary engine size and thus engine weight m_M is primarily a function of the magnitude of specific thrust $\sigma_L = F/\dot{m}_L$ which the engine achieves in the upper range of flight Mach numbers through which it passes. In order that unnecessary excess thrust and power plant drag are avoided in the lower range of flight Mach numbers, moreover, the magnitude of σ_L should decrease as little as possible with increasing flight Mach number.

In summary, we can list the following requirements that must be placed on the air-breathing engine of a space vehicle carrier. /9

-- adequate takeoff thrust and sufficient excess thrust in the transonic range, suitable up to flight Mach numbers above $M_\infty = 6$;

-- high specific thrust with respect to air flow, $\sigma_L = F/\dot{m}_L$, particularly in the upper range of flight Mach numbers;

-- high specific thrust with respect to fuel flow, $\sigma_B = F/\dot{m}_B$, within the entire range of flight Mach numbers covered;

-- high specific thrust with respect to weight, $\sigma_G = F/(m_M \cdot g_o)$, with an uncomplicated, highly reliable power plant design.

2.2. Engines Based on Conventional Aeronautical Power Plants

Among the conventional air-breathing jet engines, it can be seen from Fig. 2.3 that only the turbojet and the turbofan, each in its own version with afterburning (PC), are suitable for flight Mach numbers up to beyond $M_\infty = 2.5$ and are at the same time capable of takeoff.

The range of flight Mach numbers for air-breathing turbojets is given an upper limit by the permissible compressor outlet temperature. In the conventional type of turbine blade cooling with compressor air, this limit is on the order of about $M_\infty \approx 3.25$ for the turbojet with afterburning. The turbofan with afterburning already reaches the temperature limit at somewhat lower flight Mach numbers, due to the higher compressor pressure ratio in the first circuit.

If it proves possible to precool the turbine cooling air via heat transfer to the flow of fuel or to use fuel directly for blade cooling, the range of flight Mach numbers can be extended to /10

about $M_\infty \approx 4.5$, depending on the compressor pressure ratio. At that point, the compressor outlet temperature reaches a value of about $T_{t2} = 1200$ K, which for technical reasons is considered the maximum permissible for the present discussion involving a compressor with uncooled blades.

The same flight Mach number limit of course applies also to the turborocket (TR), in the experimental stage for the past few years ([4, 5]), in which the turbine, which covers the compressor's power requirement, is driven by a separate gas flow -- e.g. from the reaction of fuel with liquid oxygen. Since the compressed air does not expand partially in the turbine again after heating has taken place, as in the turbojet, the compressor pressure ratio need only assume smaller values in the thrust nozzle for the same expansion pressure gradient.

Fig. 2.4 shows schematics of the turbojet, the turbofan and the turborocket -- each equipped with an afterburner chamber. As reference values, the compressor pressure ratios $\pi_{tV} = p_{t2}/p_{t1}$ and the associated compressor outlet temperatures T_{t2} which yield about the same nozzle pressure ratio at $M_\infty = 4$ are shown for the three types of power plants. With the vehicle on the ground (design starting point), the total pressure ratios for the compressors naturally assume significantly higher values.

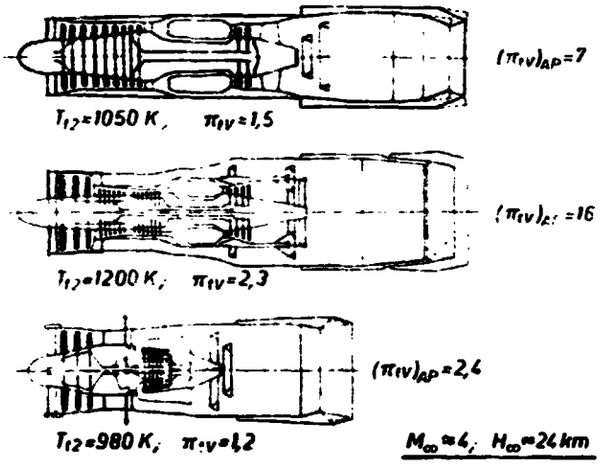

Fig. 2.4. Compressor outlet temperatures for "turbo" engines at $M_\infty = 4$.

The turbo engines described are no longer suitable for throughflow at Mach numbers above $M_\infty = 4.5$ if we disregard the much too expensive possibility of cooling the entire blade system and, ultimately, even all of the flow channels with fuel. If these engines, acting as power plants for takeoff and initial acceleration, are combined with a ramjet, their internals must be hermetically sealed against throughflow in the upper range of flight Mach numbers, and their outer skin must also be cooled with fuel to prevent a flow of heat into the inside of the power plant from its hot surroundings. The latter approach is only conditionally feasible if kerosene is used. /11

Schematics are shown in Fig. 2.5 for combinations of a turbojet, a turbofan or a turborocket and a ramjet. /12

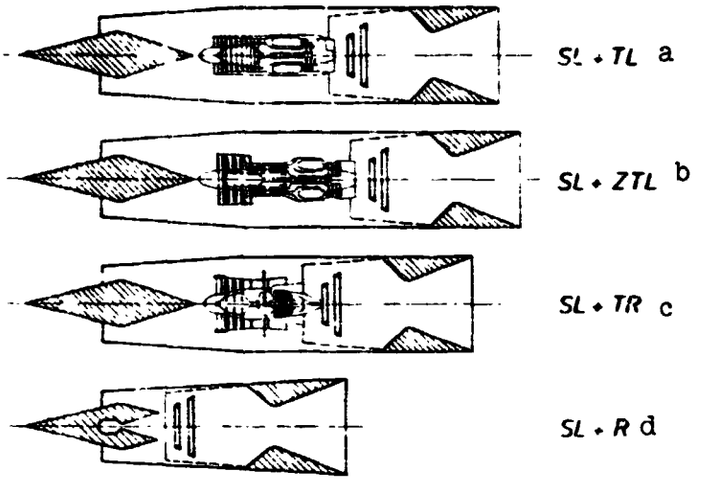

Fig. 2.5. Combination engines.

Key: a. Ramjet + turbojet;
b. Ramjet + turbofan;
c. Ramjet + turborocket;
d. Ramjet + rocket.

This series of combination engines is supplemented with the combination of a ramjet and a rocket, which is characterized by a relatively low engine weight but has high fuel consumption in the take-off phase. The schematics show the integrating arrangement of the engines to be combined in each case (combination mode), which permits the common use of intake and thrust nozzle. The separate arrangement of engines side by side (composite mode) has the advantage of eliminating interaction problems to a large extent.

2.3. Possibilities for Controlling Thermodynamic Processes Arising from the Peculiarities of the Application /13

The possibility of using liquid hydrogen as a fuel is obtained for the air-breathing engines from the peculiarities of this application in an accelerated space vehicle carrier system. Aside from the higher energy content per unit mass and the considerable savings in fuel which result relative to the use of conventional hydrocarbons (e.g. ATK, JP4), the flow of fuel provides a heat sink which can be used to precool the flow of air drawn in by the compressor.

A consideration of the course of thermodynamic processes in conventional jet engines immediately shows that the state from which expansion to the applied back-pressure commences in the thrust nozzle should have the highest possible temperature values and low entropy so that a large enthalpy difference is available in the nozzle for expansion and a high jet exhaust velocity can thus be achieved.

As Fig. 2.6 shows in the example of a turbojet, this can be achieved through a reduction in the outlay for compression Δh_{tV} for a given compressor pressure ratio π_{tV} or through an increase in compressor pressure ratio for a given compression outlay, or through a combination of the two. A possibility for this is

provided, for example, by precooling the air upstream from the inlet to the compressor with the flow of hydrogen used as fuel. In the former case (Fig. 2.6a), the turbine need provide only relatively low power ($\rightarrow(\Delta h_{tT})_{VK} < \Delta h_{tT}$). The enthalpy h_{t4} at the nozzle inlet increases, and thus so do temperature T_{t4} and pressure p_{t4}. In the second case (Fig. 2.6b), heat input in the combustion chamber takes place at a higher process pressure ratio p_{t2VK}/p_o up to the same heating temperature T_{tmax}; for a given enthalpy ($h_{t4VK} = h_{t4}$), this ultimately produces reduced entropy in state $4t_{VK}$ and thus increases jet exhaust velocity. /15

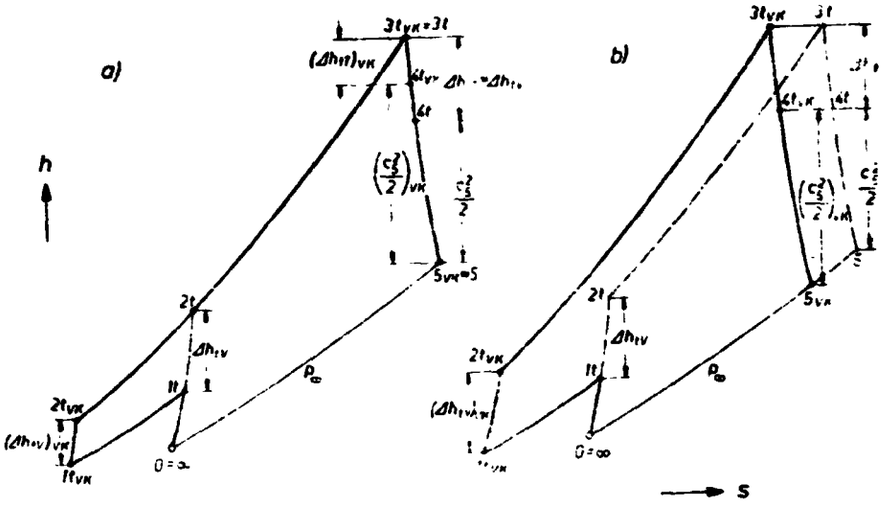

Fig. 2.6. Effect of precooling on expansion in the thrust nozzle.

As jet exhaust velocity is increased, precooling the air prior to compression increases not only specific thrust $\sigma_L = F/\dot{m}_L$ with respect to air but also specific thrust $\sigma_B = F/\dot{m}_B$ with respect to fuel. Although heat input in the combustion chamber is higher in the case of precooling as seen, for example, in the process shown in Fig. 2.6b, the flow of fuel required per kg air at a given heating temperature T_{tmax} -- i.e. the fuel/air ratio $\beta = \dot{m}_B/\dot{m}_L$ -- remains the same, according to the principle of the conservation of energy. The heat absorbed in the heat exchanger need no longer be added to the hydrogen in the combustion chamber.

In addition to increasing specific thrust σ_L and σ_B, precooling allows the range of flight Mach numbers of air-breathing turbo engines to be extended considerably because of the drop in compressor outlet temperature; it is only then that they become interesting as power plants for aerodynamic space vehicle carriers.

2.31. Turbojet with Upstream Turbine

A turbojet engine called the "inverted turbojet," in which the air is supposed to be precooled ahead of the compressor inlet with the liquid methane or hydrogen used as fuel, was proposed in 1961 by Mordell, Evre and Sreenath [6]. The special feature of this type of power plant is that the turbine which covers the power requirements of the compressor is placed directly downstream from the engine intake and initially expands the compressed air prior to admission to the heat exchanger (Fig. 2.7). This arrangement makes it possible to feed heat in the combustion chamber up to the technically feasible heatup temperature for a ramjet at a process pressure ratio which, particularly at higher flight Mach numbers, is appreciably above that for the ramjet. To be sure, it is precisely in this flight range that additional compression exceeding that of the ram effect is less effective than at lower flight Mach numbers. The main disadvantage of this type of engine is that, like the ramjet, it is unsuitable for the lower range of flight Mach numbers. /16 /17

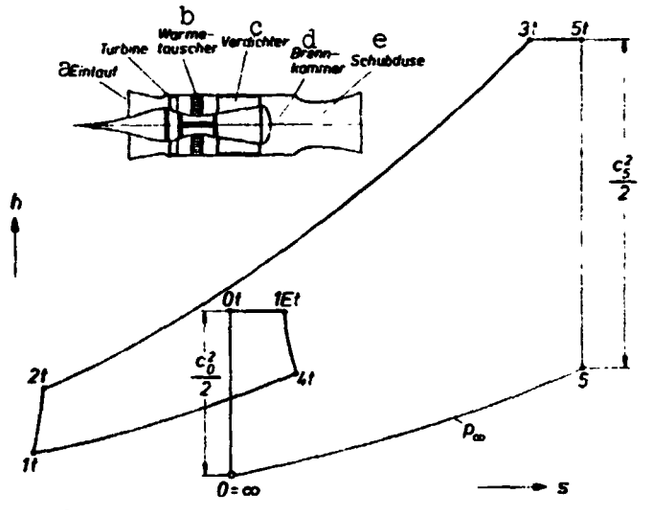

Fig. 2.7. Schematic and curve of processes for the inverted turbojet.

Key: a. Intake; b. Heat exchanger; c. Compressor; d. Combustion chamber; e. Nozzle.

The project proposal made by B. Becker [7] represents a turbojet with an upstream turbine of basically different design. In a supersonic turbine -- definition of turbine: turbomachine with a shaft power output that takes overall enthalpy from fluid and converts it to blade work -- the only slightly compacted air is compressed further and retarded to subsonic velocity (Fig. 2.8). After heat input in subsonic combustion, a completely run-up supersonic compressor returns the energy withdrawn in the turbine to the combustion gas during simultaneous expansion, the fluid already being accelerated to supersonic velocity. Residual expansion occurs in a purely divergent supersonic nozzle. /18

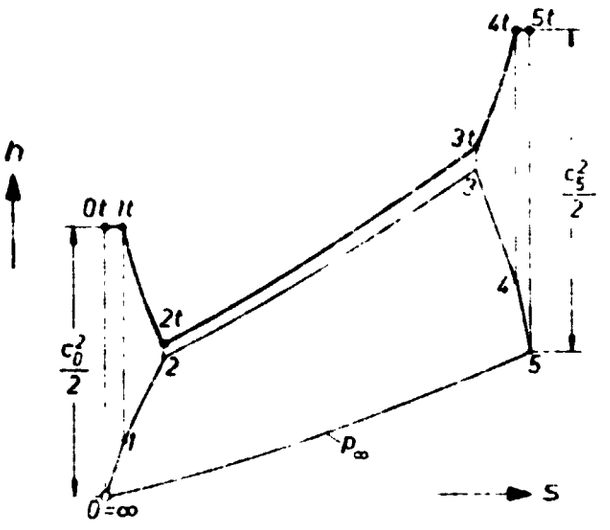

Fig. 2.8. Curve of processes in turbojet with upstream supersonic turbine.

The static curve of state for this project is similar to that for the ramjet with supersonic combustion, whose advantages and disadvantages this type of engine also shares:

-- low losses in the intake and nozzle, and a low level of static temperatures even at extremely high flight Mach numbers;

-- suitability only for the high Mach number range, heat input at a relatively low process pressure ratio and additional low flexibility, plus high thermal stresses on the compressor (T_{t4}).

2.32. Turborocket with Precooling

It seemed reasonable to extend the turborocket's advantage of making the entire process pressure ratio available for expansion in the nozzle to flight Mach numbers above $M_\infty \approx 4.5$ by placing a heat exchanger upstream from the compressor. This allows the major disadvantage of the turborocket, the high on-vehicle mass flow requirements, to simultaneously be reduced at least in the middle and upper range of flight Mach numbers. The necessary heat can now be transferred to the flow of hydrogen required as fuel in the afterburner chamber through heat exchange with the compacted flow of air prior to its expansion in the turbine, so it becomes unnecessary to heat it in a separate combustion chamber by reacting it with additional liquid oxygen carried on the vehicle. Fig. 2.9 shows the schematic of a turborocket with precooling proposed by Texaco Experiment Inc. [8] and called the "air turbo exchanger" (ATE).

The course followed by thermodynamic processes is similar to that in the inverted turbojet (Fig. 2.7). The primary difference is that expansion of the air that is compacted in the intake, which makes the inverted turbojet unusable for relatively low flight Mach numbers, can be dispensed with here. An additional /19

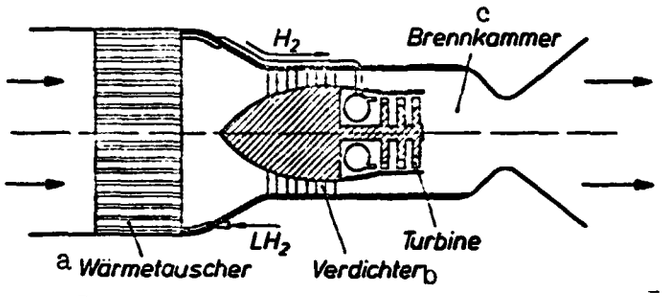

Fig. 2.9. Turborocket with precooling.

Key: a. Heat exchanger; b. Compressor; c. Combustion chamber

advantage to be considered, also of particular importance in the lower range of flight Mach numbers, is that the LH_2 coolant can heat almost to stagnation temperature $T_{t\infty}$ in the heat exchanger, due to the absence of the upstream turbine, and can thus absorb a greater quantity of heat from the air to be cooled than in the inverted turbojet. Nevertheless, the output of the hydrogen-fed turbine at flight Mach numbers below $M_\infty = 2$ is only sufficient for a quite small compressor pressure ratio ($\pi_{tV} < 1.5$), for which reason the thrust achieved in this range of flight Mach numbers, particularly takeoff thrust, must be considered inadequate.

It is possible to increase the output of the turbine by increasing the applied pressure differential only within narrow limits, since the turbine already has to have quite a large number of stages, due to the low mass flow and due to the very small pressure ratio between stages which can be obtained with hydrogen. /20
A slight improvement in takeoff thrust is possible if the hydrogen is used to cool the afterburner chamber after it leaves the heat exchanger and is heated further there.

An effective rise in thrust in the lower range of flight Mach numbers can only be achieved, however, if the hydrogen is heated by its reaction with an oxidizer before it enters the turbine, as happened in the turborocket without precooling. The increase in on-vehicle mass flow consumption due to the additional flow of oxygen must necessarily be accepted in the lower flight Mach number range because the heat exchanger cannot have hydrogen flowing through it during the takeoff phase and during the climb to about $H_\infty = 10$ km. Due to the high absolute humidity in the lower atmosphere, there is a danger of heat exchanger icing.

2.33. Turbojet with Precooling

In addition to the limitation on their usability, which is sometimes a decisive factor in important ranges of operation, the unconventional power plant concepts described have the disadvantage that their technological requirements deviate quite far from the standard which prevails at present in the production of propulsion systems.

Because of its largely conventional design, however, a turbojet with afterburning and air precooling prior to compression appears to be particularly suitable as a high-velocity power plant even for the near future (Fig. 2.10).

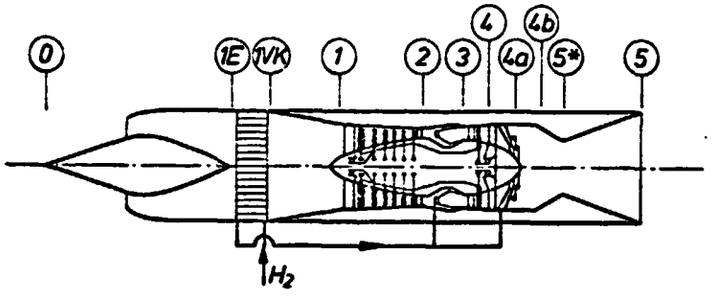

Fig. 2.10. Turbojet with precooling.

Even without precooling, which cannot be turned on initially because of icing, this type of power plant develops the high initial thrust required for takeoff and subsonic climb with moderate fuel consumption. With precooling, it exhibits a comparatively favorable consumption curve throughout the entire range of flight Mach numbers covered, from the transonic phase to maximum flight Mach number, as will be shown later. /21

Due to the reduction in temperature at the compressor inlet, the flow of air taken in by the compressor and thus the thrust of the power plant increase to such a degree that in spite of the added equipment weight due to the required heat exchanger, the erginer exhibits a more favorable thrust/weight ratio than the corresponding conventional turbojet with afterburning. The important advantage of air precooling for its intended use, however, is that the range of flight Mach numbers can be considerably extended, since the engine always feels a lower "apparent" flight Mach number. /22

The flow of hydrogen required for fuel in the main and afterburner chambers is heated in the countercurrent heat exchanger almost to the particular stagnation temperature $T_{t\infty}$ (Fig. 2.11). As flight Mach number increases, it can absorb more and more heat from the airstream, which is also transferred by the heat exchanger, since the mean temperature difference between the fluids involved increases with increasing $T_{t\infty}$.

In addition to liquid hydrogen (LH_2), liquid methane (CH_4) can also be used as fuel in a turbojet with precooling of the air that is to be compressed. While preference is to be given to the use of hydrogen for the accelerated flight of a space vehicle carrier, methane is suitable for prolonged flight times at less extreme flight Mach numbers, e.g. in a high velocity transport aircraft (SST) designed for about $M_\infty \approx 4.5$. In addition to its simpler storage and handling, it has a considerable advantage over /23

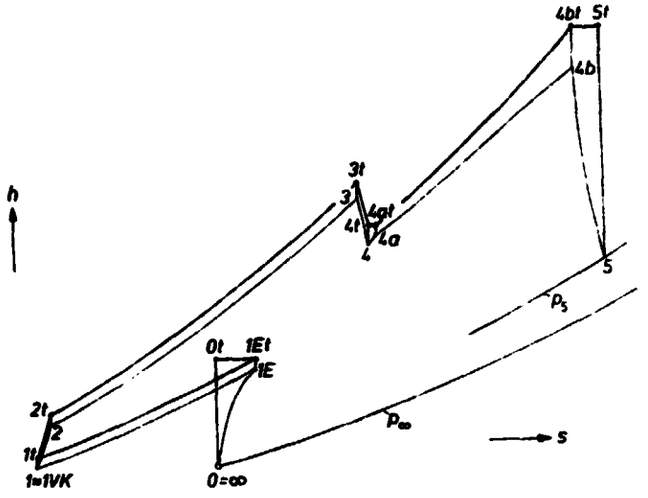

Fig. 2.11. Course of thermodynamic process in turbojet with precooling.

LH_2 in its higher density in the liquid state. This allows smaller tank volumes, in spite of its lower calorific value (H_{uH_2} = $120 \cdot 10^6$ J/kg; H_{uCH_4} = $55 \cdot 10^6$ J/kg; $H_{ukerosene}$ = $43 \cdot 10^6$ J/kg), which calls for higher on-vehicle consumption by weight. Due to its lower heat capacity, however, the effect of precooling is considerably lessened.

An exact analysis of the turboject with precooling, making use of a project design, is the topic of this dissertation.

2.34. Turbofan with Precooling

The higher flexibility of the turbofan with afterburning as compared to the simple turbojet with afterburning suggests the idea of also providing an afterburner-equipped turbofan with a precooling system, thereby making it usable for propelling an aerodynamic space vehicle carrier. In terms of design and the control of thermodynamic processes, this power plant concept offers a wide range of variation. Fig. 2.12 shows four possible configurations.

The configuration with the heat exchanger ahead of the fan inlet (version a) in principle has the precooling effect obtained with the turbojet plus precooling: The overall power plant feels a lower apparent flight Mach number. /24

In a turbofan, the specific power requirement for compressing primary-circuit air mass flow $\dot{m}_{LI}$ is considerably higher than for compressing the bypass mass flow $\dot{m}_{LII}$. Since the same relative savings in power is achieved when compressor inlet temperature is reduced equally in both circuits, the absolute reduction in the shaft power required per kg airflow is considerably greater in the primary circuit because of the higher compressor pressure ratio there. It is thus desirable to use the heat capacity of the fuel available for heat absorption primarily or even exclusively for precooling the primary-circuit air. It can then be cooled considerably more intensively since, in the last-mentioned case for example, the flow of coolant available for the /25

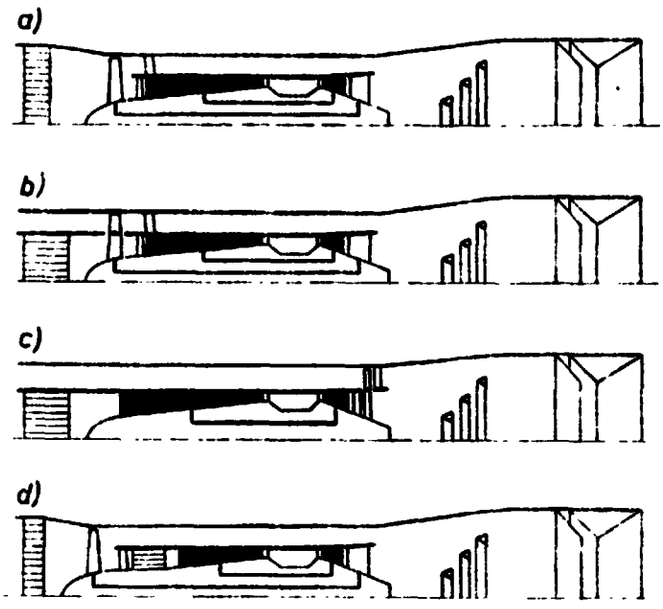

Fig. 2.12. Turbofan with precooling.

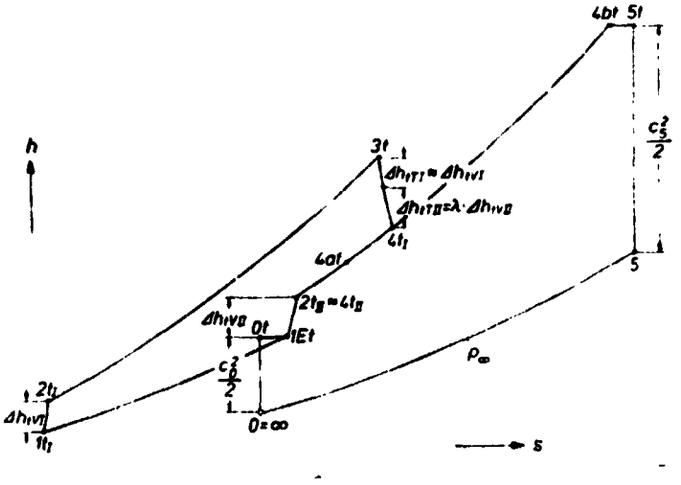

Fig. 2.13. Course of thermodynamic processes in turbofan with precooling.

airflow to be cooled is multiplied by a factor corresponding to the bypass ratio $\lambda = \dot{m}_{LII}/\dot{m}_{LI}$.

The thermodynamic processes through all states are shown for this configuration in simplified form in Fig. 2.13.

Fig. 2.12 shows two possible forms in versions b and c. In addition to the familiar disadvantages for the application under consideration, the aftfan configuration offers a slight advantage in the decoupling of the two circuits. For both forms, the bypass ratio is reduced considerably under some circumstances if precooling is turned on after the end of the takeoff and subsonic climb phases by allowing fuel to flow through the heat exchanger. In order to prevent overspeeding of the fan, it is necessary to accept the drop in turbine inlet temperature, with the attendant disadvantages. /26

The configuration shown as version d in Fig. 2.12 permits greater flexibility. In addition to more or less intense precooling of the overall airflow through the power plant (cf. version a), further intermediate cooling of the primary-circuit air is possible here in an additional heat exchanger. Through distribution of the free heat capacity of the

coolant between the two heat exchangers, it is possible to freely vary turbine inlet temperature, rotor rpm and -- within limits -- the bypass ratio.

Compared to the turbojet with precooling, the turbofan with precooling has the disadvantage of higher structural weight and, normally, also a higher compressor outlet temperature, which is a consequence of the higher compressor pressure ratio in the primary circuit and rather markedly restricts the flight Mach number range covered, at the upper end. Provisional comparative calculations as part of studies on the topic of this work indicated no advantages in consumption on the part of the turbofan with precooling.

2.35. Turbofan with Air Liquefaction in Primary Circuit /27

If we increase the bypass ratio of a turbofan with precooling in configuration b or c (Fig. 2.12) to values above about $\lambda = 7$, a sufficiently large heat sink becomes available in the flow of hydrogen which is required for stoichiometric consumption of the entire airflow to use to liquefy the primary-circuit airflow. This can then be highly compressed in the liquid state with negligible compression effort and be heated in a high-pressure combustion chamber after the addition of suitably substoichiometric or highly superstoichiometric quantities of fuel. The turbine fed with the combustion gases, small in diameter but of many stages, drives not only the pumps for the fuel and liquid air but also the secondary circuit compressor, via a reduction gear system. Except for the heat exchanger, the design of the power plant corresponds to that of a turborocket. The liquid oxygen required in the latter is merely replaced with previously liquefied air, which now does not need to be carried on the vehicle any more.

Since the heat capacity of the entire flow of hydrogen is fully utilized for liquefying the primary circuit air, but not for its cooling to liquefaction temperature, an additional heat exchanger can be placed in front of the engine, as in the version of the turbofan with precooling shown in Fig. 2.12d or in the turborocket with precooling.

The primary disadvantage of this type of engine relative to the turbojet with precooling, aside from its much less conventional design, can be considered the fact that it, like the turborocket with precooling, delivers inadequate thrust in the takeoff and subsonic climb phases. Due to the danger of icing, cooling and /28 liquefaction of the air must be dispensed with at the lower altitudes, so the turbine can again only be fed with fuel in this flight range if an additional supply of oxygen is not to be used.

2.36. Precooling with the Compressed Air

In the turbofan with air liquefaction in the primary circuit described, only a small portion (less than an eighth) of the flow of air fed to the engine is liquefied through heat exchange with the flow of fuel needed to heat the entire airflow. Now it is conceivable for the entire flow of air entering the inlet to be liquefied, then heated after compression in the liquid phase in a high-pressure combustion chamber which is similar to a rocket combustion chamber. Fig. 2.14 shows the schematic for such a power plant, proposed by D.A. Anderton [9] and later by Jeffs and Beeton [10], who designated it the "liquid air cycle engine" (LACE).

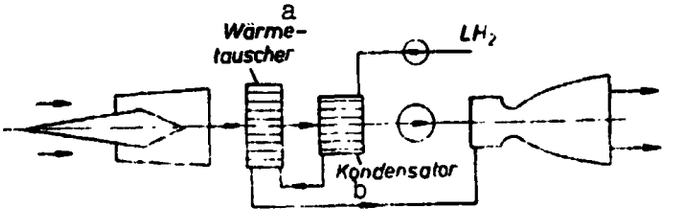

Fig. 2.14. Liquid air cycle engine (LACE).

Key: a. Heat exchanger; b. Condenser

Its high specific fuel consumption can be considered the decisive disadvantage of this operating principle. It is a consequence of the fact that more than eight times the stoichiometric supply of fuel is required to liquefy the air. The aim of the following discussion is to reduce this disadvantage.

A systematic extension of the idea of precooling the air to be compressed with the liquid hydrogen or methane required for fuel leads to utilization of the heat sink available in the already compressed airflow /29
for further cooling the air which is compacted in the intake. This allows the positive effects of precooling to be considerably enhanced without additional consumption of outside coolant. Even at high flight Mach numbers, air cooling can thus be extended close to the phase boundary curve, producing a considerable reduction in compression effort. A qualitative curve of the overall changes in state during compaction, heat exchange and compression is shown for this process in Fig. 2.15.

The air which becomes compacted to state (1Et) in the intake is cooled to state (1At) in the air/air heat exchanger. The heat q_L removed from it heats the already-compressed air from state ($2t_{VK}$) downstream from the compressor to state (2t) at the combustion chamber inlet. The remaining cooling of the air from state (1At) to compressor inlet state ($1t_{VK}$), which may lie close /30
to the phase boundary curve, is done in the air/H_2 heat exchanger. The magnitude of the quantity of heat $\beta \cdot q_{H_2}$ which the hydrogen must

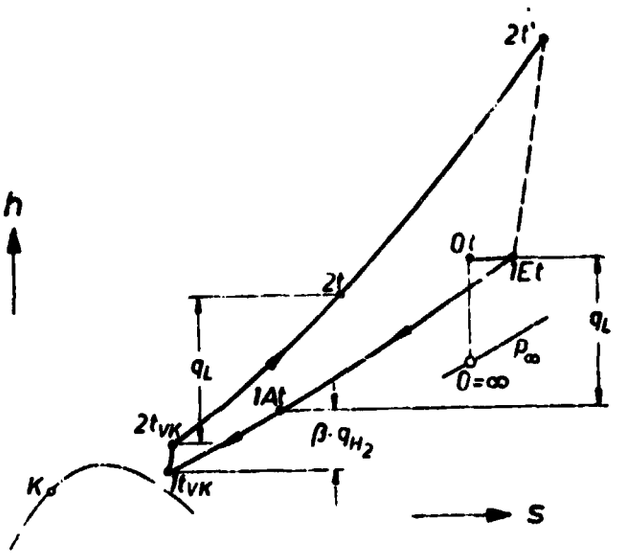

Fig. 2.15. Precooling with compressed air.

absorb here is determined by the magnitude of the increase in enthalpy during compression and by the transfer loss which occurs in the air/air heat exchanger due to the finite character of the required temperature differences between the heat-exchanging fluids.

Particularly because combustion in the high-pressure chamber preferable takes place with a slight excess of fuel, the heat sink available in the flow of fuel which is necessary anyway is adequate to precool the air throughout the range of flight Mach numbers covered, /31 up to the vicinity of the boundary curve. Partial or even complete liquefaction of the air is not appropriate in this process, since this would increase hydrogen requirements several-fold for reasons already discussed.

This engine concept has already been subjected to a critical analysis during the studies which led to the present work. It permits a further extension of the flight Mach number range and a slight improvement in consumption relative to the turbojet with precooling. A detailed presentation of it will not be attempted here, however.

The major disadvantage of this engine is again the fact that it is normally not suitable for altitudes below H_∞ = 10 km, due to the danger of icing in the heat exchanger.

The basic thermodynamic effect of precooling on the process and the generation of thrust by thermal jet engines will be illustrated using the limiting case -- thought of as a conceptual model -- in which a heat sink is provided to the operating fluid, air, exclusively by the flow of hydrogen. During the course of the thermodynamic process, consequently, total enthalpy can at no point assume a value which is higher than the total enthalpy of the airstream entering the intake.

Fig. 2.16 shows an h-s diagram in which the thermodynamic principle of precooling is illustrated. The qualitative process is somewhat equivalent to that in Fig. 2.15. As an idealization,

it has also been assumed that the flow of heat can even occur at infinitely small temperature differences between the fluid involved. As can be seen from the h/s diagram, precooling alone can provide positive process power $\dot{m}_L \cdot (c_5^2 - c_\infty^2)/2$ and thus positive thrust even though just heat from the surroundings is added to the process. /32

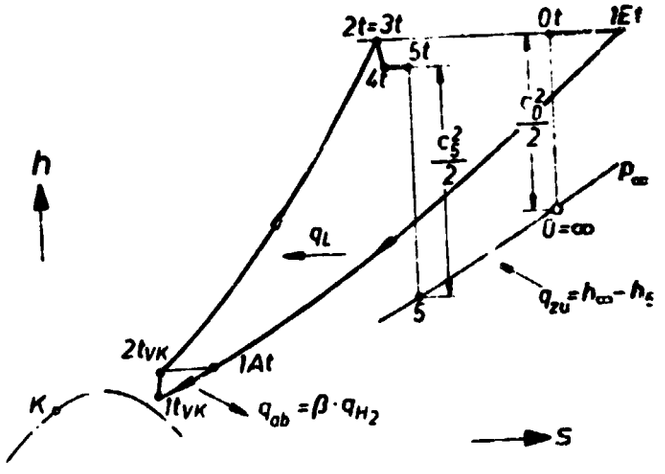

Fig. 2.16. Thermodynamic principle of precooling.

2.37. Liquefaction and Separation of Air into its Components

The concepts presented represent air-breathing engines that are more or less well suited as power plants for a space vehicle carrier. During the first phase of flight, within the dense atmosphere, they remove all of the oxygen necessary for consumption from the air, in contrast to the rocket propulsion used so far. It also appears consistent to obtain the oxidizer required for the second phase of flight outside the atmosphere from the surrounding air shortly prior to stage separation. Since this portion of the fuel then no longer need be carried from takeoff on, the ratio of payload to launch weight can be improved slightly under given circumstances. /33

For this purpose, additional air can be scooped in toward the end of the first phase of flight, liquefied by heat exchange with the fuel flow required in the air-breathing engines, and stored in tanks in the rocket stage, which takes over the job of continued acceleration after burnout of the booster stage.

It is also conceivable to branch off a portion of the air scooped up by the engine intakes and to break it down into its components after liquefaction [2, 11]. The possibility then exists of storing only the liquid oxygen obtained here, which represents a higher-energy fuel component than liquid air, in the upper stage. The gaseous nitrogen obtained can be fed to the air-breathing engines again. This has the advantage that during the collection phase, in contrast to the first version, only the inlet momentum of the separated oxygen need be compensated for by engine thrust as an additional drag. On the other hand, about

three times the total quantity of air must be liquefied for the same "integral total momentum" in this alternative approach. To this is added the large amount of equipment for the oxygen collecting system, required primarily by the separator [36], which removes a predominately oxygen-bearing fraction from the liquid air delivered. The weight of this system appreciably reduces the savings in weight achieved. To this is added the indirect increase in weight due, for example, to the aspects which must be taken into consideration in selecting the flight profile. /34

If the separation of liquid air is dispensed with, the amount of equipment is considerably reduced. The major disadvantage of this version, however, is the lower specific thrust $\sigma_B = F/\dot{m}_B$ (so-called "specific momentum") of the air/H_2 rocket relative to the H_2/O_2 system, with its consequences for the total weight of the upper stage and thus the launch weight of the entire carrier system.

To reduce the amount of equipment, finally, it appears desirable to combine the collecting system with the engine concept presented in Section 2.36 and thus simultaneously provide the basis for further extending its range of application to higher flight Mach numbers.

2.38. Combustion with Excess Fuel

This section will point out a basic possibility or necessity which results from the peculiarities of the application and which must be considered with respect to the thermodynamic processes.

Among the conventional air-breathing engines, the ramjet with subsonic combustion is suitable for the highest flight Mach numbers. Since constantly stoichiometric fuel/air ratios are used for calculations in those studies published so far in which the ramjet was used for comparison purposes, limiting Mach numbers above $M_\infty = 9$ are indicated. Combustion chamber temperatures assume values here which are obtained only experimentally even in rocket combustion chambers. /35

If we limit the maximum permissible combustion chamber temperature, by supplying substoichiometric quantities of fuel, to a technologically reasonable value of, say, $T_{tmax} = 2400$ K, the ramjet no longer delivers adequate thrust beyond about $M_\infty = 5.5$ or 6. The supply of energy in the combustion chamber, which decreases more and more markedly with increasing flight Mach number, ultimately covers only the more and more rapidly increasing losses.

If we maintain the maximum permissible combustion chamber temperature through combustion with a suitable excess of fuel, however, jet exhaust velocity is markedly increased, since the molar mass of the combustion gases decreases. If hydrogen is used

as the fuel, the engine is now suitable for speeds up to more than $M_\infty = 7$. Generally, it would still provide a usable specific thrust $\sigma_L = F/\dot{m}_L$ even if the temperature of the air at the combustion chamber inlet has already exceeded the permitted heating temperature. However, this advantage is purchased at the cost of a loss of thrust relative to fuel flow, $\sigma_B = F/\dot{m}_B$.

Superstoichiometric combustion allows the maximum limiting flight Mach number to be shifted farther out to a corresponding degree even for a turbojet. Since the flow of fuel is simultaneously the flow of coolant here, combustion with an excess of fuel does not just produce a direct increase in jet exhaust velocity, as in the ramjet. Due to the enhanced precooling effect, temperature at the power plant inlet and thus the relative weight required for compression and the compressor outlet temperature are also reduced further. The result is an increase in the thrust generated by the engine and an appreciable extension of the flight Mach number range covered to more than $M_\infty = 6.5$. /36

The increase in thrust due to superstoichiometric combustion produces an improvement in the thrust/weight ratio σ_G for the engine or, for a given installed engine weight, a reduction in the time of accelerated flight. As is shown later, this can ultimately lead to a reduction in the total weight of fuel required, e.g. when turbojets with precooling are used, if the missile is accelerated with such engines to flight Mach numbers above about $M_\infty = 4$. This case occurs in the mission of a space vehicle carrier system under consideration.

3. Mathematical Principles for Determining the Real-Gas Behavior of the Fluids Involved /37

A numerical analysis of the processes to be studied is feasible only with electronic computers. It is necessary here that all operating data be made available in programmed form. We especially need to have the thermal and caloric variables of state assigned to each of the fluids involved in the cyclic processes.

In view of the size of the range of states covered, it was necessary to obtain these results taking the real gas behavior of the mass flows into consideration. Since air is partly cooled very close to the phase boundary curve or even liquefied in the engines with precooling, a real gas program was written to calculate its variables of state, as well as those of hydrogen, oxygen and nitrogen. A combustion gas program was developed for the reaction calculations and for determining the changes in state of the combustion gases, taking the varying molar compositions into consideration. It is designed for the reaction of any hydrocarbons with air, oxygen or a mixture of them.

A brief, orienting outline of the thermodynamic principles and of the basic ideas needed to take real gas behavior into consideration in thermodynamic process calculations for air-breathing jet engines will first be provided on the following pages. Initial conditions and the main features of the computational process are then shown, along with an outline of the subprogram systems written for this.

3.1. Delimiting the Ranges of States /38

a) The Ideal Gas

Assumed (definition):

-- gas of constant composition

-- individual molecules have punctiform mass (molecules have no volume of their own)

-- no intermolecular field forces.

For this relationship between thermal variable of state we then have

$$p = \rho \cdot R \cdot T \tag{3.1}$$

with

$$R = \mathcal{R}/\mathcal{M} = \text{const.} \tag{3.2}$$

For the isentropic exponent k -- since the specific heats of the ideal gas are not functions of pressure or density -- we also have

$$\begin{aligned} k &\equiv \left(\frac{\frac{\partial p}{p}}{\frac{\partial v}{v}}\right)_s = -\left(\frac{v \cdot dp}{p \cdot dv}\right)_s = \left(\frac{dh}{du}\right)_s = \frac{c_p}{c_v} \equiv \kappa \\ c_p &= c_p(T) \\ k &= \kappa = f(T) \end{aligned} \tag{3.3}$$

Specific heat $c_p(T)$ can be determined from the classical statistical mechanics of molecular motion.

b) The Real Gas

/39

Deviation from ideal gas behavior:

-- at high densities in the low-temperature range: Intermolecular attractive forces can no longer be neglected when mean free paths approach the order of magnitude of "molecular diameter."

$p = p_{kin} - \Delta p$

p_{kin} = f(gas kinetics energy density)

= $f(T,\rho)$

Δp = f(intermolecular field forces)

= cohesion pressure

We have

$$p = Z(\rho, T) \cdot \rho \cdot R \cdot T \qquad (3.4)$$

$$\kappa = k(\rho, T) \neq \kappa = \kappa(\rho, T) \qquad (3.5)$$

-- at very high density: The potential of intermolecular attractive forces is ultimately exceeded by the repulsive forces between somewhat compressible molecules of finite inherent volume.

$p = p_{kin} + \Delta p$

-- at high temperatures (and low densities): Due to dissociation (cleavage into simpler components, e.g. $N_2 \rightarrow 2N$), gas composition varies with temperature and with density or pressure: /40

$$\nu_j = n_j/n_{ges} = \nu_j(\rho,T) \qquad (3.6)$$

where
n_j = number of moles of component J
n_{ges} = total number of moles.
Otherwise, the real gas behaves like a mixture of ideal gases in this range.

The caloric variables of state, enthalpy h and entropy s, in a given state can be formulated for a homogeneous fluid which is in thermodynamic equilibrium and has a constant composition with the aid of the Second Law and statistical mechanics if the thermal quantities of state are known. If gas composition changes as the result of dissociation or recombination, additional attention must be given to the quantities of heat converted.

c) Delimiting the Ranges of State

The state diagram (T-s diagram) for air shown in Fig. 3.1 is divided into

-- a low-temperature range,

-- a medium-temperature range and

-- a high-temperature range.

The medium-temperature range is delimited in such a way that within it, the air can be viewed as a quasi-ideal gas.

No changes of state of conventional cyclic engine processes occur in the low-temperature range. It is still needed, for example, for cyclic process designs with precooling. /42

Generally, cyclic processes in air-breathing jet engines take place in the medium-temperature range, whose upper limit for combustion gas is somewhat lower than plotted in Fig. 3.1, however. The changes in state in power plants with afterburning and in ramjets extend into the high-temperature range.

3.2. Low-Temperature Range

A program system had to be developed with which it is possible to calculate all missing thermodynamic variables of state, p, T, ρ, h and s, for a given state from any two that are given in each case for the fluids H_2, O_2, N_2 and air. The range of states represented should extend from p = 0.001 bar to p = 150 bars and from the liquefaction region to T = 1000 K (H_2), T = 2000 K (O_2) or T = 3000 K (N_2 and air). In particular, the equations used should be formulated in such a way that the thermodynamic properties of any materials can be calculated with the program system after changing blocks of constants.

The thermal and two caloric equations of state used are first given below. The method used to improve these equations is also discussed.

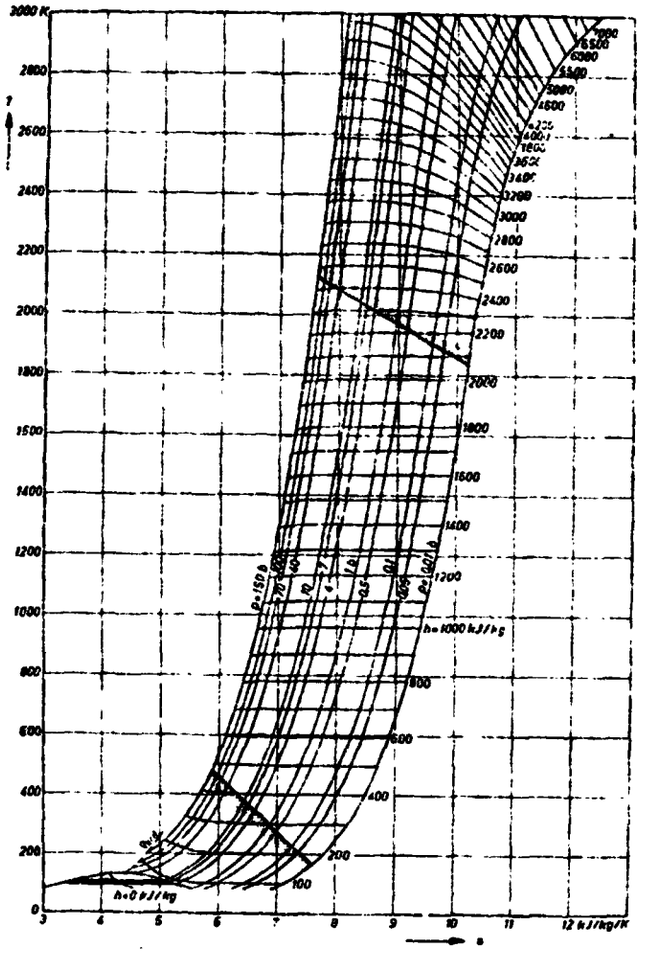

Fig. 3.1. T-s diagram for air, broken down into ranges.

3.21. Thermal Equation of State

The so-called gas equation relates the thermal state variables:

-- the temperature T corresponding to the molecules' state of excitation

-- the volume v_{kin} (specific net volume) available for translational motion of the molecules

-- the pressure p_{kin} corresponding to energy density

to one another via the gas constant $R = \mathcal{R}/m$, whose value can be determined from gas kinetics theory:

$$p_{kin} \cdot v_{kin} = R \cdot T.$$

While $p_{kin} = p$ and $v_{kin} = v$ for the ideal gas, cohesion pressure acts against kinetic pressure in the real gas, and kinetic volume is increased by an amount equal to the co-volume:

$$\left(p + \frac{a}{v^2}\right) \cdot (v - b) = R \cdot T \qquad (3.7)$$

where

a/v^2 = cohesion pressure; b = co-volume.

The constants a and b can be determined from statistical gas kinetics.

This equation, named for van der Waals, is quantitatively inaccurate. However, it allows a complete overview of the basic state behavior of all materials. Higher precision can be achieved with equations of state of purely mathematical form or with equations which are based on theoretical formulations but have then been improved empirically.

The Beattie-Bridgeman equation of state used belongs to the latter type; in its original form it reads /44

$$p = \frac{R \cdot T}{\mathcal{V}^2} \cdot (1 - \cdot) \cdot (\mathcal{V} + b) - \frac{A}{\mathcal{V}^2} \qquad (3.8)$$

with the terms

$$A = A_0 \cdot \left(1 - \frac{a}{\mathcal{V}}\right)$$

$$B = B_0 \cdot \left(1 - \frac{b}{\mathcal{V}}\right)$$

$$c = \frac{c}{\mathcal{V} \cdot T^3}$$

where $\mathcal{V}$ is molar volume, R is the general gas constant, and A_0, B_0, a, b and c are constants which depend upon the material.

In virial notation, the equations appear as follows:

$$p(\rho,T) = R \cdot T \cdot \rho + \left(\frac{R}{m} \cdot B_0 \cdot T - \frac{A_0}{m^2} - \frac{R}{m} \cdot \frac{c}{T^2}\right) \cdot \rho^2$$

$$+ \left(-\frac{R}{m^2} \cdot B_0 \cdot b \cdot T + \frac{A_0 \cdot a}{m^3} - \frac{b}{m^2} \cdot \frac{B_0 \cdot c}{T^2}\right) \cdot \rho^3$$

$$+ \left(\frac{R}{m^3} \cdot \frac{B_0 \cdot b \cdot c}{T^2}\right) \cdot \rho^4 \qquad (3.9)$$

or

$$p(\rho,T) = R \cdot T \cdot \rho + A_2(T) \cdot \rho^2 + A_3(T) \cdot \rho^3 + A_4(T) \cdot \rho^4$$

In its "physical form," this equation has the basic advantage over the so-called "technical form" ($\rho = \rho(p,T)$) that it can also represent the region of states in the vicinity of the critical point. Moreover, it is easier to mathematically adapt the material-dependent constants to available measured data for the "physical form" of the equation of state than for the "technical form," since the isochors ρ = const. are almost linear over a wide area of the region of states (Fig. 3.2). /45

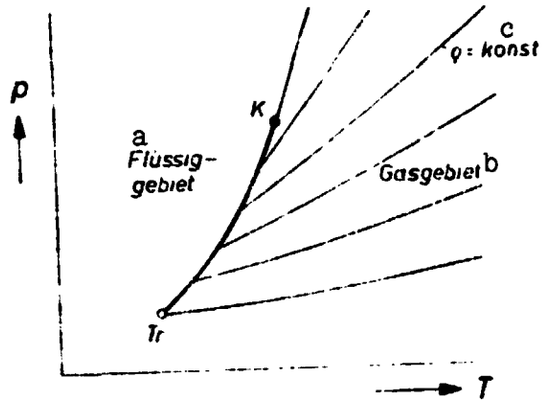

Fig. 3.2. Vapor pressure curve and isochors in p-T diagram.

Key: a. Liquid region; b. Gas region; c. Constant

The virial coefficients A(T) in the Beattie-Bridgeman equation, dependent only upon temperature, are known for almost all technically important fluids. The relationship $p = p(\rho,T)$ has been calculated for the entire region of states of interest in each case with the constants given by Beattie and Bridgeman for H_2, O_2, N_2 and air. A comparison with the values tabulated in [12-15] shows that the Beattie-Bridgeman equation does not satisfy requirements for higher accuracy. In particular, /46 it does not correctly represent real gas behavior in the lower temperature range as the wet vapor region is approached, as well as at high temperatures in the dissociation range. A way therefore had to be found to improve the equation.

The simplest method available was to add a correction term to equation (3.9):

$$p(\rho,T) = p(\rho,T)_{B.B.} + \Delta p(\rho,T)$$

It was found that the relative error $\Delta p/p$ in the first equation is inversely proportional to temperature and increases with pressure. The error function, which can be approximated with a linear equation, can thus be given as:

$$f_1 = \frac{\Delta p_1}{p} \cdot \frac{T}{p} = \frac{\Delta p_1(\rho,T)}{R^2 \cdot \rho^2 \cdot T} \qquad (3.10)$$

The equation for ideal gases can be used here for conversion. If we introduce the linear equation for the error function, the correction term reads

$$\Delta p_1(\rho,T) = (A_1 + A_2 \cdot T) \cdot R^2 \cdot \rho^2 \cdot T$$
$$= (a_1 \cdot T + a_2 \cdot T^2) \cdot \rho^2 \qquad (3.11)$$

The constants a_1 and a_2 can be determined from a graphic evaluation of the error function. This first correction is covered in the equation of state by extending the second virial coefficient in equation (3.9) with the additional term $(a_1 \cdot T + a_2 \cdot T^2)$.

If we use the equation of state improved in this manner to obtain the remaining deviation from tabulated values and plot it for various pressures over temperature, we obtain, in principle, something like the mean error distribution shown in Fig. 3.3 for all four materials studied. /47

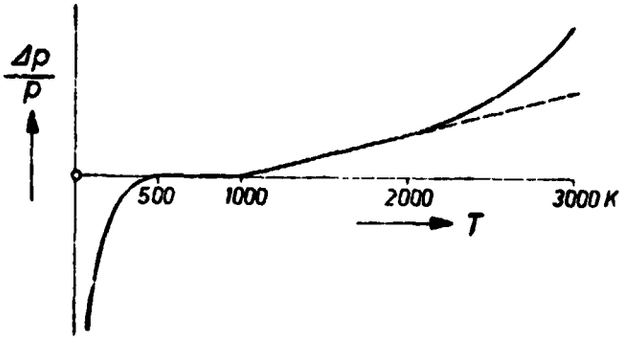

Fig. 3.3. Relative error after first correction.

Since it is difficult to represent the behavior of this function wit a single equation, it is desirable to break up the temperature range.

While the error $\Delta p/p$ in the "normal temperature range" (500 K to 1000 K) remains below the desired limits of error $\varepsilon = 0.1\%$ after just the first correction, additional error functions must be defined for the low-temperature range (subscript T), which extends up to 500 K, and for the high-temperature range (subscript H) above 1000 K. These error functions should again be formulated in such a manner that they can be represented approximately with linear equations whose coefficients can be calculated from the boundary conditions. A comparison with the error curve shown in Fig. 3.3 yielded /48

$$F_{2T} = \frac{\Delta p_{2T}}{p} \cdot \left(\frac{T}{p}\right)^2 = \frac{\Delta p_{2T}(\rho,T)}{R^3 \cdot \rho^3 \cdot T} \qquad (3.12)$$

$$F_{2H} = \frac{\Delta p_{2H}}{p} \cdot \frac{1}{T} = \frac{\Delta p_{2H}(\rho,T)}{R \cdot \rho \cdot T^2} \qquad (3.13)$$

Error functions (3.12) and (3.13), when rewritten in the form of

equation (3.11), yield additional constants by which the third and/ /or first virial coefficient must be extended.

For air, the equation of state improved thusly must also be extended by a third correction term $\Delta p_{3H}(\rho,T)$ in the high-temperature range, since an appreciable dissociation effect occurs above about 2000 K. The residual error remaining after the second correction is proportional here to a higher power of temperature and approximately inversely proportional to the square root of pressure:

$$F_{3H} = \frac{\Delta p_{3H}(\rho,T)}{R \cdot T^7 \cdot \rho^{1/2}} \qquad (3.14)$$

In the abbreviated virial notation of equation (3.9), the triply extended Beattie-Bridgeman equation reads as follows for the case at hand, for example:

/49

$$\begin{aligned} p(\rho,T) &= p(\rho,T)_{B.B.} + \Delta p_1(\rho,T) + \Delta p_{2H}(\rho,T) + \Delta p_{3H}(\rho,T) \\ p(\rho,T) &= (R \cdot T + b_1 \cdot T^2 + b_2 \cdot T^3) \cdot \rho \\ &\quad + (A_2(T) + a_1 \cdot T + a_2 \cdot T^2) \cdot \rho^2 \\ &\quad + A_3(T) \cdot \rho^3 + A_4(T) \cdot \rho^4 \\ &\quad + (c_1 \cdot T^7 + c_2 \cdot T^8) \cdot \rho^{1/2} \end{aligned} \qquad (3.15)$$

For the low-temperature range, too, it was necessary to extend the equation of state by a third correction term. This resulted from the condition that at the phase boundary between the moist vapor and gas regions, it must satisfy the corresponding values of the separately determined boundary curve representation so that a continuous transition to the moist vapor region is guaranteed. In order to change the curvature as little as possible, matching was extended over the entire low temperature range by adding a parabolic term. A continuous and smooth connection is made with the "normal temperature range."

3.22. Caloric Equations of State

If the caloric state variables for a fluid are known at a reference point "0" with $h_O = h(\rho_O,T_O)$ and $s_O = s(\rho_O,T_O)$, the caloric state variables h_A and s_A at any point A in the region of states can be determined via a state change from 0 to A:

$$h_A = h_0 + \int_0^A dh$$

$$s_A = s_0 + \int_0^A ds$$

Since h and s are variables of state and thus dh and ds are exact differentials, the path of integration is arbitrary. For example, it can proceed along two isotherms and an isobar as shown in Fig. 3.4:

$$h_A = h_0 + \int_0^1 (dh)_T + \int_1^2 (dh)_p + \int_2^A (dh)_T \qquad (3.16)$$

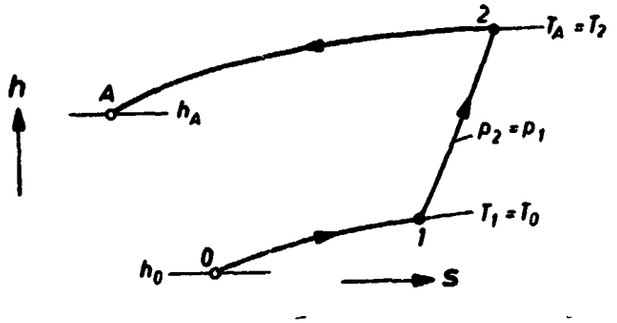

Fig. 3.4. Path of integration for determining enthalpy.

Integrations between the reference point and the state being sought are represented by the caloric equations of state. To formulate them we need the Second Law of Thermodynamics, which relates the thermal and caloric state variables to one another:

$$T \cdot ds = du + p \cdot dv = dh - \frac{dp}{\rho}$$

With the Second Law, the exact differential for enthalpy can be represented as:

/51

$$dh = T \cdot \left(\frac{\partial s}{\partial \rho}\right)_T \cdot d\rho + T \cdot \left(\frac{\partial s}{\partial T}\right)_\rho \cdot dT + \frac{1}{\rho} \cdot \left(\frac{\partial p}{\partial \rho}\right)_T \cdot d\rho + \frac{1}{\rho} \cdot \left(\frac{\partial p}{\partial T}\right)_\rho dT \qquad (3.17)$$

Equation (3.17) can be simplified for integration along the isotherm:

$$(dh)_T = \left(\frac{\partial h}{\partial \rho}\right)_T \cdot d\rho = \left[T \cdot \left(\frac{\partial s}{\partial \rho}\right)_T + \frac{1}{\rho} \cdot \left(\frac{\partial p}{\partial \rho}\right)_T\right] \cdot d\rho \qquad (3.18)$$

Using the Second Law and the definition of free energy $f \equiv u - T \cdot s$, we can derive

$$\left(\frac{\partial s}{\partial \rho}\right)_T = -\frac{1}{\rho^2} \cdot \left(\frac{\partial p}{\partial T}\right)_\rho$$

If we substitute this relationship into equation (3.18), we can express the differentials required in equation (3.16) for the change in enthalpy at constant temperature exclusively in terms of the independent thermal state variables and the derivatives of the thermal equation of state $p = p(\rho,T)$:

$$(dh)_T = \left[\frac{1}{\rho} \cdot \left(\frac{\partial p}{\partial \rho}\right)_T - \frac{T}{\rho^2} \cdot \left(\frac{\partial p}{\partial T}\right)_\rho\right] \cdot d\rho \qquad (3.19)$$

The partial differential needed for integration along the isobar

$$\left(\frac{\partial h}{\partial T}\right)_p = c_p\,(p,T)$$

is defined as specific heat at constant pressure. If we integrate from point 1 to point 2 along the isobar $p = 0$, $c_p(p,T)$ becomes the specific heat of the ideal gas $c_p^o(T)$, which can be determined relatively simply and accurately from the classical statistical mechanics of molecular motion: /52

$$(dh)_{p=0} = c_p{}^o(T) \cdot dT \qquad (3.20)$$

The solution to equation (3.16) can be further simplified if we locate reference point 0 in a region in which the ideal gas equation is valid with sufficient accuracy. The result of this is that the value of the first integral expression in (3.16) becomes zero, for the enthalpy of an ideal gas remains constant during an isothermal change of state. Reference point enthalpy h_o, which basically can be selected arbitrarily, can then likewise best be calculated from statistical mechanics as $h_o = h^o(T_o)$.

Thus the caloric equation of state for determining enthalpy at point A can be formulated

$$h_A = h_o + \int_{T_o}^{T_A} c_p{}^o(T) \cdot dT + \int_{\rho=0}^{\rho_A} \left[\frac{1}{\rho} \cdot \left(\frac{\partial p}{\partial \rho}\right)_T - \frac{T}{\rho^2} \cdot \left(\frac{\partial p}{\partial T}\right)_\rho\right] \cdot d\rho \qquad (3.21)$$

Entropy in state A can be derived in a similar manner:

$$s_A = s_o + \int_{T_o}^{T_A} c_p^o(T) \cdot \frac{dT}{T} + \int_{\rho \to 0}^{\rho_A} \left[\frac{R}{\rho} - \frac{1}{\rho^2} \cdot \left(\frac{\partial p}{\partial T} \right)_\rho \right] \cdot d\rho - R \cdot \ln \frac{\rho_A \cdot T_A}{\rho_o \cdot T_o} \qquad (3.22)$$

The two caloric equations of state (3.21) and (3.22) are closely related to the thermal equation of state (3.15) via the partial derivatives -- and via the thermal state variables themselves in implicit solutions. This justifies the high accuracy requirements satisfied in their formulation. /53

The specific heat of air in the imaginary ideal gas state had to be given an additional correction for the dissociation region, since only the values for normal composition were provided by $c_p^o(T)$. A third-degree polynomial was used for fitting in the temperature range represented, up to T = 3000 K.

3.23. Representation of Boundary Curves

The moist vapor region is inferred from its two phase boundary curves. Since the isobars and isotherms of fluid materials coincide in the moist vapor region, we generally require an additional state variable, vapor content x, to define a state with given p and T. All missing state variables can then be calculated with the aid of the "lever law of phase proportions" if the corresponding values on the boundary curves are known.

Explicit equations for the following boundary curve representations have been developed for the four materials used for this purpose:

$$\begin{array}{ll} T' = T'(p) & T'' = T''(p) \\ \rho' = \rho'(T') & \rho'' = \rho''(T'') \\ h' = h'(T') & h'' = h''(T'') \\ s' = s'(T') & s'' = s''(T'') \end{array} \qquad (3.23)$$

A single prime indicates the phase boundary between liquid and moist vapor; a double prime, the phase boundary between moist vapor and gas. The two equations for T'(p) and T"(p) are identical for the pure fluids H_2, N_2 and O_2. /54

Using suitable iteration methods, it is possible to evaluate all 14 combinations of specified variables coming under consideration with the above eight boundary curve representations. The corresponding representations were carried out for the four fluids with the same explicit function types in each case.

At this point it will also be pointed out that the boundary curve equation as well as the thermal and the two caloric equations of state were reduced in the computer program with the applicable data for the critical point and therefore have a rather generally valid form. The program system can easily be extended to real gas calculations for other fluids by changing or adding blocks of constants.

3.24. Computing System and Ranges of States Represented

The real gas program that was written was designed as a closed subprogram system. It is called by the statement

CALL ZUSTGL (K,N1,N2,P,T,RHO,H,S,X)

Parameter K indicates the fluid (H_2, O_2, N_2, air) for which the four missing state variables for a given state are to be determined. Parameters N_1 and N_2 indicate by which of the two known variables the given state is defined. /55

The following prespecified combinations are conceivable and are provided for:

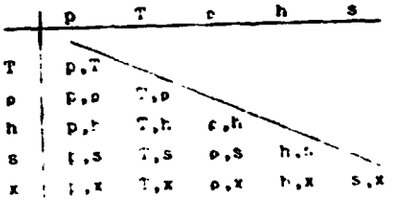

The missing state variables can generally be calculated for these prespecified combinations, provided they uniquely characterize a state, throughout the range of states provided for, including the immediate vicinity of the critical point. The program decides whether the particular state lies within the moist vapor region or the gaseous region.

The computing system is designed as follows for calculating states within the gaseous region:

-- The three equations of state used are available explicitly only in the form $p = p(\rho,T)$, $h = h(\rho,T)$ and $s = s(\rho,T)$.

-- If only one of the independent variables ρ and T is specified, the other must be estimated and determined iteratively. This applies to the prespecified combinations (p,T), (p,ρ), (T,h), (T,s), (ρ,h) and (ρ,s).

-- If both independent variables in the equations of state are unknown, as in the case of the prespecified combinations (p,n), (p,s) and (h,s), the solution can be obtained only via three-dimensional iteration: /56

1. The temperature to be expected in the particular state is estimated (e.g. $T_1 = T(p,h)$).

2. The corresponding value for the second of the given state variables (e.g. $h_1 = h(p,T_1)$) is determined iteratively for this temperature and one of the given state variables.

3. The estimate T_1 is improved iteratively and item 2 repeated, until the second of the given state variables, too, has been approached within a limit of error (e.g. $h_1 = h$).

The computational process is basically similar for the moist vapor region. The individual state variables must be determined from the associated boundary curve values, however, via the "lever law of phase proportions."

If vapor content x is one of the two known state variables or is estimated as a starting value during the course of an iteration, calculation of the missing variables with the aid of the above boundary curve representations (3.23) takes a relatively simple form:

-- For specification of (p,x), the unknown state variables can be calculated explicitly.

-- Specified (T,x) can be reduced to the case (p,x) by iterative calculation of the associated vapor pressure.

-- For specified combinations (ρ,x) (h,x) and (s,x), the corresponding values ρ_1, h_1 and s_1 are calculated for an initial value T_1 and are fitted to the specified values ρ, h and s by the iterative improvement of T_1. /57

Figs. 3.5, 3.6, 3.7, and 3.1 show the ranges of states of the materials H_2, O_2, N_2 and air represented with the real gas program. In addition, a section of the low-temperature range is plotted in Fig. 3.8 for air. Since calculations must be made for different processes in to the liquid region but the Beattie-Bridgeman equation is unsuitable for representing this range of

states in spite of all correction terms, the liquid region and the wedge between ρ_{crit} and p_{max} was determined with an auxiliary construction.

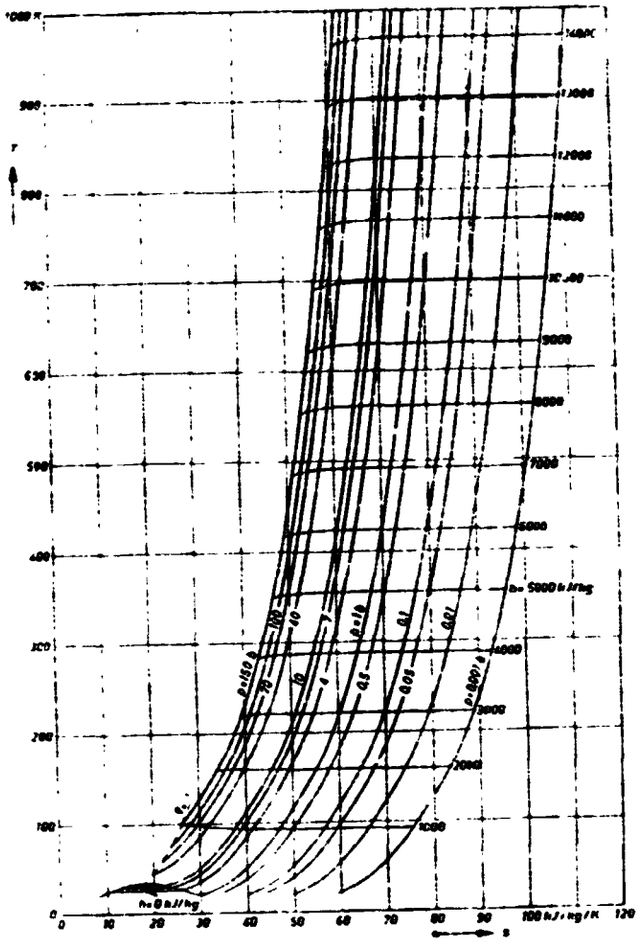

Fig. 3.5. T-s diagram for hydrogen.

All of the T-s diagrams shown were calculated pointwise by the computer (CD 6400) with the program that was written and were plotted automatically with a plotter (Zuse Z-64). It was possible to keep the mean deviation from the values tabulated in [12-16] below 0.1% for the entire range of states represented. The errors are larger only in the immediate vicinity of the critical point. But even there they remain below 2%.

The range of states represented in the real gas program was extended to T = 3000 K for air, taking dissociation into consideration, although the real gas behavior of air in the upper temperature range can also be represented with the combustion gas program, which had to be written anyway. This appeared desirable, however, in order to allow changes of state of air, which can extend from the low-temperature range on into the dissociation range during the course of a variation problem, to be calculated in closed form and without junctions. It was also desirable to need to use only one real gas program if no combustion gas calculations were necessary in certain sub-calculations, as in the study of the oxygen collecting system or in separate intake studies. /62

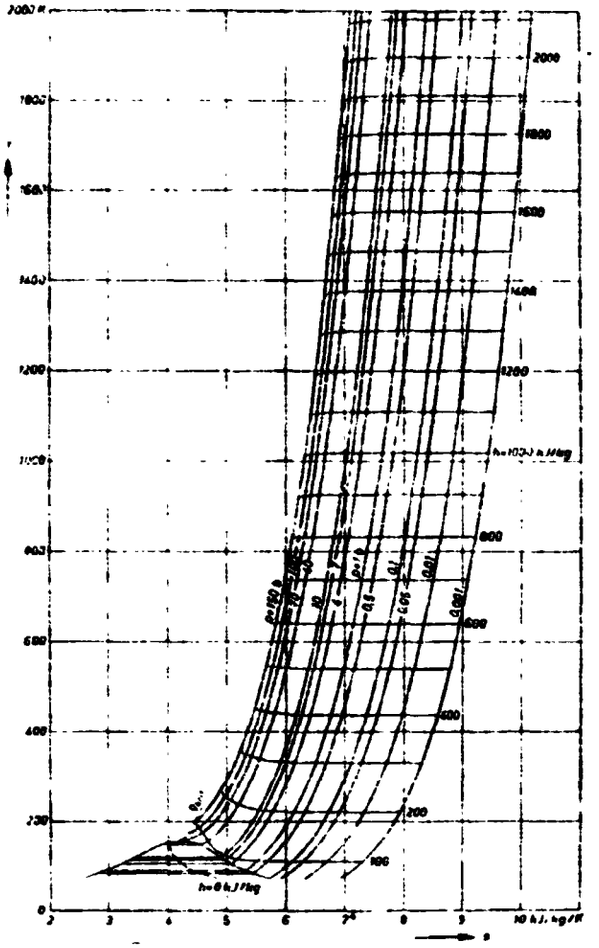

Fig. 3.6. T-s diagram for oxygen.

3.3. Medium-Temperature Range

In the medium-temperature range delimited in Fig. 3.1, the fluids behave like quasi-ideal gases. Their thermal state variables obey the ideal gas equation. The caloric state variables can be determined from so-called "vibrational calculations" with the aid of statistical gas kinetics.

The enthalpy h° and/or the derived caloric quantity c_p° of the ideal gas is required in the real gas program described in Section 3.2. Moreover, since the combustion gas is treated as a mixture of ideal gases for calculating its state variables and thus the caloric quantities h°, c_p° and s° for the individual components are also needed there, their determination from vibrational calculations will be mentioned briefly here.

According to classical statistical mechanics, a molecule may contribute to the internal energy of the gas with the following energies, depending upon the type of degrees of freedom:

1) translational kinetic energy

2) rotational kinetic energy

3) vibrational kinetic and potential energy.

On an average in time and space, according to Boltzmann's equidistribution principle, the same energy is allotted to each degree of freedom of the molecules in a gas at absolute temperature T, namely /63

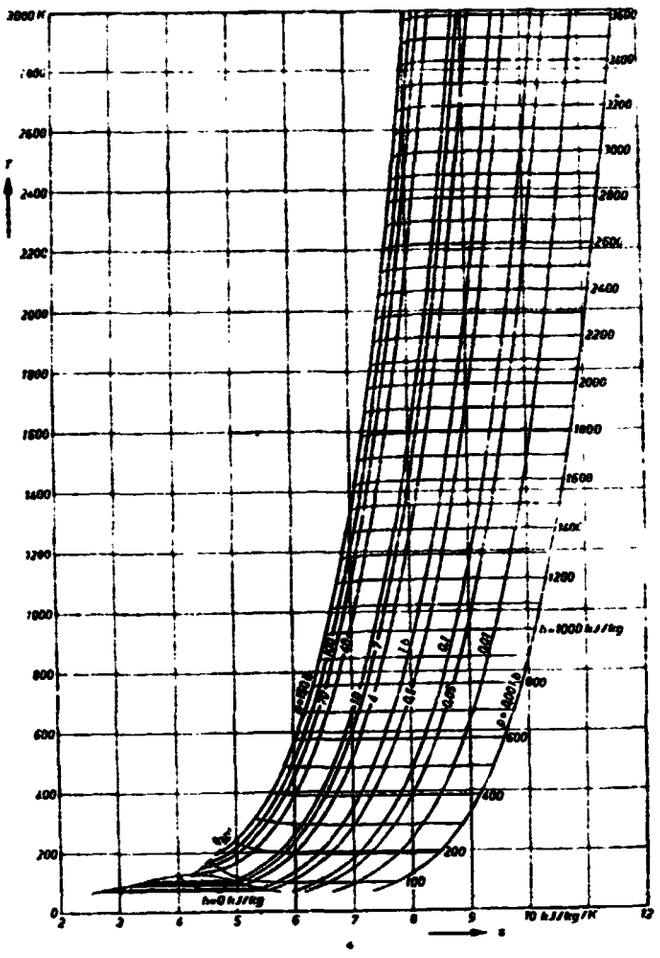

Fig. 3.7. T-s diagram for nitrogen.

$$E_T = E_R = \frac{1}{2} \cdot k \cdot T$$

(translation, rotation)

$$E_S = k \cdot T \quad \text{(vibration)}$$

where k is the Boltzmann constant in [J/molecule/K]. The vibrational component is $2 \cdot ((1/2)kT) = kT$, since both the kinetic and the potential energies of vibration must be taken into consideration. We thus obtain the following for the specific internal energy of an ideal gas:

$$u^\circ = \frac{1}{2} \cdot R \cdot T \cdot (f_T + f_R + 2 \cdot f_S) \quad [J/kg] \qquad (3.24)$$

where f_T, f_R and f_S refer to the number of degrees of freedom for translation, rotation and vibration.

The transition from molecular motion without vibration at low temperatures to motion with completely excited vibrational states is continuous. For the energy of a diatomic gas (harmonic oscillator), for example, we must therefore use the following in place of $E_S = k \cdot T$, according to statistical quantum mechanics:

$$E_S = k \cdot \frac{\vartheta}{e^{\vartheta/T} - 1}$$

where the characteristic vibrational temperature ϑ is defined by

$$\vartheta = h \cdot \nu / k,$$

where h = Planck's constant
ν = eigenfrequency.

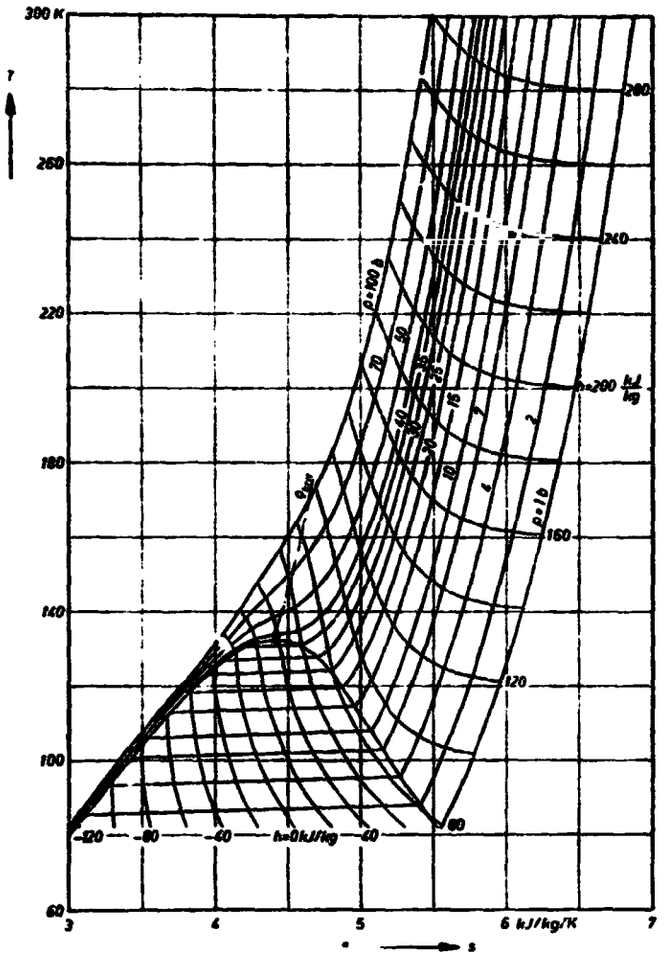

Fig. 3.8. T-s diagram for air (detail).

We thus obtain the following for the specific internal energy of a diatomic gas with three translational degrees of freedom, two rotational degrees of freedom and one vibrational degree of freedom, from Equation (3.24):

$$u^{o} = R \cdot T \cdot \left(\frac{5}{2} + \frac{\Theta/T}{e^{\Theta/T}-1}\right) \quad [J/kg]$$

From the definition of enthalpy: $h = u + p \cdot v$, and from the gas equation, we obtain

$$h^{o} = R \cdot T \cdot \left(\frac{7}{2} + \frac{\Theta/T}{e^{\Theta/T}-1}\right) \quad [J/kg]$$

(3.25)

and for the specific heat of a diatomic gas:

$$c_p^{o} = \frac{7}{2} \cdot R + R \cdot \left(\frac{\Theta/2T}{\sinh(\Theta/2T)}\right)^2 \quad [J/kg/K]$$

(3.26)

The statistical theory of gases consisting of polyatomic molecules is quite similar to that of gases consisting of diatomic molecules; a larger number of degrees of freedom then exist for the individual molecule, however.

The enthalpy of any ideal gas can be calculated as follows:

$$h_o = R \cdot T \cdot \left[\frac{f_T + f_R}{2} + 1 + \sum_{i=1}^{f_S} \frac{\Theta_i/T}{e^{\Theta_i/T}-1}\right] \quad [J/kg] \qquad (3.27)$$

3.4. High-Temperature Range

As vibrational energy increases, the field forces operant between the individual atoms of the molecules eventually are no longer able to keep the molecular unit together. The molecules decompose into smaller components, e.g. /65

$$CO_2 \rightarrow C + O_2 \qquad O_2 \rightarrow 2O$$

Since the energy levels of the individual molecules in a gas are the same for all molecules only on a time and space average, this "dissocation" does not occur suddenly as a given temperature is reached; it extends over a relatively large temperature range. The temperature intervals for the individual decomposition reactions can be shifted toward one another in the process.

In addition to temperature, pressure has a decisive effect on the extent of dissociation. As pressure decreases, the degree of dissociation increases.

In the high-temperature range, the composition of a fluid (e.g. combustion gas) and thus molar mass

$$M = \sum_{j=1}^{n} \nu_j \cdot M_j \ [\text{kg/kmol}] \qquad (3.28)$$

are functions of temperature and pressure. The mole fractions $\nu_j = n_j/n_{ges}$ here give the contributions of the different components "J" in kmoles to each kmole of combustion gas.

Since a dissociated fluid behaves like a mixture of ideal gases, moreover, we have

$$\rho = \frac{p}{R \cdot T} \cdot M(T,p) \qquad (32.9)$$

for the thermal equation of state in this region. The caloric state variables /66

$$h = \sum_{j=1}^{n} \nu_j \cdot h_j \ [\text{J/kmol}] \qquad (3.30)$$

$$s = \sum_{j=1}^{n} \nu_j \cdot s_j \ [\text{J/kmol/K}] \qquad (3.31)$$

can be determined additively from the corresponding values for the individual mixture components only when instantaneous gas composition is known. In the limiting case, this can correspond to the state of chemical equilibrium associated with the instantaneous state specified. In the usual case, it deviates from equilibrium composition, since the latter can be adapted to varying conditions only sluggishly during a change of state, due to the finite reaction velocity. In the case of combustion gases, the deviation is also a consequence of the more or less incomplete combustion.

For the engine designs which are to be analyzed within the scope of this work, combustion gas temperatures occur which reach high into the dissociation range. It was therefore necessary to also determine real gas behavior as exactly as possible in this range of states, since the quantitative validity of the results is largely determined thereby. This applies particularly with regard to the use, justified above, of superstoichiometric fuel/air ratios. A combustion gas program was therefore written with which the input of heat in the combustion chamber and expansions in the turbine and nozzle can be calculated, taking combustion gas composition into consideration in each case.

The mathematical principles on which the program system used /67
to determine combustion gas composition, both in the equilibrium state and in the case of incomplete combustion, and to calculate changes of state in the case of labile or "frozen" chemical equilibrium were based will be outlined in the following sections.

3.41. Equilibrium Composition

Due to the decomposition phenomena described above, a kerosene/air combustion gas, for example, consists of more than the complex composition products CO_2, H_2O, N_2 and excess air (N_2, O_2, Ar, etc.) at high temperatures. In addition to the so-called stoichiometric reactions, a large number of sub-reactions take place parallel to these, e.g.

$$\tfrac{1}{2} H_2 + \tfrac{1}{2} O_2 \rightleftharpoons OH$$

$$\tfrac{1}{2} O_2 \rightleftharpoons O$$

A state of equilibrium is set up between the reactions proceeding in both directions; it is reached when as many units of each reaction product are produced as decompose per unit time. This state of equilibrium shifts toward the more complex components

-- with decreasing molecular and/or atomic energy potential, i.e. with decreasing temperature T,

-- with increasing density at constant temperature, i.e. with increasing p at T = const.

It is described by the equilibrium constants $K_n = f(T,p)$ of the partial reactions. The K_n relate the concentrations of reaction products on one side of the partial reaction equation to the concentrations of reaction products on the other side. The magnitudes of the K_n can be determined from statistical mechanics via the characteristic vibrational 0 temperatures. /68

Combustion gas composition can now be calculated from the relationships for the equilibrium constants and the principle of the conservation of mass.

It is assumed that the combustion gas consists of the following 14 components:

$$O_2,\ N_2,\ H_2,\ C_f,\ O,\ N,\ H,\ C_g,\ NO,\ OH,\ CO,\ H_2O,\ CO_2,\ Ar.$$

The argon component of air (0.93%) does not participate in the reaction. The CO_2 component of air (0.03%) and its remaining components (<0.01%) and the NO_2 and N_2O components of dissociated air can be neglected in the combustion gas calculations. In addition, the dissociation component CN and other insignificant species can be neglected.

The reaction equation thus reads:

$$\sum_{i=1}^{m} m_i\, I \longrightarrow \sum_{j=1}^{n} n_j\, J$$

$$\begin{aligned} m_{Ar}\,Ar + m_{O_2}\,O_2 + m_{N_2}\,N_2 + m_{H_2}\,H_2 + m_{C_f}\,C_f \\ \longrightarrow n_{Ar}\,Ar + n_{O_2}\,O_2 + n_{N_2}\,N_2 + n_{H_2}\,H_2 + n_{C_f}\,C_f \\ + n_O\,O + n_N\,N + n_H\,H + n_{C_g}\,C_g \\ + n_{NO}\,NO + n_{OH}\,OH + n_{CO}\,CO \\ + n_{H_2O}\,H_2O + n_{CO_2}\,CO_2 \end{aligned} \qquad (3.32)$$

where m_i = number of moles or molecules of reactants I, /69
m_j = number of moles or molecules of products J.

The hydrocarbons participating in the reaction can be conceived of as a mixture of solid carbon (graphite) C_f and hydrogen H_2 for the purpose of determining chemical equilibria. The number of moles $n_{C_{10}H_{20}}$ occurring among the product can be neglected.

The fractions of gaseous carbon C_g and of atomic nitrogen N are quite small at the temperatures which occur (T < 3000 K), but have been included because the program system as written was basically to be suitable for calculations up to T = 5000 K. The equations for the nine partial reactions on which calculations were based then read

1. $\frac{1}{2} O_2 \rightleftharpoons O$
2. $\frac{1}{2} N_2 \rightleftharpoons N$
3. $\frac{1}{2} H_2 \rightleftharpoons H$
4. $C_f \rightleftharpoons C_g$
5. $\frac{1}{2} N_2 + \frac{1}{2} O_2 \rightleftharpoons NO$
6. $\frac{1}{2} H_2 + \frac{1}{2} O_2 \rightleftharpoons OH$
7. $C_f + \frac{1}{2} O_2 \rightleftharpoons CO$
8. $H_2 + \frac{1}{2} O_2 \rightleftharpoons H_2O$
9. $C_f + O_2 \rightleftharpoons CO_2$

The equilibrium constant defined by the molar concentrations of the reaction products, required to describe the state of equilibrium of reversible partial reactions, is a function of temperature and pressure: /70

$$K_n = K_n(T,p).$$

It can be calculated easily with "Dalton's law," however, from the equilibrium constant $K_p(T)$ based on partial pressures, which is independent of pressure. Using the change in Gibbs free energy accompanying the partial reaction under consideration, we can formulate this as

$$K_p = e^{-\frac{\Delta \vartheta_T^o}{\mathcal{R} \cdot T}} \qquad (3.33)$$

For the partial reaction

$$H_2 + \frac{1}{2} O_2 \rightleftharpoons H_2O, \qquad K_{p_{H_2O}} = \frac{p_{H_2O}}{p_{H_2} \cdot p_{O_2}^{1/2}}$$

for example, the change in free energy at T = 2000 K here is

$$\Delta \varphi^{\circ}_{2000} = (\varphi^{\circ}_{2000})_{H_2O} - \left[(\varphi^{\circ}_{2000})_{H_2} + \frac{1}{2} \cdot (\varphi^{\circ}_{2000})_{O_2}\right]$$

The values for free energy φ°_T at pressure p = 0 can be determined from statistical mechanics (Section 3.3) using the relationship

$$\varphi^{\circ}_T = h^{\circ}_T - T \cdot s^{\circ}_T$$

In the combustion gas program as written, however, approximate functions presented in [23] were used for this. They are based on the results, confirmed and extended with experimental data, of a comprehensive vibrational calculation which also takes electronic excitation into consideration. /71

We can now use the relation

$$K_{n_j} = K_{p_j} \cdot \left(\frac{n_{ges}}{p}\right)^{\Delta n} \qquad (3.34)$$

to calculate the equilibrium constants K_n based on numbers of moles; in contrast to the K_p, these are a function of pressure.

Δn = Change in the stoichiometric number of gaseous moles in a partial reaction

n_{ges} = Total number of moles of all reaction products, including n_{Ar}

p = Total pressure during the reaction.

For example, conversion yields

$$K_{n_O} = \frac{n_O}{n_{O_2}^{1/2}} = K_{p_O} \cdot \left(\frac{n_{ges}}{p}\right)^{1/2}$$

$$K_{n_{NO}} = \frac{n_{NO}}{n_{N_2}^{1/2} \cdot n_{O_2}^{1/2}} = K_{p_{NO}}$$

$$K_{n_{H_2O}} = \frac{n_{H_2O}}{n_{H_2}^{1/2} \cdot n_{O_2}^{1/2}} = K_{p_{H_2O}} \cdot \left(\frac{n_{ges}}{p}\right)^{-1/2} \qquad \text{/72}$$

Since only the gaseous components contribute to total pressure $p = \Sigma p_i$, however,

$$K_{n_{CO_2}} = \frac{n_{CO_2}}{n_{C_f} \cdot n_{O_2}} = K_{p_{CO_2}} = \frac{p_{CO_2}}{p_{O_2}}$$

applies to partial reaction 9, for example. The total number of moles n_{ges} is not yet known. For the time being, it can only be estimated from the "complex" reaction equation (reaction products: H_2O, CO_2 and excess fuel or oxidizer):

$$m_{O_2} O_2 + m_{N_2} N_2 + m_{H_2} H_2 + m_{C_f} C_f \longrightarrow$$

$$n'_{O_2} O_2 + n'_{N_2} N_2 + n'_{H_2} H_2 + n'_{C_f} C_f + n'_{H_2O} H_2O + n'_{CO_2} CO_2$$

1. In a reaction with excess oxygen ($m_{O_2} > 1/2\ m_{H_2} + m_{C_f}$), $n'_{H_2} = 0$ and $n'_{C_f} = 0$. The total number of moles of the six complex reaction products is then calculated to be

$$\begin{aligned} n'_{ges_1} &= n'_{O_2} + n'_{N_2} + n'_{H_2O} + n'_{CO_2} \\ &= \left[m_{O_2} - \left(\tfrac{1}{2} m_{H_2} + m_{C_f}\right) \right] + m_{N_2} + m_{H_2} + m_{C_f} \qquad (3.35) \\ n'_{ges_1} &= m_{O_2} + m_{N_2} + \tfrac{1}{2} m_{H_2} \end{aligned}$$

2. In a reaction with insufficient oxygen ($m_{C_f} < m_{O_2} < 1/2\ m_{H_2} + m_{C_f}$), we set $n'_{O_2} = 0$ and $n'_{C_f} = 0$:

$$
\begin{aligned}
n'_{ges_2} &= n'_{N_2} + n'_{H_2} + n'_{H_2O} + n'_{CO_2} \\
&= m_{N_2} + \left[m_{H_2} - 2(m_{O_2} - m_{C_f}) \right] + 2(m_{O_2} - m_{C_f}) + m_{C_f} \qquad (3.36) \\
n'_{ges_2} &= m_{N_2} + m_{H_2} + m_{C_f}
\end{aligned}
$$

A reaction with $m_{O_2} < m_{C_f}$ can be neglected.

The provisional value for the total number of moles n_{ges} so determined must be improved later by several iterations of the entire computational process.

With the equilibrium constants K_{n_j} now known, we can formulate nine equations for calculating the 14 unknown numbers of moles n_j, e.g.:

$$
\begin{aligned}
n_O &= K_{n_O} \cdot n_{O_2}^{1/2} \\
n_{NO} &= K_{n_{NO}} \cdot n_{N_2}^{1/2} \cdot n_{O_2}^{1/2} \\
n_{H_2O} &= K_{n_{H_2O}} \cdot n_{H_2} \cdot n_{O_2}^{1/2}
\end{aligned}
$$

The condition of equal number of atoms before and after reaction (conservation of mass) provides five additional equations for calculating the n_j:

/74

$$
\begin{aligned}
m_{Ar} &= n_{Ar} \\
2m_{O_2} &= 2n_{O_2} + n_O + n_{NO} + n_{OH} + n_{CO} + n_{H_2O} + 2n_{CO_2} \\
2m_{N_2} &= 2n_{N_2} + n_N + n_{NO} \\
2m_{H_2} &= 2n_{H_2} + n_H + n_{OH} + 2n_{H_2O} \\
m_{C_f} &= n_{C_f} + n_C + n_{CO} + n_{CO_2}
\end{aligned}
$$

The nonlinear system consisting of 14 equations allows determination of the 14 unknown numbers of moles n_j of the components contained in the reaction product for given temperature and pressure values, as well as the composition m_i of the reactants occurring in equation (3.32). If the total number of moles

$$
n_{ges} = \sum_{j=1}^{14} n_j
$$

deviates from the value n'_{ges} estimated with equation (3.35) or equation (3.36), the equilibrium constants K_{n_j} must be corrected with the value determined for n_{ges} and the system of equations solved again.

The molar components ν_j of the individual product components are obtained from the relationship

$$\nu_j = \frac{n_j}{n_{ges}}$$

The solution to the system of nonlinear equations is not unique. If it is based, for example, on the implicit calculation of n_{H_2}, various values n_{H_2} exist for which the system is satisfied.

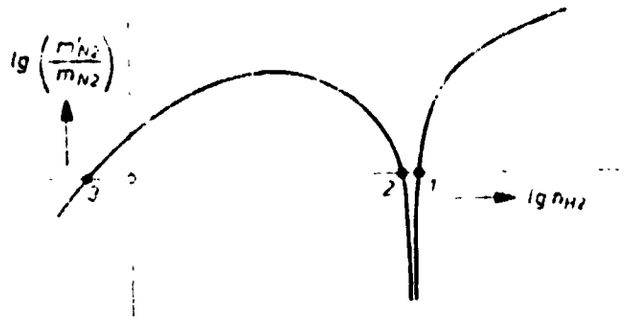

Fig. 3.9. Solutions to the system of equations for combustion gas composition.

At all three labeled points (Fig. 3.9), for example, the number of moles of N_2, m'_{N_2}, required mathematically, agrees with the number of moles n_{N_2} actually fed to the reaction. However, x-intercepts 2 and 3 are extraneous solutions. Either the slope $\delta m'_{N_2}/\delta n_{H_2}$ has a physically incorrect sign, or numbers of moles occur for individual components which are negative or exhibit higher values on the product side than on the reactant side. /75

In order to always obtain a reliable solution, the following approach was therefore used in writing the program for determining combustion gas composition:

1. The numbers of moles m_{Ar}, m_{O_2}, m_{N_2}, m_{H_2}, m_{C_f} (see equation (3.32)) fed to the reaction per kg $\dot{m}_{Ox}$ can be calculated from the known molar composition of the fuel source $\dot{m}_B$ (e.g. kerosene) and the oxygen source $\dot{m}_{Ox}$ (e.g. air) and from their mass ratio $\beta = \dot{m}_B/\dot{m}_{Ox}$. /76

2. The total number of moles of products n'_{ges} is estimated on the basis of equation (3.35) or (3.36).

3. The equilibrium constants $K_n(T,p)$ for the nine partial reactions can now be calculated with equation (3.34) from the constants $K_p(T)$ determined previously with equation (3.33).

4. The number of moles n_{H_2} is estimated with a suitable formula, and the provisional mole number $n'_{O_2} = f(n_{H_2},...)$ is determined from the corresponding equilibrium conditions and the balance of mass for hydrogen atoms. If n'_{O_2} lies between the physically possible boundaries for n_{O_2}, computation can continue. Otherwise, a value is picked for n'_{O_2} and the associated n_{H_2} determined by iteration. The first and second partial derivatives of N_{O_2} with respect to n_{H_2} are required here to make the second-order Newton's method converge rapidly.

5. The provisional value $n'_{C_f} = f(n_{H_2},n'_{O_2},...)$ can now be calculated from the balance of masses for m_{C_f} and the equilibrium conditions. If it lies outside physically possible limits, the method described in item 4 is also used here. The same applies to the corresponding determination of $n'_{N_2} = f(n_{H_2},n'_{O_2}, n'_{C_f},...)$, based on the balance of mass for m_{O_2}.

6. Finally, the number of moles m'_{N_2} needed on the reactant side, associated with the estimate n_{H_2} and the resultant values n'_{O_2}, n'_{C_f} and n'_{N_2} can be determined from the balance of masses for nitrogen. If it deviates a greater amount from number of moles n_{N_2} actually fed to the reaction than permitted by the relative limit of error specified as $\varepsilon = 0.5 \cdot 10^{-3}$, n_{H_2} is corrected by the above-mentioned iteration method, and steps 4, 5 and 6 are repeated. Since the physically meaningless solutions are already eliminated at the earliest point during each intermediate step in the computation process, the method describes converges very rapidly to the one meaningful solution to the system of equations. /77

7. The numbers of moles still missing can now be determined easily from the equilibrium relationships and the computation process continued as describes above.

Program BGZ, in which combustion gas composition is determined, is based on reaction equation (3.32). The fuel may be any hydrocarbon or even pure hydrogen. During the course of the study, calculations were made for kerosene (represented by $C_{10}H_{20}$), octane (C_8H_{18}), methane (CH_4) and hydrogen (H_2). Air, oxygen or air enriched with additional oxygen was used as the oxidizer here.

The numbers of moles of the specified reactants are compiled in a block of constants which can be expanded for any other C,H,O,N,Ar systems. They are always referred to 1 kmole of fuel source.

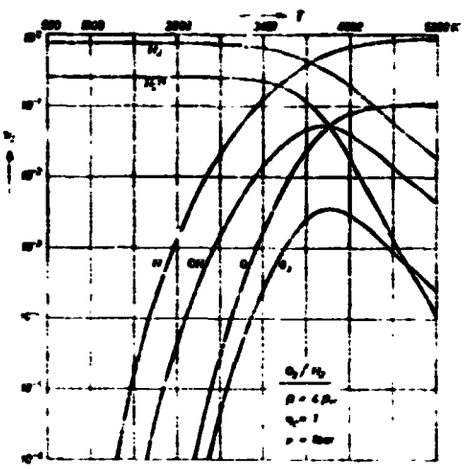

Fig. 3.10. Molar equilibrium composition of O_2/H_2 combustion gas.

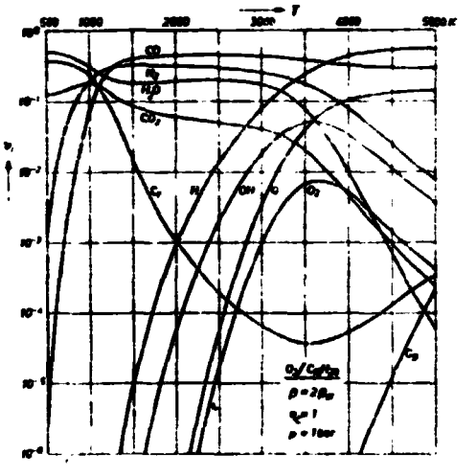

Fig. 3.11. Molar equilibrium composition of O_2/ /kerosene combustion gases.

Test runs showed that the following ranges of variation are reliably covered by the program for the combinations mentioned: /80

$$300\ \text{K} < T < 5000\ \text{K}$$
$$0{,}001\ \text{bar} < p < 1000\ \text{bar}$$
$$0{,}001 \cdot \beta_{st} < \beta < 20 \cdot \beta_{st}$$

where

$$\beta = \dot{m}_{fuel}/\dot{m}_{oxidizer},$$

and β_{st} is the corresponding stoichiometric ratio.

Equilibrium compositions of the systems

O_2 / H_2

O_2 / kerosene

air / H_2

air / kerosene

are shown in Figs. 3.10 through 3.13 as examples for a pressure of p = 1 bar and characteristic β values.

3.42. Combustion Gas Composition in the Case of Incomplete Combustion

The following assumption appears reasonable for taking incomplete combustion into consideration mathematically:

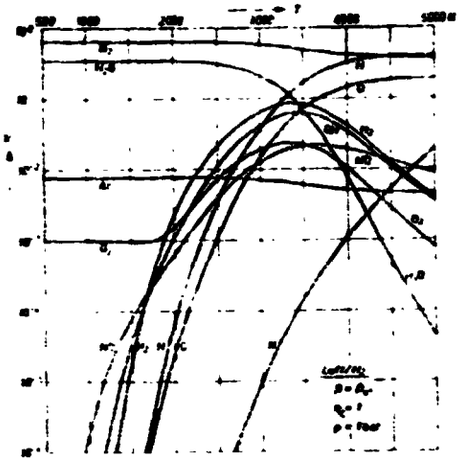

Fig. 3.12. Molar equilibrium composition of air/H_2 combustion gas [Luft = air].

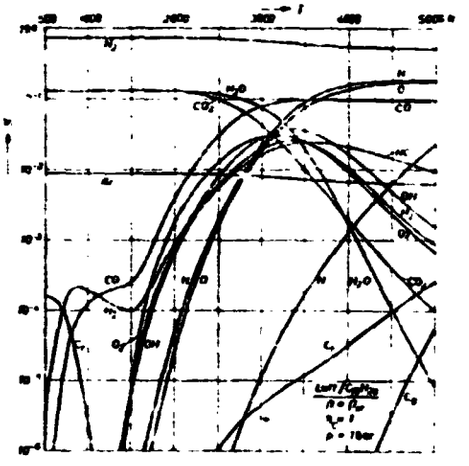

Fig. 3.13. Molar equilibrium composition of air/kerosene combustion gas [Luft = air].

In the case of incomplete combustion, a portion of the fuel fed in leaves the combustion chamber again unconsumed, without having participated in the reaction. This component is to be covered by a combustion efficiency or degree of burnup /81

$$\eta_C = \frac{\text{fuel involved in reaction}}{\text{fuel fed to reaction}} .$$

We can of course define a combustion efficiency differently. But the definition given appears meaningful particularly with regard to air-breathing engine applications.

Only the fuel fraction $\eta_C \cdot (m_{H_2}H_2 + m_{C_f}C_f)$ need be assigned a value in equation (3.32) in order to determine the "equilibrium composition" of the combustion gas. The fraction $(1 - \eta_C) \cdot (m_{H_2}H_2 + m_{C_f}C_f)$ does not participate in the reaction, but it can be assumed that it dissociates at the prevailing final combustion temperature into the components $n'_{H_2}H_2 + n'_H H + n'_{C_f}C_f + n'_{C_g}C_g$.

If we assume that this dissociation reaction is in equilibrium itself, we can calculate the numbers of moles n'_{H_2}, n'_H, n'_{C_f} and n'_{C_g}:

$$(1-\eta_C)\cdot m_{H_2}\,H_2 \longrightarrow n'_{H_2}\,H_2 + n'_H\,H = n'_{H_2}\,H_2 + K_{n_H}\cdot n_{H_2}^{'\,1/2}\,H$$

$$2\cdot(1-\eta_C)\cdot m_{H_2} = 2\cdot n'_{H_2} + K_{n_H}\cdot n_{H_2}^{'\,1/2}$$

$$n_{H_2}^{'\,1/2} = -K_{n_H}/4 \pm \sqrt{K_{n_H}^2/16 + (1-\eta_C)\cdot m_{H_2}}$$

Since the negative sign is eliminated from the root, /82

$$n'_{H_2} = \left(\sqrt{K_{n_H}^2/16 + (1-\eta_C)\cdot m_{H_2}} - K_{n_H}/4\right)^2 \qquad (3.37)$$

and $n'_H = K_{n_H} \cdot n'^{1/2}_{H_2}$

Moreover,

$$(1-\eta_C)\cdot m_{C_f} C_f \longrightarrow n'_{C_f} C_f + n'_{C_g} C_g = n'_{C_f} C_f + K_{nC_g} \cdot n'_{C_f} C_g$$

$$(1-\eta_C)\cdot m_{C_f} = n'_{C_f} \cdot (1 + K_{nC_g})$$

$$n'_{C_f} = (1-\eta_C)\cdot m_{C_f}/(1+K_{nC_g}) \qquad (3.38)$$

and

$$n'_{C_g} = K_{nC_g} \cdot n'_{C_f}$$

The numbers of moles n'_{H_2}, n'_H, n'_{C_f} and n'_{C_g} so calculated must be added to the molar numbers n_{H_2}, n_H, n_{C_f} and n_{C_g} determined from the reaction equation with $\eta_C \cdot (m_{H_2}H_2 + m_{C_f}C_f)$.

In the case of incomplete combustion, the reaction system described can of course no longer be in equilibrium, although the two subsystems, i.e. the system consisting of the fuel component $\eta_C \cdot \dot{m}_B$ involved in the reaction and the oxidizer and the system consisting of the unconsumed fraction of fuel $(1 - \eta_C)\cdot\dot{m}_B$, are in themselves each in equilibrium. An interaction between the two systems is possible only via the total number of molecules n_{ges}, which affects the size of the equilibrium constants K_{n_j} based on the molar numbers as per equation (3.34).

Fig. 3.14 shows molar composition for an air/kerosene combustion gas in the technically important range of 1000 K < T < < 3500 K for p = 1 bar. /83

Combustion efficiency is $\eta_C = 0.95$ at the stoichiometric fuel/air ratio. A comparison with Fig. 3.13 clearly shows the effect of incomplete combustion on combustion gas composition.

3.43. Final Combustion Temperature

The combustion temperature of a chemical reaction can be easily determined from the principle of the conservation of energy. The sum of chemical energy potential and total enthalpy of a

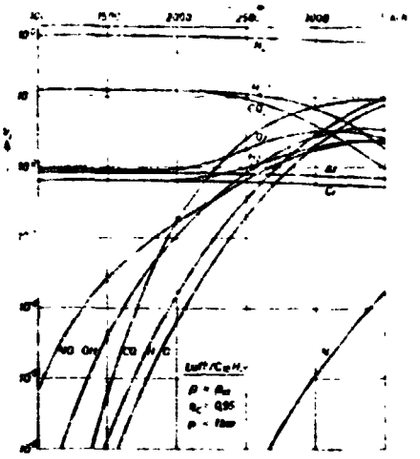

Fig. 3.14. Molar composition of air/kerosene combustion gas in the case of incomplete combustion [Luft = air].

fluid must be the same before and after an adiabatic reaction:

$$\sum_{i=1}^{m} n_i \cdot \left[(\varepsilon_i + \zeta_i)_{T_{CE}} + m_i \cdot \frac{c_{CE}^2}{2} \right] = \sum_{j=1}^{n} n_j \cdot \left[(\varepsilon_j + \zeta_j)_{T_{CA}} + m_j \cdot \frac{c_{CA}^2}{2} \right] \quad (3.39)$$

/84

where T_{CE} = temperature at combustion chamber inlet
T_{CA} = temperature at combustion chamber outlet.

The required statistical total energy values $(\varepsilon_i + \zeta_i)$ of the individual components can be calculated immediately for the temperature range 300 K < T < < 5000 K with the functions for H_T given in [23]:

$$(\varepsilon_i + \zeta_i)_T = H_{Ti}^{\circ}.$$

They again apply to quasi-ideal gases. If the reactants are fed into the combustion chamber at temperatures T_{CE} < 300 K, this must be taken into consideration with an additional term. If they lie within the liquid phase, heat of vaporization must be included in the calculations.

The program as written was based on the general case of adiabatic combustion. It is immaterial here whether the additional energy flux consists of a flow of heat through the wall or whether mechanical energy is introduced via the system boundaries.

Once the total energy per kg combustion gas at the combustion chamber inlet has been determined for a given β, the expected final combustion temperature T_{CA} is estimated and the combustion gas composition determined for this. In a separate subprogram HBRENGA, the associated total energy is calculated in J/kg and is calculated with total energy at the combustion chamber inlet, taking the adiabatic energy flow into consideration. T_{CA} must now be corrected until the conservation of energy is satisfied.

The method of tangents was used for the rapid convergence of iteration. In order to determine tangent slope, it is now necessary to also calculate combustion gas composition and total

/85

energy in case for a nearby temperature value. Although combustion gas composition must thus be determined twice for each iteration step, the total computer time required (CD 6400) to determine combustion temperature for the most expensive combustion gas system (air/kerosene) averages only about 0.3 sec. The error permitted is less than 1 K.

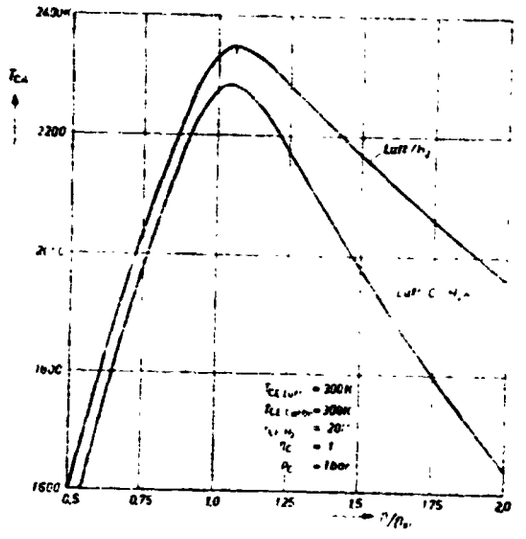

Fig. 3.15. Final adiabatic combustion temperatures of air/kerosene and air/LH_2 [Luft = air].

Fig. 3.15 shows the final combustion temperatures which can be reached in the adiabatic combustion of kerosene ($C_{10}H_{20}$) and of liquid hydrogen (LH_2) with air in approximately ambient conditions ($\eta_C = 1$). The curves are plotted over the relative fuel/air ratio $\beta/\beta_{st} = \dot{m}_B/\dot{m}_{Bst}$. /86

The effect of combustion chamber pressure on T_{CA} can be seen from Fig. 3.16. The final combustion temperatures which can occur in the combustion chamber of a ramjet engine heated with hydrogen at a flight Mach number of about $M_\infty = 5$ are shown here as a function of fuel/air ratio, with combustion chamber pressure as the parameter. The same temperature values will also occur under the same conditions in the afterburner chambers of turbojets with or without precooling. /87

A comparison with Fig. 3.15 shows that the fuel/air ratio at which maximum final combustion temperature is reached at $p_C = 1$ has shifted toward higher values of β. This is caused by the higher degree of dissociation, which is a consequence of the increased combustion chamber inlet temperature T_{CE}. For the same reason, the maxima in the curves shift towards higher β with decreasing pressure.

Fig. 3.17, when compared with Fig. 3.16, shows the effect of the degree of burnup η_C on the location of the temperature maximum. While this occurred at about 1.12 times the stoichiometric fuel/air ratio for $p_C = 1$ bar and $\eta_C = 1$ (Fig. 3.16), it has shifted to $\beta/\beta_{st} \approx 1.15$ for $\eta_C = 0.95$. In addition, it can be seen from Fig. 3.17 that jet exhaust velocity c_D only reaches its maximum at a considerably higher fuel/air ratio. This is primarily caused by the fact that the molar mass m of the combustion gas decreases with increasing fuel fraction and that

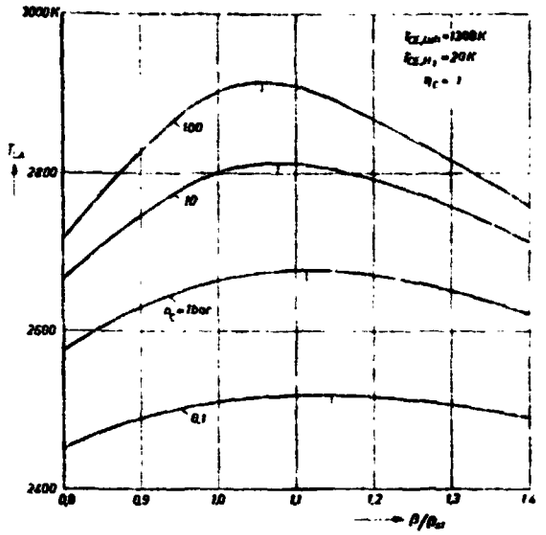

Fig. 3.16. Final combustion temperatures of air/LH_2 at $M_\infty \approx 5$ and $\eta_C = 1$ [Luft = air].

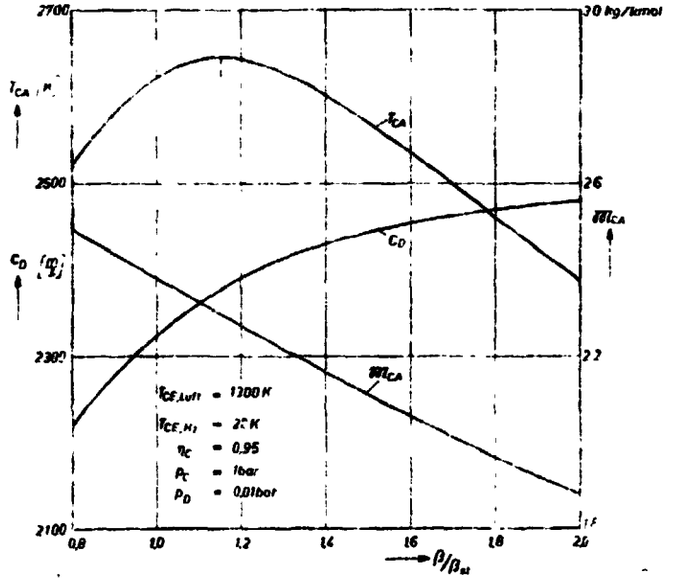

Fig. 3.17. Effect of fuel/air ratio on final combustion temperature, molar mass and jet exhaust velocity at $M_\infty \approx 5$ and $\eta_C = 0.95$ [Luft = air].

$c \sim \sqrt{T_{CA}/m_{CA}}$ applies approximately. In the case at hand, jet exhaust velocity was determined under the specified conditions and under the assumption of lossless expansion to an ambient pressure $p_\infty = 0.01$ bar ($H_\infty \approx 30$ km) with a "frozen" combustion gas composition.

3.44. Changes of State in Combustion Gases of "Frozen" Composition or in Labile Chemical Equilibrium

/88

During each change of state in a combustion gas, the conditions for chemical equilibrium between the individual components change. This results in a change in gas composition. Since this only proceeds at finite velocities, chemical equilibrium can be maintained only /89 during an infinitely slow change of state. Gas composition remains unchanged during a change of state, on the other hand, if the latter takes place suddenly. At each point, it corresponds to the state of equilibrium or disequilibrium (e.g. $\eta_C < 1$) existent prior to the change of state.

Between the limiting cases in these two conceptual models:

-- labile chemical equilibrium

-- "frozen" combustion gas composition

lies the actual path of a change of state. The higher the reaction velocities of the partial reactions controlling the state of equilibrium and the lower the rate at which the conditions for each state of equilibrium change, i.e. the slower the change of state proceeds, the closer this path approaches that associated with labile chemical equilibrium.

The actual path can be determined only with a high computational outlay if reaction kinetics (relaxation) are taken into consideration. For changes of state in the combustion gas, e.g., in the turbine, the mixing chamber or the thrust nozzle, it is therefore replaced in this work by the conceptual model which is expected to approximate it best. The Bray criterion [31] is used for this purpose for expansion in the nozzle.

The computational process used to calculate a change of state for a "frozen" composition will be described briefly using the example of the imagined change of state between a static state and the associated overall state. Combustion gas composition is actually the same in both states for this case.

According to the Second Law, /90

$$ds = \frac{dh}{T} - R \cdot \frac{dp}{p}$$

Integration yields

$$s = s^{\circ}(T) - R \cdot \ln p. \qquad (3.40)$$

Because $s \overset{!}{=} s_t$, we obtain

$$s^{\circ}(T) - \frac{\alpha}{m} \cdot \ln p = s^{\circ}(T_t) - \frac{\alpha}{m_t} \cdot \ln p_t$$

Since the compositions and thus the molar masses are the same in both states, we have

$$R \cdot \ln \frac{p_t}{p} = s^{\circ}_{T_t} - s^{\circ}_{T}$$

With equation (3.31), then,

$$\ln \frac{p_t}{p} = \frac{1}{R} \cdot \sum_{j=1}^{n} \nu_j \cdot (\mathcal{S}^{\circ}_{T_t} - \mathcal{S}^{\circ}_{T})_j \qquad (3.41)$$

The values $\mathcal{S}^{\circ}_{T,j}$ for molar entropies at a reference pressure p° can be determined from the vibrational calculations or from the functions given in [23].

If T, T_t and p were given, total pressure p_t can be determined from equation (3.41). However, each of the three other state variables can also be calculated by internal iteration with the subroutine /91

ISENTE (I,T,TT,P,PT).

When it is called, I = 1,...4 indicates which state variable is unknown.

A separate subroutine

EXPAN (I,J,T2,T1,P2,P1,ETA)

was developed for the frequently required calculation of an expansion involving losses (e.g. in the turbine or in the thrust nozzle), to be represented optionally by the two limiting cases of "frozen" composition or labile chemical equilibrium. The parameter I again indicates whether temperature T_2 or pressure p_2 is being sought for expansion end point 2. Parameter J indicates whether expansion is to occur at a "frozen" composition or in labile chemical equilibrium or disequilibrium. For the latter case, provision is also made that the degree of burnup n_C also changes during expansion. Thus an application can be represented in which "combustion" is prolonged into the convergent portion of a nozzle. ETA is used to indicate the static/polytropic efficiency of expansion.

The entropy values for the individual states required during computation are determined in subroutine SBRENGA from an evaluation of the relation

$$\mathcal{S}_T = \sum_{j=1}^{n} \nu_j (\mathcal{S}^{\circ}_{T,j} - R \cdot \ln \nu_j) - R \cdot \ln p, \qquad (3.42)$$

which can be expanded from equation (3.40) making use of equation (3.31) with $p_j = p \cdot \nu_j$.

We thus have the working material which we need to characterize the real gas behavior of the fluids involved in the low-temperature range and in the high-temperature range. /92

4. Special Requirements Placed on Individual Structural Components and the Computational Methods Used /93

A comparison of the performances of air-breathing engines for the high flight Mach number range must be based on calculations made with the most realistic possible assumptions and computational methods, since the danger of a completely distorted picture can otherwise easily arise. This is particularly true if the performance data obtained are to serve as the basis for optimizing and comparing booster systems equipped with different types of engine designs.

In addition to the real gas behavior of the working fluids, information on the instantaneous characteristic properties of all structural components, particularly their operating behavior, and the boundary conditions, also taking technical feasibility into consideration, must be accessible to the computer.

4.1. Intake

The supersonic intake of an air-breathing jet engine is a relatively simple structural component if it is designed only for low flight Mach numbers and can be configured with a fixed geometry. Even just for the Concorde airliner, which is designed for a flight Mach number of $M_{\infty AP} = 2.2$, however, an involved inlet design was required in order that a reasonable total pressure drop in the internal flow and a low drag in the external flow could be achieved in any operating state. In addition to possibilities for varying throat cross section A_H and the angle of attack δ of deflecting surfaces, the inlet, which was best designed in planar form, requires a sensitively reacting control system that always guarantees approximately optimum operation. /94

4.11. Special Requirements and Configuration

The special requirements which arise in the upcoming design of a supersonic intake for the air-breathing engine in a space vehicle carrier result primarily from the unconventionally high maximum flight Mach number.

Due to the magnitude of the stagnation temperatures which occur, the intake must be of heat resistant material and must also be cooled in the areas of the throat cross section and the entire subsonic section above about $M_\infty = 5$. The fuel, required anyway,

is available as a coolant, but an ablative system is generally also conceivable for special use in accelerated flight.

While the drag of the missile and thus the necessary minimum thrust is proportional to $\rho_\infty \cdot c_\infty^2 \cdot$ const as a first approximation beyond about $M_\infty = 2$, the flow of air $\dot{m}_L$ which reaches the intake in "freestream tube" A_∞ varies only proportionally to $\rho_\infty \cdot c_\infty$. Thus as M_∞ increases, a larger and larger "freestream tube" A_∞ must enter the intake to provide the flow of air needed to generate the necessary thrust, particularly because specific thrust $f/\dot{m}_L$ generally decreases with increasing flight Mach number.

Maximum flight Mach number M_∞ therefore normally determines the size of geometric scoop cross section A_E for the intake, as well as the smallest constriction ratio A_H/A_E for the convergent supersonic section. While the required scoop cross section A_E decisively affects the size of the overall engine negatively, the pronounced contraction of throat cross section A_H in conjunction with the boundary layers running along the central body can cause unstable flow behavior at high flight Mach numbers. /95

The pronounced reduction of throat cross section also causes an extreme ratio of divergence for the subsonic diffuser. It has therefore been assumed for the calculations that flow separates with retardation to below $M_{1E} = 0.2$ in the last diffuser section.

Moreover, the occurrence of unavoidably high overall pressure drops accompanying the retardation of supersonic flow can be considered an important consequence of the high maximum flight Mach number M_∞, which incidentally need not be identical to the Mach number M_O of oncoming flow at the intake. Fig. 4.1 shows the maximum overall pressure ratios p_{t1b}/p_{to} which can be reached in the supersonic part of a planar intake with various shock wave configurations, as a function of the Mach number M_O of oncoming flow.

Overall pressure drop can be considerably reduced by an increase in the number of shock waves. The distribution of retardation over the largest possible number of low-loss shock waves leads to a special shape for the isentropic intake here ($n = \infty$), whose field of flow represents the reverse of Prandtl-Meyer flow. The pressure ratios were determined by a method described by K. Oswatitisch [24] for plane flow, under the assumption that retardation is optimally distributed in each case among the individual shock waves, i.e. that the optimum shock wave and lip angles are present for each oncoming flow Mach number M_O. With a fixed intake geometry, however, the associated maximum overall pressure ratio can be achieved only for one design Mach number of oncoming flow. /96

The angle of optimum overall deflection δ_{opt} can be taken from Fig. 4.2 for various numbers of shock waves. The greater total

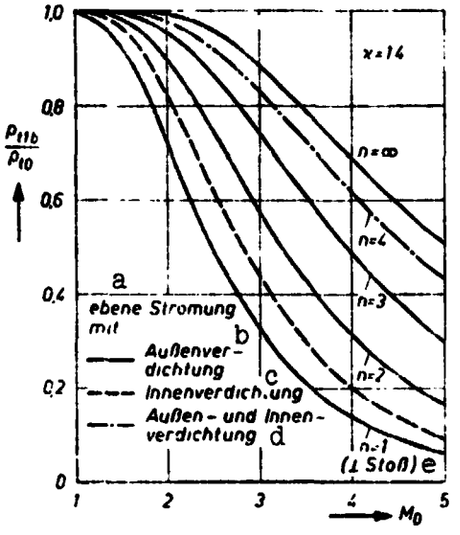

Fig. 4.1. Maximum overall pressure ratio for planar supersonic intakes.

Key: a. Plane flow with: b. External compression; c. Internal compression; d. External and internal compression; e. Shock wave

deflection is, the lower the loss associated with the final perpendicular shock wave at constant flight Mach number. The angle of attack of the cowling edge also increases with deflection, however, so the oblique shock wave generated on it ultimately separates in the external flow, forms a perpendicular shock wave in front of the intake, and destroys the shock wave system. In the case of pure external compression, a maximum angle of deflection δ_{max} may therefore not be exceeded. /97

A retardation of flow in oblique compression waves exceeding this limit can be achieved only through a combination of external and internal compression. Here, internal flow is deflected again in a primarily axial direction, e.g. in the last oblique shock wave, which propagates from the cowling edge, as a result of which the cowling angle is markedly reduced (lower drawing, Fig. 4.2).

The configuration of a plane four-shock-wave intake with combined external and internal compression appears to be particularly suitable for the application under consideration. Due to the size of the range of flight Mach numbers covered, it is necessary here to make not only throat cross section A_H but also the lip angles of the deflecting surfaces adjustable. Only in this way can the intake operate with the most favorable values for overall pressure ratio p_{t1b}/p_{to} under each of the various operating conditions. /98

The plane configuration makes it possible to achieve adjustability with a relatively small outlay in design. The advantage of the rotationally symmetrical intake, providing a slightly higher overall pressure ratio under equivalent conditions, falls off with increasing number of shock waves and is insigificant in the case at hand. In contrast, the undesirable effect of the lateral boundary walls is more important in the plane configuration. On the other hand, rotationally symmetrical intakes cannot be mounted side by side because of the interference effect of their shock wave systems, for which reason they usually cannot be used in multijet high-speed vehicles.

A decisive special requirement to be placed on the intake used arose from the fact that the throughflow behavior of the turbo

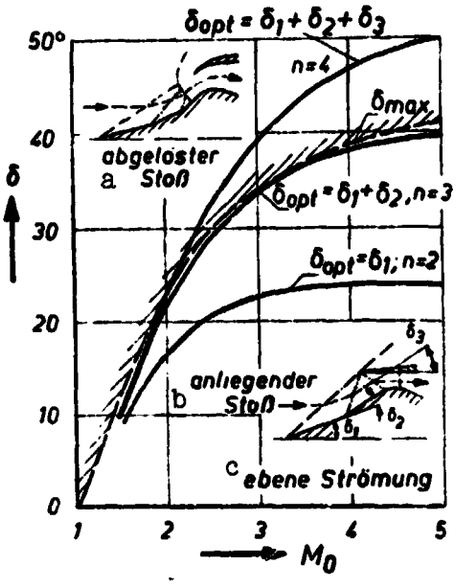

Fig. 4.2. Optimum and maximum angles of deflection.

Key: a. Separated shock wave; b. Adhering shock wave; c. Plane flow

engine designs to be studied differs quite considerably from that of the intake with increasing flight Mach number. This is particularly true of turbo engines with precooling in which the ratio of coolant flow to airflow assumes higher and higher values with increasing flight Mach number, due to combustion with an increasing excess of fuel. While the ramjet -- except in the transonic flight Mach number range -- can always be fed the stream of air which the intake provides, the use of turbojets makes it necessary to match the airflow which is taken in to the air requirements of the engines. This matching is made problematical by the fact that it often cannot be achieved without an increase in intake drag or in overall pressure drops in internal flow. A suitable compromise must then be sought. /99

4.12. Possible Matching Methods, Operating Behavior, Drag

In order for the highest engine efficiency to be achieved, the intake must be tuned to the engine in such a manner that it operates close to its optimum conditions throughout the flight Mach number range covered and in the important engine load states with regard to total pressure drop and drag. The mass flow provided by the intake in each case during so-called "critical" operation -- perpendicular shock wave in narrowest cross section A_H -- must correspond as much as possible to the air requirements of the engine.

Matching an intake of fixed geometry to the air requirements of the engine at maximum oncoming flow Mach number M_{Omax} generally has the consequence that a more or less pronounced shortage of air occurs at all lower oncoming flow Mach numbers, depending upon lip angle and the design characteristic of the compressor. "Supercritical" operation of the intake -- perpendicular shock wave sucked into the divergent section of the subsonic diffuser -- with a correspondingly reduced overall pressure ratio would be the necessary results of such a desig..

The extent to which these matching problems can be eliminated by an axial shift in the central body and/or by variation of the lip angles has already been shown in detail in a previous publication [38]. /100

The effect of shifting the central body on the intake's throughflow behavior was demonstrated using the example of a design for a two-shock intake for a turbojet engine with afterburning. The engine characteristic (upper solid curve), which gives the air requirements of the engine as a function of flight Mach number, is shown in Fig. 4.3.

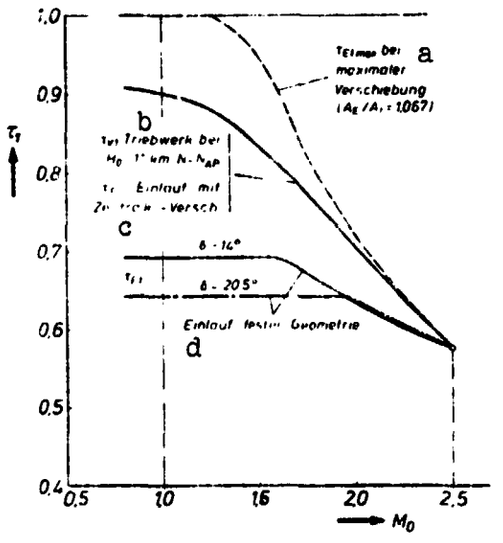

Fig. 4.3. Effect of central body displacement on the throughflow behavior of a two-shock intake.

Key: a. With maximum displacement; b. Engine at ...; c. Intake with central body shifted; d. Intake with fixed geometry

If the intake were designed with a fixed geometry for an oncoming flow Mach number of $M_0 = 2.5$ with the associated optimum lip angle $\delta_{opt} = 20.5°$, the intake characteristic shown in the diagram as a curve of dashes and dots would be obtained, showing the throughflow behavior of the intake in critical operation. The solid curve is the corresponding characteristic of an intake that is also matched to the engine for $M_0 = 2.5$ but whose lip angle represents a compromise value at $\delta = 14°$. Consideration was given in its selection to the fact that the optimum lip angles assume smaller values below $M_0 = 2.5$ and, moreover, the drag of the intake cowling increases with increasing lip angle. /101

Shifting the central body completely covers the air requirements of the engine while retaining the intake's critical operation. If the central body were always shifted far enough with decreasing oncoming flow Mach number that the oblique shock wave is tangent to the lip of the cowling, the dashed curve would be obtained for the relative mass flow delivered by the intake in critical operation.

The curve of total pressure ratio p_{t1}/p_{t0} for the intake with a lip angle of $\delta = 14°$ is compared in Fig. 4.4 with the corresponding

values for a two-shock intake, with the optimum lip angle in each case. While the optimum curve can be approached to a large degree through lip displacement, a pronounced drop relative to the optimum values can be seen for the fixed geometry which is a consequence of the highly supercritical operation.

Aside from the improvement of overall pressure ratio, the additional drag of the intake is already considerably reduced by the Mach-number-dependent shift x in the central body. It could be completely eliminated if the entire flow of air approaching in the "flow tube" $A_0 = A_E$ were accepted by the intake at the corresponding central body displacement $x = x_{max}$ and the excess air were branched off upstream from the compressor. /102

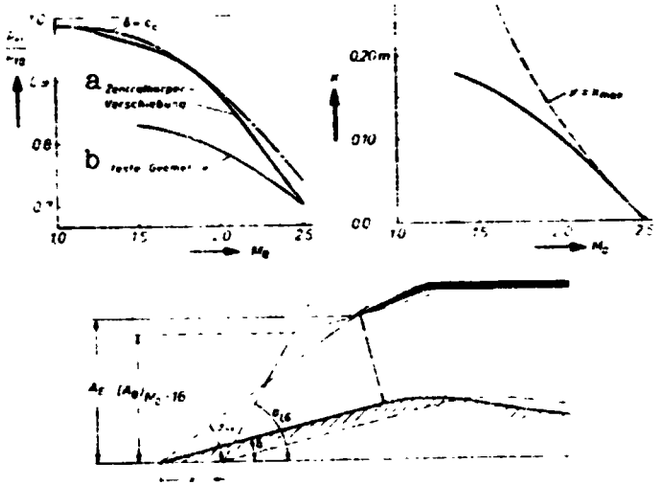

Fig. 4.4. Total pressure ratio, central body displacement and geometry of a plane two-shock intake.

Key: a. Central body displacement; b. Fixed geometry

In the following, the possibility of matching through the variation of lip angles will now be studied using the example of the intake design for a turbojet with precooling, imagined to be the propulsion unit for an aerodynamic space vehicle carrier. Although it is reasonable to mount the engine pods, with their plane intakes, directly under the missile's wing, the effects of wing precompression will be neglected here for the time being. It is thus assumed that flight Mach number is also the oncoming flow Mach number for the intake ($M_\infty = M_0$). /103

The air requirements of the turbojet with precooling at constant rotor rpm $N = N_{AP}$ are plotted in Fig. 4.5 versus flight Mach number range, limited to $M_\infty = M_0 = 5$ for this example. The corresponding curve for the simple afterburner engine is shown for comparison. Final afterburning temperature increases with flight Mach number with the stoichiometric afterburning intended. When it reaches its intended maximum value, it is kept constant by a suitably superstoichiometric fuel/air ratio. The increased flow of fuel, which acts simultaneously as the coolart flow, causes /104

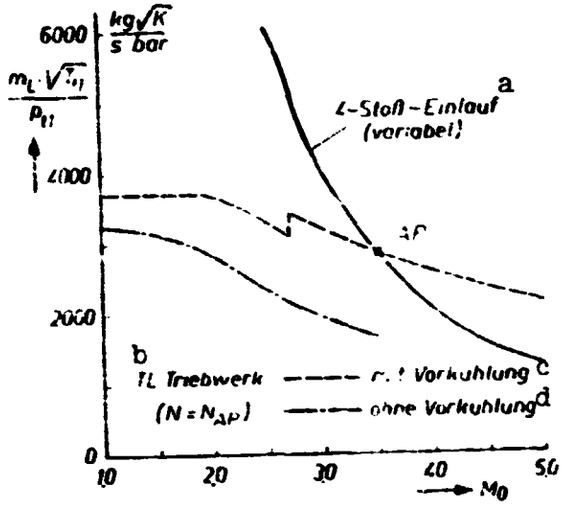

Fig. 4.5. Characteristics for four-shock intake and engine.

Key: a. Four-shock intake (variable); b. Turbojet; c. With precooling; d. Without precooling; AP = "design stage"

enhancement of the precooling effect and thus the jump shown in the mass flow curve at $M_\infty = M_0 \approx 2.7$.

The intake is designed for $M_0 = 3.5$ with regard to its scoop cross section A_E. It is supposed to be designed as a plane four-shock intake with combined external and internal compression. The variation of lip angle makes it possible for the airflow taken in by the intake to correspond to maximum scoop cross section $A_0 = A_E$ in the Mach number range between design Mach number $M_0 = 3.5$ and maximum oncoming flow Mach number $M_0 = 5$.

At oncoming flow Mach numbers below $M_0 = 3.5$, lip angle δ_1 for the first oblique shock wave is supposed to be adjusted so that the overall pressure ratio for the intake approaches that achievable with optimum lip angles in each case as much as possible. At the same time, the shock front should be located only a short distance upstream from the cowling lip so that the added drag remains small. For design reasons, lip angle δ_1 may not drop below a minimum value here. Lip angle δ_2 for the second oblique shock wave, which is tangent to the cowling edge, is varied over the entire flight Mach number range to obtain a high total pressure ratio in a manner which at the same time is simple to achieve in terms of design.

The curve of reduced mass flow taken in by the intake in critical operation is likewise plotted in Fig. 4.5. The excess air at oncoming flow Mach numbers below $M_0 = 3.5$ is mixed into the jet of gases in the thrust nozzle, considerably reducing the problems of nozzle matching. The air deficit at oncoming flow Mach numbers above $M_0 = 3.5$ cannot be compensated for without enlarging the in ake. The unnecessary drop in overall pressure ratio p_{t1}/p_{to} associated with supercritical operation can be eliminated, however, by matching the engine's air requirements to the air provided by the intake in each case through a reduction in rotor rpm N. /105

Fig. 4.6 shows intake geometry and shock wave configuration at design Mach number $M_{0AP} = 3.5$, at maximum oncoming flow Mach /106

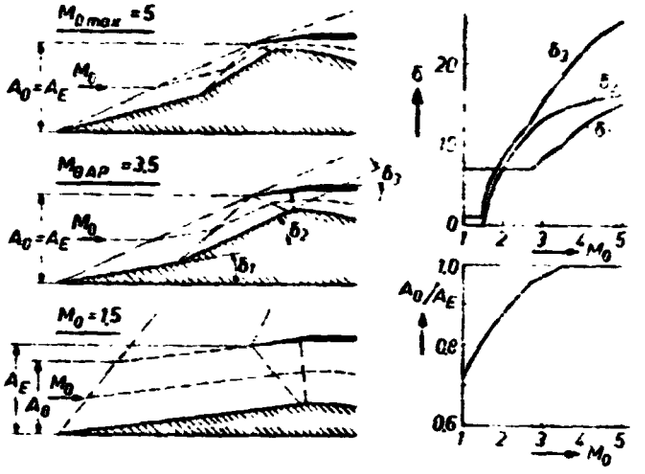

Fig. 4.6. Intake geometry.

number $M_{0max} = 5$ and at $M_0 = 1.5$. As can be seen from the curve of lip angle δ, the second external compression wave disappears at oncoming flow Mach numbers below $M_0 \approx 1.5$.

In the selection of lip angles, care was taken that the external lip angle and the axial lengths of the oblique cowling lip assume only small values, in order to achieve low external drag on the intake cowling. The area ratio A_0/A_E, which primarily determines the magnitude of additional drag, can be kept at high values because of small lip angle δ_1.

The curve of overall pressure ratio versus oncoming flow Mach number obtained with the intake presented comes quite close to the values for the four-shock intake achievable with optimum lip angles in each case (Fig. 4.7). This closeness could be further improved with a superimposed "central body shift," and the added drag produced in the lower flight Mach number range could simultaneously be reduced further.

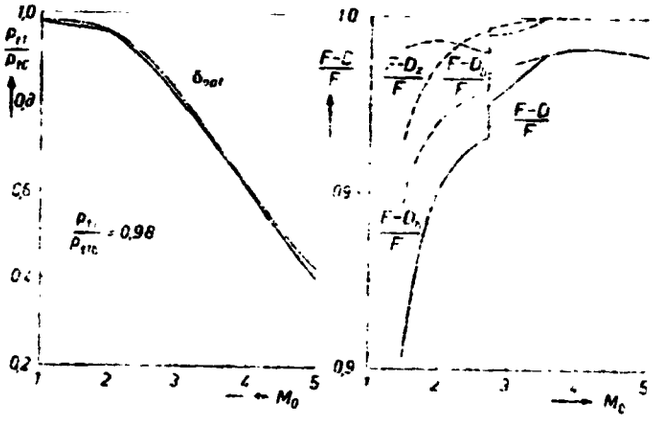

Fig. 4.7. Total pressure ratio and drag for the four-shock intake.

The reduction in engine thrust F due to added drag D_z, cowling drag D_h and bypass drag D_b, which is a consequence of the overall pressure loss that is a function of the excess air taken in through the intake and mixed into the hot gas in the nozzle, is shown in the right half of the diagram. Although the major portion of the flow of air taken in through the intake goes through the bypass at low flight Mach numbers, bypass drag makes up

only a fraction of total intake drag D in the transonic range, in which added drag and cowling drag assume their maxima. If the large excess of air were swept off over the cowling by shock wave deflection or by subcritical operation of the intake, the resultant added and cowling drags would significantly dissipate thrust in the transonic range. /107

Fig. 4.8 shows the schematic of a plane intake with combined "central body" shift and lip angle adjustments. An intake of such a design is based on performance calculations for different engine configurations. It is assumed here that it is located under the wing of the missile under consideration, behind the oblique shock wave initiated at the leading edge of the wing. /108

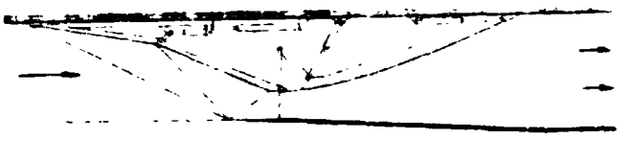

Fig. 4.8. Schematic of four-shock intake.

A slight axial adjustment of the tip of the central body makes it possible for the first two oblique shock waves to be tangent to the fixed cowling lip from about oncoming flow Mach number $M_0 \approx 2$ to maximum oncoming flow Mach number. Lip angles δ_1 and δ_2 can be set largely independently to those values which produce the lowest overall pressure drops. In addition, the pivot point for the second deflecting surface can be fixed on the first.

The shock wave system can be stabilized with boundary layer blowoff both at the lip projections and ahead of the smallest cross section in the front of the intake. This also facilitates control of the hydraulically adjustable intake, which is naturally best designed with fluidic elements. /109

4.13. Wing Precompression

The matching problems described can be reduced quite considerably if the intakes are placed within the pressure field under the wing of the missile. This can result in the following important advantages:

-- For a given geometric scoop cross section A_E for the intake, the cross section A_∞ of the "freestream tube" and thus the scooped-in flow of air is increased.

-- Flight Mach number M_∞ is reduced to an intake oncoming flow Mach number $M_0 < M_\infty$ by the lag in the oblique shock wave initiated by the leading edge of the wing.

Enlargement of the cross section of the "freestream tube" can be expressed easily with the angular function

$$\frac{A_\infty}{A_0} = \frac{\sin\sigma}{\sin(\sigma-\alpha)} \quad , \tag{4.1}$$

based on the drawing in Fig. 4.10, where σ is the angle of the oblique shock wave propagating at the wing, which is at angle of attack α. It is of course already an advantage that the geometric scoop cross section A_E of the intake can be dimensioned smaller as a result of enlargement ratio A_∞/A_0 if it is to take in a given flow of air at a given flight Mach number M_∞ and altitude H_∞. An appreciable reduction in matching problems also results from the fact that this enlargement ratio increases with flight Mach number. /110

This effect, which also occurs at constant angle of attack α, is further enhanced if the angle of attack assumes higher values with increasing flight Mach number. This is already generally the case if the flight profile has been optimized without consideration for such aspects. Let us point out the possibility, however, of influencing the match between intake and engine through the choice of flight profile.

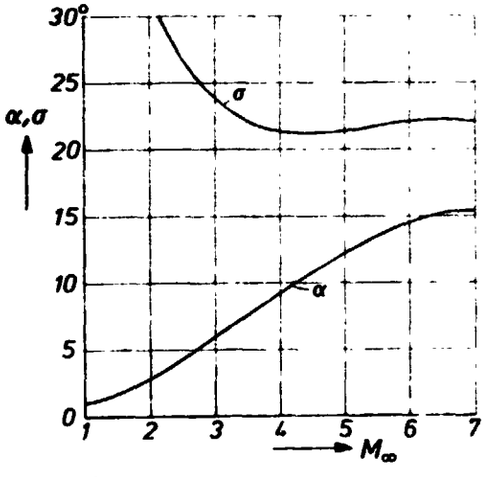

Fig. 4.9. Wing angle of attack α and shock wave angle σ.

The curves of angle of attack α and the associated shock wave angle σ are shown over flight Mach number M_∞ in Fig. 4.9 as obtained from a sample calculation for the accelerated flight of a space vehicle carrier along a flight path with p_{t1E}/T_{t1E} = const. /111

The area ratio A_∞/A_0 obtained here is shown in Fig. 4.10. The increase in freestream scoop cross section A_∞ with flight Mach number causes the intake characteristic in Fig. 4.5 to assume a flatter shape, thereby reducing the difference between the scooped-in stream of air and the stream of air required by the engine.

The reduction in intake oncoming flow Mach number has been mentioned as a second important advantage of wing precompression. /112

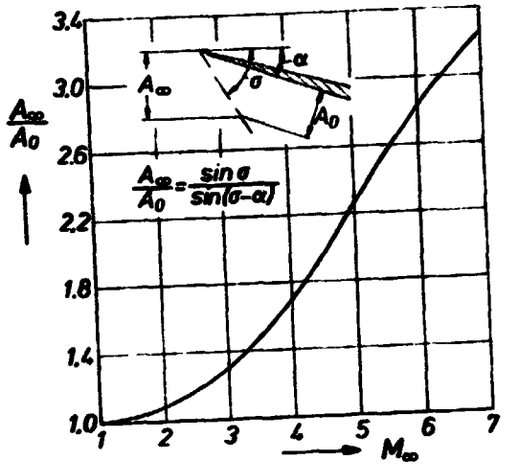

Fig. 4.10. Enlargement ratio of freestream scoop cross section in the case of wing precompression.

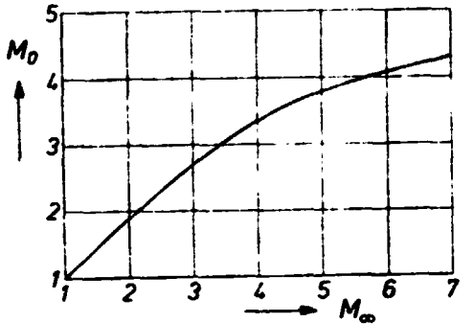

Fig. 4.11. Reduction in oncoming flow Mach number in the case of wing precompression.

It is shown in Fig. 4.11 for the boundary conditions under consideration.

As can be seen from the graph, the intake need be designed only for an oncoming flow Mach number slightly above $M_0 = 4$, in spite of maximum flight Mach number $M_\infty = 7$. The reduction in the oncoming flow Mach number range offers important advantages for designing the intake. The danger of unstable operation at high oncoming flow Mach numbers is also reduced, since contraction ratio A_H/A_0 assumes less extreme minima.

Finally, retardation of the flow of air fed to the engine is distributed between five shock waves due to wing precompression. As will be shown below, wing angle of attack α, whose magnitude can be affected by the choice of flight profile and area loading, can be made to vary with increasing flight Mach number M_∞ in a manner somewhat like the optimally varied first lip angle of a five-shock intake without serious disadvantages to the overall design of the vehicle system. The consequence of this is that overall pressure ratio $p_{t1}/p_{t\infty}$ in the intake flow can be increased by wing precompression. This is shown in Fig. 4.12 for the intake illustrated in Fig. 4.8. The curve made up of dots and dashes indicates the overall pressure ratio $p_{t0}/p_{t\infty}$ for the oblique wing shock wave here.

4.2. Heat Exchanger

/114

A suitable design for the heat exchanger is critically important for the performance of engines with precooling.

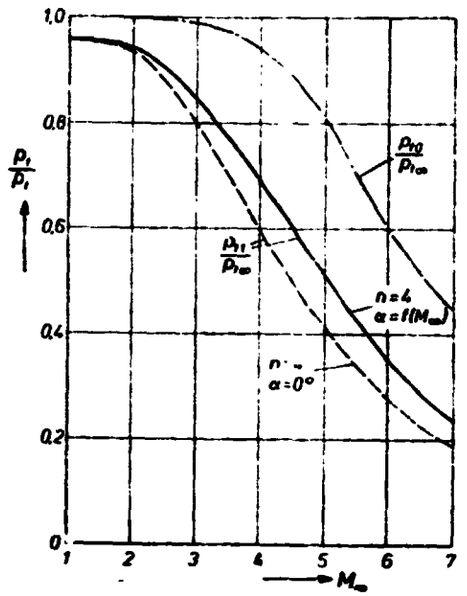

Fig. 4.12. Overall pressure ratio for the four-shock intake with and without wing precompression.

4.21. Special Requirements, Configuration and Design

The necessary heat exchanger must have an extremely low weight for its intended application in a missile engine. Since the missile is to be accelerated to high flight Mach numbers, the heat exchanger is also operated -- at least briefly -- at an unusually high temperature level. Finally, the limitation of possible frontal area results in high throughflow velocities, as a result of which the pressure drop may not increase by an impermissible level, however, since this would negate the positive effect of precooling.

The problem of heat exchanger fouling which takes place during heat exchange between air and carbon- or sulfur-bearing combustion gases and which makes the use of heat exchangers difficult and frequently impossible in gas turbine systems, does not occur in the present case, however. The heat-exchanging fluids contain practically no solid components.

The special requirements mentioned must be taken into consideration in selecting the type of heat exchanger and its configuration and in determining the cooling task at the design stage. The requirement for low inherent weight results in a high exchange surface density (exchanger surface area / unit volume). This cannot be achieved with pipe-bundle systems, even if ribbed pipes are used. Regenerators with periodic flowthrough, which can be made very compact in designs with rotating matrices, /115 are unsuitable for heat exchange between air and hydrogen, on the other hand, due to the necessary mixing of the two fluids.

To satisfy the need for compact heat exchangers which operate by the conventional recuperative principle (heat exchange through the wall), a large number of matrix types have been developed which are characterized by a high exchanger surface density at low inherent weight per unit volume and are thus particularly suitable for the application at hand. Their thermodynamic and flow-mechanics behavior has been studied experimentally within a large range of variation in boundary conditions and summarized in [29]. Fig. 4.13 shows the example of a combination of two characteristic matrix types to form a cross-current heat exchanger.

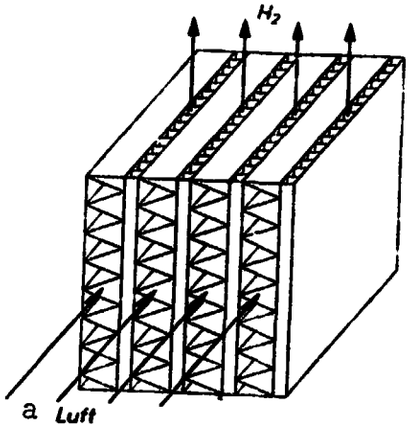

Fig. 4.13. Heat exchanger for gaseous fluids.

Key: a. Air

Combinations can be selected from these types of matrices which are particularly desirable for a wide range of different cooling tasks. The pressure drops, the quantity of heat transferred and/or the necessary heat exchanger size can be calculated from the experimental data for given boundary conditions. For the sake of better matching of the flow velocities of the two fluids, slight variation is permitted here in the geometry of the matrix type being sought, taking the laws of similarity into consideration. /116

The high exchange surface density of the matrices studied is achieved through the suitable incorporation of conducting ribs into the flow channels. This reduces the length and inherent weight of the heat exchanger for a given heat transfer capacity and frontal area. The increased pressure drop caused by the ribs is low, due primarily to the reduction of flow length.

To a decisive degree, the exchanger surface area required can be kept low in spite of the large heat flows tranferred, by consistently dispensing with high levels of exchange. The structural volume and inherent weight of the heat exchanger and the pressure drops which occur remain within a suitable scope.

Due to the intentionally low exchange levels, the smallest temperature differences between the heat-exchanging fluids hardly fall below a value of ΔT_{min} = 100 K. In spite of the size of the temperature differences and of the temperature gradients in the direction of flow, the thermal stresses which occur may be expected to remain within manageable limits because of the relatively elastic matrix. /117

Aside from purely thermodynamic aspects, it is desirable -- just in terms of these thermal stresses -- to design the heat exchanger for operation based on the countercurrent principle. The development of temperature distortion at the compressor inlet can be avoided to a large extent thereby. This normally occurs downstream from a cross-flow system and can jeopardize the reliable operation of an engine.

4.22. Computational Method

A computer program was written which calculates the thermodynamic, flow-mechanics and geometric variables for the heat exchanger required from the experimentally determined data on heat exchanger matrices studied in [29], via a system of dimensionless parameters. The thermodynamic state variables of the fluids covered (air, N_2 and H_2) required during computation are determined here with the real gas program described above. The dependence of the remaining materials constants upon temperature -- e.g. viscosity and conductivity -- were approximated with polynomials.

The program is set up in such a way that it can be used to do either of the following for both the countercurrent principle and for crosscurrent:

-- calculate the dimensions, inherent weight and pressure drops of the heat exchanger in known inlet states for both mass flows and with a given heat flow; /118

-- or calculate the transferrable heat flow and the outlet states of the mass flows for a given heat exchanger geometry with known inlet states.

Since it was not possible to see at the outset which of the 48 types of matrices initially selected from [29] are particularly suitable for the application at hand, provisions were made for the most desirable of the usable matrix combinations to be determined independently for the particular task as the program was being run. The target variables for optimization are frontal area A_{St}, inherent weight m_{WT} and overall pressure drop $\Delta p_t/p_1$. The parameters varied here include not only matrix type but also flow velocities $c_{1,h}$ and $c_{1,k}$ of the two fluids at the hot end of the heat exchanger and the smallest temperature different ΔT_{min} occurring between the heat-exchanging mass flows. A slight variation is also made in matrix geometry, for the reasons mentioned.

Aluminum, copper, stainless steel (V2A) and carbon steel are covered as matrix materials; their constants are included in the program.

The basic computation cycle will be illustrated below with the example of the heat exchanger designed for a turbojet with precooling. It makes use of the method described in [29], which has been revised at various points. The designation of planes and the given data are shown in Fig. 4.14. The planes upstream and downstream from the heat exchanger are called 1a and 2a. The ends of the matrix channels are designated 1 and 2.

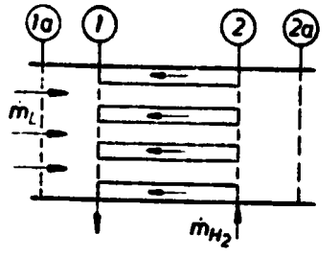

Given:

$\dot{m}_L$	$\dot{m}_{H_2}$
$h_{t1a,L}$	h_{t2,H_2}
$p_{t1a,L}$	p_{t2,H_2}
$c_{1,L}$	ΔT_{min}

Fig. 4.14. Schematic of heat exchanger and data given.

Qualitative curves of temperature over exchanged heat are shown in Fig. 4.15 for both fluids. /119

It is conventional, and also permissible in the normal case, to set the static states of the fluids equal to the overall states in a heat exchanger design. In the present case, howevever, this simplification is not generally justifiable because of the unusually high flow velocities in plane 1, since this would yield low values, deviating by up to 5% from the true values, for the free flow surfaces and thus for frontal area and heat exchanger weight.

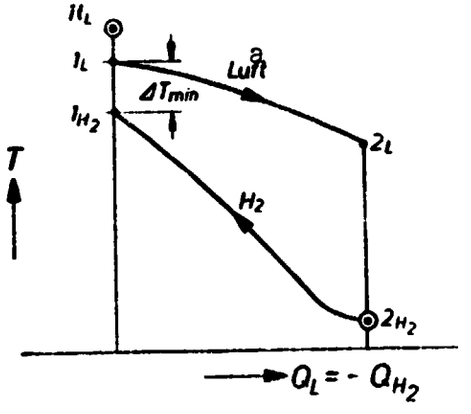

Fig. 4.15. Temperature curves in heat exchanger.

Key: a. Air

For the same reason, the pressure drop which occurs between planes 1a and 1 in the airflow and which is a result of the sudden reduction in cross section and of the additional separation phenomena in the matrix inlet will also be taken into consideration here for determining heat exchanger geometry. This irreversibility is considered in [29] only for the purpose of determining the pressure drop in the entire heat exchanger, i.e. to determine pressures in plane 2a, and is taken as $p_{1,L} = p_{t1a,L}$ elsewhere. /120

As for the hydrogen system, it is not worthwhile to determine the deviation of the static state from the overall state, since the Mach numbers remain very small even in plane 1, due to the high sonic velocity.

State Variables in Planes 1 and 2:

State 1_L is first determined: The conservation of energy gives us $h_{1,L}$. ZUSTGL is used to determine the pressure $(p_{1,L})_s$ which would occur in plane 1 in lossless flow, from $h_{1,L}$ and /121

$s_{1a,L}$. Entropy $s_{1a,L} = f(p_{t1a,L}, h_{t1a,L})$ has likewise been calculated previously with ZUSTGL.

Taking losses into consideration, $p_{1,L}$ can now be determined by iteration from

$$p_{1,L} = (p_{1,L} - \frac{\rho_{1,L} \cdot c_{1,L}^2}{2} \cdot K_E$$

The coefficient K_E here describes irreversibilities at the inlet end. Its dependence upon porosity α_P and upon Reynolds number N_{Re}

$$K_E = f(\alpha_P, N_{Re})$$

is demonstrated in [29] and is available in approximate functions. The porosities

$$\alpha_P = \frac{A_F}{A_{St}} = \frac{A_T}{V_{WT}} \cdot r_h \qquad (4.2)$$

where A_F = free flow area
A_{St} = frontal area
A_T = transfer area (exchange area)
$V_{WT} = A_{St} \cdot \ell$ = total volume of heat exchanger
ℓ = matrix length

can be calculated from the matrix parameters, of which hydraulic radius

$$r_h = A_F \cdot \ell / A_T \qquad (4.3)$$

is also known. Viscosity $\mu_{1,L} = F(T_{1,L})$, whose value is likewise to be determined with approximate functions, is needed for Reynolds number /122

$$(N_{Re})_{1,L} = \frac{c_{1,L} \cdot 4 \cdot r_h}{\mu_{1,L} / \nu_{1,L}} \qquad (4.4)$$

Finally, $T_{1,L}$ and $\rho_{1,L}$ can be determined for $p_{1,L}$ and $h_{1,L}$ from ZUSTGL.

The pressure drops which occur in the two fluids as they flow through the matrix must be estimated provisionally and used to calculate pressures $p_{2,L}$ and p_{1,H_2} for establishing states 2, 1_{H_2} and 2_{H_2}. Enthalpies $h_{2,L}$, h_{1,H_2} and h_{2,H_2} and missing temperature $T_{2,L}$ can then be determined by calling real gas program ZUSTGL or from the principle of the conservation of energy.

Capacities and Mean Temperatures:

The heat capacities of the mass flows are calculated from

$$C = \dot{m} \cdot \frac{h_1 - h_2}{T_1 - T_2} \left[\frac{J}{K \cdot s}\right]$$

The ratio of capacities in the mass flows is

$$\gamma = C_{min}/C_{max}. \qquad (4.5)$$

The calculation of mean temperature difference $\overline{\Delta T}$ between the heat-exchanging fluids must take into consideration the fact that the necessary transfer areas $A_{T,L}$ and A_{T,H_2}, and also -- as an approximation -- the pressure drops which occur, increase proportionally to the quantity of heat to be transferred locally and inversely proportionally to the local temperature differential: /123

$$A_T \sim \int_{h_2}^{h_1} \frac{dh}{\Delta T} \quad ; \quad \frac{\Delta p}{p} \sim \int_{h_2}^{h_1} \frac{dh}{\Delta T}$$

We can write the following for the assumption c_p = const, which presupposes linear curves in Fig. 4.15:

$$\int_{T_2}^{T_1} \frac{dT}{\Delta T} = \frac{T_1 - T_2}{\overline{\Delta T}}$$

With

$$\Delta T = \Delta T_1 + (\Delta T_2 - \Delta T_1) \cdot \frac{T_1 - T}{T_1 - T_2}$$

we obtain

$$\frac{1}{\overline{\Delta T}} = \frac{1}{T_1 - T_2} \cdot \int_{T_2}^{T_1} \frac{dT}{\Delta T_1 + (\Delta T_2 - \Delta T_1) \cdot \frac{T_1 - T}{T_1 - T_2}}$$

Integration yields

$$\overline{\Delta T} = \frac{\Delta T_2 - \Delta T_1}{\ln(\Delta T_2 / \Delta T_1)} \qquad (4.6)$$

The mean gas temperatures of the fluids $\overline{T}_L$ and $\overline{T}_{H_2}$ and mean material temperature $\overline{T}_{Mat.}$ of the heat exchanger can now likewise be determined using (4.6). /124

Exchange Efficiency and Heat Transfer Capacity:

Exchange efficiency is determined by the given boundary conditions:

$$\varepsilon = \frac{h_{1,H2} - h_{2,H2}}{(h_{1,H2})_{\overline{\Delta T}=0} - h_{2,H2}}$$

where

$$(h_{1,H2})_{\Delta T=0} = f\,(T_{1,L}, p_{1,H_2}) \qquad \text{from ZUSTGL.}$$

The heat transfer capacity of the heat exchanger is described by the transport coefficient:

$$N_{Tr} = \frac{A_T \cdot \overline{k}_{Tr} \cdot \overline{\Delta T}}{(\dot{m} \cdot \overline{c}_p)_{min} \cdot \overline{\Delta T}} = \frac{A_T \cdot \overline{k}_{Tr}}{C_{min}} \qquad (4.7)$$

where $\overline{k}_{Tr}$ = mean heat transmission coefficient.

N_{Tr} is the dimensionless factor used to calculate the required transfer area. It relates the quantity of heat which the heat exchanger can transfer at mean temperature difference $\overline{\Delta T}$ to the

quantity of heat which the fluid of lower capacity can absorb or lose if its temperature changes by $\overline{\Delta T}$.

The required heat transfer capacity can be calculated from the given boundary conditions using equation (4.5): /125

$$\ddot{}_{Tr} = \frac{\ln (1 - \varepsilon) / (1 - \varepsilon \cdot Y)}{Y - 1}$$

Material Properties and Prandtl Numbers:

The material properties of viscosity $\overline{\mu}$, thermal conductivity $\overline{\lambda}$ and specific heat $\overline{c_p}$ can now be determined for the mean gas temperatures from approximate functions or from ZUSTGL. The mean Prandtl numbers can thus be calculated:

$$\ddot{}_{Pr} = \frac{\overline{\mu} \cdot \overline{c_p}}{\overline{\lambda}} \qquad (4.8)$$

Reynolds Numbers, Stanton Numbers, Friction Factors:

The calculation of heat transfer and pressure drops due to friction also requires

$$\ddot{}_{Re} = \frac{\overline{c} \cdot 4r_h}{\overline{\mu} / \overline{\rho}} \qquad (4.9)$$

with reference length $4r_h$. For reasons of continuity, $\overline{\rho} \cdot \overline{c}$ can be replaced by the known quantities at the ends of the matrix in each case:

$$\ddot{}_{Re,L} = \frac{c_{1,L} \cdot 4r_{h,L}}{\overline{\mu}_L / \rho_{1,L}}$$

and

$$\ddot{}_{Re,H_2} = \frac{c_{1,H2} \cdot 4r_{h,H2}}{\overline{\mu}_{H_2} / \rho_{1,H2}}$$

where /126

$$c_{1,H_2} = c_{1,L} \cdot \frac{\dot{m}_{H2}}{\dot{m}_L} \cdot \frac{a_{p,L}}{a_{p,H2}} \cdot \frac{\rho_{1,L}}{\rho_{1,H2}} .$$

The Stanton number

$$\bar{N}_{St} = \frac{\bar{N}_{Nu}}{\bar{N}_{Re} \cdot \bar{N}_{Pr}} = \frac{\bar{\alpha} \cdot A_F}{C} \qquad (4.10)$$

where $\bar{\alpha}$ = mean heat transfer coefficient, is stored in the program as a function of Reynolds number N_{Re} and Prandtl number N_{Pr} for the different types of matrices in the form of approximate functions. Similar provisions are made for the friction factor

$$c_f = f(\bar{N}_{Re}).$$

Heat Transfer Coefficient, Surface Area Coefficient and Heat Transmission Coefficient:

We obtain the following from (4.10) for the heat transfer coefficients:

$$\bar{\alpha} = N_{St} \cdot C/A_F.$$

The surface area coefficient η_A indicates the fraction of geometrically available exchange area A_T which may be taken as effective area for calculating the heat transmission coefficient. It is a function of the matrix parameters, mean material conductivity $\bar{\lambda}_{Mat} = f(\bar{T}Mat)$ and heat transfer coefficient $\bar{\alpha}$.

If the very low wall drag is neglected, for example, heat transmission coefficient $\bar{k}_{Tr}$ is now found to be

/127

$$(\bar{k}_{Tr})_{m2} = \frac{1}{(\bar{\eta}_A \cdot \bar{\alpha})_{H_2}} + \frac{1}{(\lambda_W)_L / (A_W)_{H_2} \cdot (\bar{\eta}_A \cdot \bar{\alpha})_L} \qquad (4.11)$$

The ratio of transfer surfaces depends upon the geometry of the types of matrices.

Geometric Dimensions:

The required transfer surfaces can be determined using equation (4.7):

$$(A_T)_{H_2} = \dot{m}_{Tr} \cdot c_{H_2} / (\bar{\kappa}_{Tr})_{H_2}$$

$$(A_T)_L = (A_T)_{H_2} \cdot \frac{(A_T)_L / V_{WT}}{(A_T)_{H_2} / V_{WT}}$$

where A_T/V_{WT} is known from the matrix parameters.

With the freestream area

$$A_{F,L} = \dot{m}_L / (\rho_{1,L} \cdot c_{1,L})$$

we can use equation (4.2) to determine frontal area, which is equivalent in the inlet planes of the two fluids in the countercurrent heat exchanger:

$$A_{St,H_2} = A_{St,L} = A_{F,L} / \sigma_{F,L}$$

The freestream area for the hydrogen system is calculated from equation (4.2) to be

$$A_{F,H_2} = A_{F,L} \cdot \sigma_{F,H_2} / \sigma_{F,L}$$

The matrix lengths, which likewise have equal values in the countercurrent heat exchanger, are found from equation (4.3) to be:

$$l_{M,H_2} = l_{M,L} = (r_h \cdot A_T / A_F)_L$$ /128

It is now possible to also calculate the inherent weight of the required heat exchanger matrix m_{MWT} from its geometric dimensions, the known matrix parameters and the density of the matrix material used.

Velocities and Pressure Drops:

The unknown velocities $c_{2,L}$, c_{1,H_2} and c_{2,H_2} can now be determined from the continuity relationships. Since the pressure drops are approximately proportional to the square of the mean flow velocity

$$\Delta p \sim \bar{c}^2,$$

we obtain the following for their mean:

$$\bar{c} = \sqrt{\frac{c_1^2 + c_2^2}{2}} \qquad (4.12)$$

The static pressure change Δp_M which occurs during flow through the heat exchanger matrix can be attributed to two causes:

1. Acceleration of flow in the matrix:

The conservation of momentum yields the following, for example (Fig. 4.14):

$$\Delta p_{B,L} = \rho_{1,L} \cdot c_{1,L}^2 - \rho_{2,L} \cdot c_{2,L}^2$$

$$= \rho_{1,L} \cdot c_{1,L}^2 \cdot \left(1 - \frac{c_{2,L}}{c_{1,L}}\right)$$

Since flow in the air system is retarded as the result of heat removal, $\Delta p_{B,L}$ assumes a positive value.

2. Wall friction in the matrix: /122

Pressure drop Δp_R is described by friction coefficient c_f (see p. 74):

$$A_F \cdot \Delta p_R = - \frac{\bar{\rho} \cdot \bar{c}^2}{2} \cdot c_f \cdot A_T$$

$$\Delta p_R = - \frac{\rho_1 \cdot c_1^2}{2} \cdot c_f \cdot \frac{l_M}{r_h} \cdot \frac{\bar{c}}{c_1}$$

Thus the air-system pressure change in the matrix, for example, can be given as

$$\Delta p_{M,L} = \frac{\rho_{1,L} \cdot c_{1,L}^2}{2} \cdot \left[2 \cdot \left(1 - \frac{c_{2,L}}{c_{1,L}}\right) - c_f \cdot \frac{l_M}{r_h} \cdot \frac{\bar{c}}{c_1}\right] \qquad (4.13)$$

Pressures $p_{2,L}$ and p_{1,H_2} at the respective matrix ends can be calculated from equation (4.13). If they do not agree with the initial estimates (see p. 71) within a specified limit of error, the entire heat exchanger calculation must be repeated with them.

Taking the drops into consideration, we can calculate $p_{2a,L}$ with sufficient accuracy as

$$p_{2a,L} = p_{2,L} + \frac{\rho_{2,L} \cdot c_{2,L}^2}{2} \cdot (1 - \alpha_p^2 - K_A)$$

The coefficient $K_A = f(\alpha p, N_{R\epsilon})$ describes irreversibility in the air system at the outlet end of the matrix (planes 2 → 2a in Fig. 4.14).

Thus all static and overall state variables still missing at the outlet of the heat exchanger can now be determined by calling real gas program ZUSTGL or from the principle of conservation of energy. /130

The method given in [29] for heat exchanger calculations was improved in the following ways:

-- consistent consideration of the real gas behavior of the fluids involved;

-- more exact calculation of the required freestream cross sections or flow velocities at the matrix inlet;

-- correct means for $\overline{\Delta T}$ (equation (4.6)), $\overline{T}_L$, $\overline{T}_{H_2}$, $\overline{T}_{Mat}$, $\overline{u}$, $\overline{c}_p$ and $\overline{\lambda}$ and for $\overline{c}$ (equation (4.12));

-- consideration of the effects of longitudinal conduction within the matrix material.

Neglecting the above corrections would result in impermissibly high cumulative errors due to the unusually high flow velocities and heat flow densities which occur in this application. Excessively small values would then be calculated for the pressure drops and for the inherent weight of the heat exchanger.

4.3. Compressor /131

The special requirements which are placed on the compressor in this application hardly exceed the state of the art in conventional engine construction.

Due to the high temperature level to which the compressor is exposed toward the end of the acceleration phase, it must be made of heat-resistant material. Since the maximum flight Mach number achievable with turbo engines under consideration is primarily determined by the permissible material temperature reached at the end of the compressor, it is reasonable to consider providing blade and rotor cooling for the compressor similar to that used in the turbine in order to extend the flight Mach number range covered.

The compressor blades could be cooled directly with the hydrogen used as fuel here. The quantity of heat absorbed by the hydrogen could thereby be increased slightly or the exchange area required in the heat exchanger and thus its inherent weight could be correspondingly reduced. This savings in weight is insignificant, however, since the total blade surface in the compressor is quite small relative to the exchange surface in the heat exchanger. Moreover, the additional structural outlay which is necessary for blade cooling quickly counteracts the savings in weight. In this type of blade cooling, it is also necessary to expect hydrogen/air mixtures to develop which, due to the high temperature levels which occur, ignite spontaneously even at very substoichiometric values, as the result of sealing problems in the rotating system.

Cooling the compressor blades with air which is branched off, /132
like the turbine cooling air, at the end of the compressor would be less problematical. In order for it to be able to remove heat from the blade material, however, it would have to go through intermediate cooling as far as possible below the permissible material temperature through heat loss to the flow of hydrogen in a separate heat exchanger. Although this type of compressor cooling can be considered a quite suitable means for further extending the flight Mach number range of turbojets, it will not be considered within the scope of these studies.

Although the compression process is influenced in the direction of isothermal compression in a power plant with precooling, both types of compressor cooling must generally impair the course of thermodynamic processes if they do not produce an appreciable increase in the total heat absorbed by the flow of hydrogen. The removal of heat prior to compression is thermodynamically more reasonable than removal of the same quantity of heat during compression.

For the upper flight Mach number range, moreover, continuous intermediate cooling during the compression process can be expected to raise the pumping limit of the compressor and the pressure ratio built up in the range of low reduced engine speeds occurring here and to increase the flow of air received by the compressor. This flow-mechanics advantage of intermediate cooling is still not fruitful, however, since the flow of air is already

limited by the intake in the upper flight Mach number range, due to the necessary compromise in intake design.

In addition to the special thermal stress on the compressor at high flight Mach numbers, it is also necessary to discuss the stress caused by unconventionally low temperatures. In the limiting case, compressor inlet temperature is about 40 K below that of the oncoming flow to the compressor in a conventional turbojet in slow high-altitude flight. This must be taken into consideration with regard to low-temperature brittleness in the selection of materials. An advantage in this respect, however, is that natural rotor rpm N must be reduced anyway when correspondingly low compressor inlet temperatures T_{t1} occur, through a reduction in turbine inlet temperature, to the extent that rotor rpm, reduced as per Mach's similarity principle, does not exceed the design value $(N/\sqrt{T_{t1}})_{AP}$ by too much. This is necessary in order to rule out the danger of compressor pumping at excessive reduced rpm. Achieving this by opening the nozzle at constant rpm appears to be less desirable in the case at hand. It is also not reasonable here, moreover, to have to take the occurrence of high overspeeds into consideration in design starting point selection, since the special requirement placed on the compressor with regard to its optimum operating range is concerned primarily with broad extension toward low reduced rpm. /133

An important aspect to be considered in designing the compressor of a turbojet with precooling is that its pressure ratio is limited to a value which makes it possible to design the turbine with one stage. This helps in designing the turbo section of the engine as simple and light as possible.

Aside from the effect on the turbo section's inherent weight, no special significance is to be assigned to frontal cross section, since the cross section of the upstream heat exchanger is considerably larger anyway. Thus the hub ratio of the first stage need not be designed extremely low and inlet Mach number M_1 undesirably high, particularly since flow upstream from the compressor inlet must be accelerated anyway, in contrast to the normal case. /134

In view of the unusually large operating range covered and in view of compressor efficiency, it appears reasonable, moreover, to design the compressor in the form of a subsonic compressor with a slightly transonic first stage in any case.

A consideration of the changes in pressure ratio, reduced mass flow and efficiency with inlet conditions in each case or with the change in rotor rpm is based on suitable generalized performance graphs. /135

The compressor performance graph shown in Fig. 4.16 served as the basis for the compressors of the turbojets studied, with

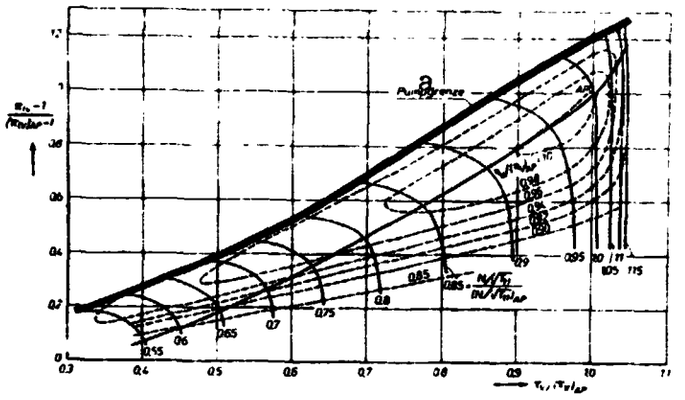

Fig. 4.16. Generalized compressor performance graph.

Key: a. Pumping limit

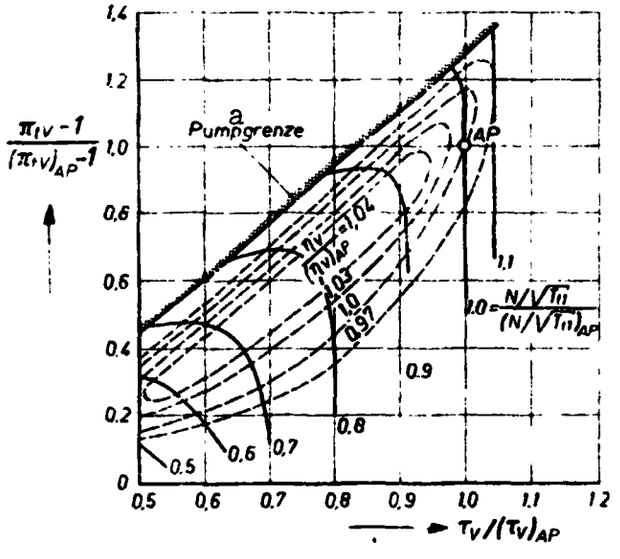

Fig. 4.17. Generalized fan performance graph.

Key: a. Pumping limit.

and without precooling. It is assumed here that it applies to compressors with about 5 to 10 stages, designed on the basis of the specified conditions.

The generalized fan performance graph shown in Fig. 4.17 [30] was used to cover the steady behavior of fan compressors in turbo-rocket engines, which were employed, and likewise analyzed, as reference engines in versions with and without precooling. We can assume that it applies to a heavily loaded fan with two to four transonic stages. /136

Due to the smaller number of stages, the reduced mass flow of the fan drops off less markedly with decreasing rotor rpm than is the case for a compressor with more stages. This effect influences the curve of thrust $F = f(M_\infty)$, as will be shown below.

4.4. Turbine

The requirements placed on the turbine of the turbojet with precooling correspond to the present state of the art. Compressor air is used to cool the turbine blades. Before it is used in the turbine, it experiences intermediate cooling through heat exchange with the flow of fuel in a small, separate heat exchanger. Only this makes it possible to extend the flight Mach number range far enough that compressor outlet temperature corresponds to the technologically

permissible material temperature. Moreover, this makes it possible to considerably reduce the requirement for cooling air, which appreciably impairs the thermodynamic process in conventional engines which operate at high compressor pressure ratios or at high flight Mach numbers with high turbine inlet temperatures.

Turbine calculations are made in steps in the cyclic process calculations; we can assume that the cooling air required in the individual stages is mixed with the gas flow again at the end of each stage. In addition to the state variables, combustion gas composition also changes here. The required cooling air per turbine cascade is taken from Fig. 4.18 and corresponds approximately to the present state of the art. /137

It was obtained with

$$\gamma = \frac{\vartheta - 0{,}05}{(1{,}05 - \vartheta)^3} + \frac{1}{1{,}05 - \vartheta} - \sqrt{1{,}05 - \vartheta}$$

where $\gamma = \dot{m}_{KL}/\dot{m}_L$ is specific cooling air flow, referred to the flow of air $\dot{m}_L$ received by the compressor. The temperature ratio /138

$$\vartheta = \frac{T_t - T_{Mat}}{T_t - T_{KL}}$$

relates the difference between the total temperature T_t of the gas at the cascade inlet and permissible material temperature T_{Mat} to the difference between T_t and cooling air temperature T_{KL} at the cascade inlet.

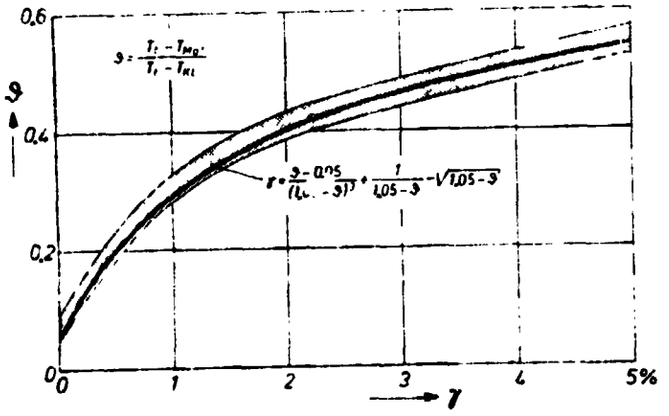

Fig. 4.18. Cooling air required per turbine cascade.

The cooling air required for the individual turbine stages as calculated in this manner is increased by the proportion of leakage air which occurs as the cooling air is admitted to the turning rotor and must also be taken into consideration.

In afterburner engines with and without precooling, the turbine

is placed downstream from a subsonic diffuser, which reduces flow Mach number toward the afterburner inlet in order to keep the pressure losses occurring there within limits.

Axial outlet Mach number M_4 must be recalculated with each deviation from the design starting point, since it determines the Mach number at the inlet of the afterburner and thus its pressure losses, due to the fixed diffuser area ratio. Because of the relatively low temperature level, of course, a frozen combustion gas composition can be assumed for expansion calculations in the turbine.

While critical operation can be assumed in each case for the turbines in the turbojets studied, the multistage turbines in the turborocket engines (with and without precooling) to be used as reference power plants always operate subcritically. Since mass flow consists mostly or even completely of hydrogen here, the /139
sonic velocities of the fluid assume very high values. In spite of high tangential velocities, only low tangential Mach numbers can be achieved for this reason, producing a low general Mach number level at suitable deflection angles. Thus calculations for the turbines must be made stepwise in terms of flow mechanics, and their operating behavior taken into consideration with a turbine performance graph (one rpm line is adequate).

4.5. Mixing Chamber

In all of the air-breathing jet engines covered here, complete mixing occurs between two mass flows of different composition at different temperatures, densities and velocities. In the combustion chambers of the turbojet with afterburning, for example, the flow of fuel, which in general is gaseous when hydrogen is used, is mixed into the air or the combustion gas already present. In the turborocket engine, the fuel-rich combustion gas coming from the turbine is mixed into the compressed airflow. In the various combination power plants involving the ramjet (e.g. ramjet plus rocket), the admixture of the flow generated in the gas generator first causes a flow of air to take place through the main combustion chamber -- even at a standstill -- to which heat can now be added.

In addition to material and heat exchange, momentum exchange is an important characteristic of jet mixing in the transport of flow energy between fluids. As an irreversible process, this always involves an increase in total entropy, even if all friction losses are disregarded. Jet-mixing calculations will be based on /140
a simplified model concept in the case at hand (Fig. 4.19).

The two mass flows enter the cylindrical mixing chamber axially at inlet plane E. Mixing is assumed to be complete at the mixing chamber outlet (plane A), i.e. homogeneous flow exists.

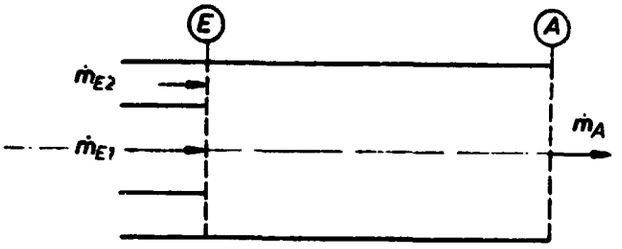

Fig. 4.19. Schematic of mixing chamber.

This can be considered permissible if we assume that the total chamber length installed for subsequent combustion is also available for mixing. Nonuniformity at the end of the chamber must then be blamed on the superimposed combustion. Mixing is also promoted by the increased turbulence of combustion.

The three principles of conservation for steady-state flow are required to calculate data on materials at the mixing chamber outlet, at first considering only thermodynamic mixing losses:

-- conservation of mass: /141

$$\dot{m}_A - (\dot{m}_{E1} + \dot{m}_{E2}) = 0 \tag{4.14}$$

-- conservation of energy:

$$\dot{m}_A \cdot h_{tA} - (\dot{m}_{E1} \cdot h_{tE1} + \dot{m}_E \cdot h_{tE2}) = 0 \tag{4.15}$$

-- conservation of momentum:

$$\dot{m}_A \cdot c_A - (\dot{m}_{E1} \cdot c_{E1} + \dot{m}_{E2} \cdot c_{E2}) + p_A \cdot A_A - (p_{E1} \cdot A_{E1} + p_{E2} \cdot A_{E2}) = 0 \tag{4.16}$$

Total enthalpy at the mixing chamber outlet, h_{tA}, can be given with equation (4.14) and (4.15).

Since separate calculations are made for mixing and for the superimposed chemical reaction, the mixing calculations are made with frozen composition. Gas composition at the mixing chamber outlet can be determined by adding the compositions of the two mass flows:

$$\nu_{j,A} = \frac{\nu_{j,E1} \cdot \dot{m}_{E1}/m_{E1} + \nu_{j,E2} \cdot \dot{m}_{E2}/m_{E2}}{\dot{m}_{E1}/m_{E1} + \dot{m}_{E2}/m_{E2}} \tag{4.17}$$

Total temperature T_{tA} and the gas constant R_A can now be calculated with HBRENGA and RGAS. Velocity $c_A = c_A'$ and static pressure p_A at the mixing chamber outlet must be determined by

iteration such that equations (4.16) and (4.18) are satisfied.

$$p_A = (\dot{m}_A \cdot R_A \cdot T_A) / (A_A \cdot c_A) \qquad (4.18)$$

Temperature $T_A = f(h_A)$ in equation (4.18) can be determined from HBRENGA with $h_A = h_{tA} - c_a^2/2$.

In addition to purely thermodynamic mixing losses, the turbulent losses which result from the turbulence of the two mass flows are important in a mixing calculation. The following approach can be used to cover them: /142

We can assume that a portion of the momentum which is exchanged between the two fluids in the main direction of flow is lost through turbulence losses.

The relationship

$$\dot{m}_{E1} \cdot (c'_A - c_{E1}) + \frac{\dot{m}_{E1}}{\dot{m}_A} \cdot A_A \cdot p_A - A_{E1} \cdot p_{E1}$$

$$= - \dot{m}_{E2} \cdot (c'_A - c_{E2}) + \frac{\dot{m}_{E2}}{\dot{m}_A} \cdot A_A \cdot p_A - A_{E2} \cdot p_{E2}$$

can be given for momentum exchange if thermodynamic mixing losses are given exclusive consideration; c'_A is velocity at the mixing chamber outlet, determined from equation (4.16) for this case. If we cover the fraction of momentum loss due to turbulence with a loss factor K_V, we obtain the following for total momentum at the mixing chamber outlet for a given value of p_A:

$$\dot{m}_A \cdot c_A + A_A \cdot p_A = \dot{m}_A \cdot c'_A + A_A \cdot p_A$$

$$\dot{m}_{E1} \cdot ABS (c'_A - c_{E1}) + \frac{A_A \cdot p_A}{\dot{m}_A} - \frac{A_{E1} \cdot p_{E1}}{\dot{m}_{E1}}$$

From this relation we obtain equation (4.19), which, in addition to equations (4.16) and (4.18), must be satisfied in the determination of c_1 and p_A by iteration: /143

$$c_1 = c'_A - K_V \cdot \frac{\dot{m}_{E1}}{\dot{m}_A} \cdot ABS (c'_A - c_{E1}) + \frac{A_A \cdot p_A}{\dot{m}_A} - \frac{A_{E1} \cdot p_{E1}}{\dot{m}_{E1}} \qquad (4.19)$$

The fact that static pressures p_{E1} and p_{E2} at the mixing chamber inlet can be unequal -- this occurs if critical or supercritical flow states exist -- is taken into consideration in subroutine MISCH. Iteration is conducted in such a manner, moreover, that the stable subsonic solution for the mixture always occurs.

4.6. Combustion Chamber

The requirements placed on the combustion chamber are less severe for hydrogen combustion than in the conventional use of kerosene. The fuel, in gaseous form, and the high reaction velocities simplify mixture preparation and result in extremely short combustion lengths. This reduces cooling problems and the cost of producing the combustion chambers themselves, as well as the engine rotor. Due to the relatively small structural volume of the afterburner chamber and the possibility of cooling it with hydrogen, it is possible to achieve high heating temperatures. In contrast to the ramjet, moreover, values for the inlet temperature of the combustion gas, for flow Mach numbers and, if the flight profile is properly selected, also for combustion chamber pressure remain almost constant in the afterburner chamber of the turbojet.

Heat input in a first combustion chamber, e.g. the main combustion chamber of a turbojet or the rocket combustion chamber of the turborocket, can easily be calculated with program TCADI, previously written. Since combustion temperature is generally given initially, the required fuel/air or fuel/oxygen ratio must be determined by iteration. /144

At the inlet to a second combustion chamber, i.e. the afterburner chambers of the turbojet, the turborocket or combination engines, the individual reaction products from the first combustion chamber are already present in the combustion gas. In order not to inflate the reactant side of equation (3.32) unnecessarily for second-combustion calculations, the two combustion chambers were combined in a model to form one equivalent combustion chamber.

This is shown in Fig. 4.20 for a turbojet with afterburning. /145
The different changes in enthalpy between states 1t and 4bt are replaced by a single change of state (dashed curve). Airflow $\dot{m}_L$ with enthalpy at point 1t and the two fuel flows $\dot{m}_{BC}$ and $\dot{m}_{BPC}$ with each of their enthalpies are fed into the "equivalent combustion chamber." Pressure p_{t4b} and degree of burnup η_{PC} are known for the end of the combustion chamber. Although the values for η_C and η_{PC} differ in the normal case, it is permissible to describe combustion losses in this form, since gas temperatures once more exceed the "freezing points" of the chemical reactions during afterburning.

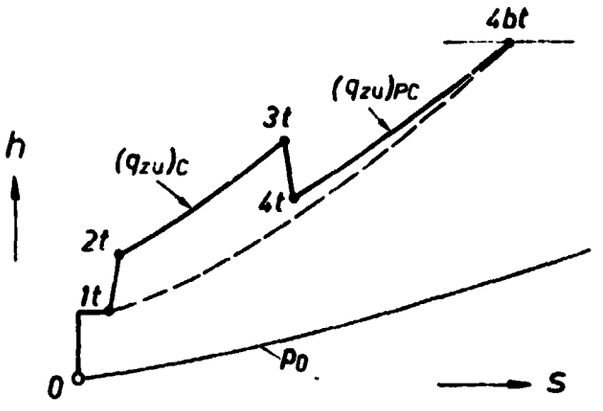

Fig. 4.20. Equivalent combustion chamber.

The combustion chambers of the turbo-rocket and the "ram-rocket" can be considered together in a corresponding manner. It is sufficient to stipulate mass flow ratios $\dot{m}_{H_2}/\dot{m}_{O_2}$, $\dot{m}_{H_2}/\dot{m}_{air}$ and $\dot{m}_{O_2}/\dot{m}_{air}$ to cover the oxidizers O_2 and air now occurring simultaneously.

Since the program TCADI was designed for the general case of adiabatic combustion, it is also possible to consider the fact that power is also removed from the system, e.g. to cover the power requirements of auxiliary drive units.

The quantities of heat which are removed from the combustion gas between the compressor inlet and the afterburner chamber outlet and are transferred to hydrogen in the oil cooler, in the heat exchanger for the intermediate cooling of turbine cooling air, and during cooling of the afterburner chamber need not be determined separately. They are not included in the combustion calculations as adiabatic heat flows if we assume, for the equivalent combustion chamber model, that the hydrogen has been heated from its tank condition to its temperature at the inlet to the combustion chamber only through the absorption of heat in the main heat exchanger and during intake cooling. /146

In calculating final combustion temperature, it is necessary to see that combustion gas composition at the end of the combustion chamber always corresponds to the static state variables existing there. Thus static temperature T_{4b} for the afterburner chamber of a combination engine, for example, is more than 200 K below total temperature T_{t4b}, since flow Mach numbers M_{4b} assume quite high values in certain ranges of flight. Neglecting this fact would cause an appreciable error in the calculation of total temperature at the end of the combustion chamber.

For this reason, the provisional values for total pressure drop Δp_{tPC} and flow Mach number M_{4b} are determined after the initial quasi-static determination of T_{t4b}. The static state change in the combustion chamber can then be calculated, the difference in kinetic energies[1] $(c_{4b}^2 - c_1^2)/2$ being taken into consideration as additional energy removed adiabatically.

[1] [Translator's note: literally, "velocity energies"]

The overall pressure drop in the main combustion chamber, which consists of an hydraulic and a thermodynamic component, can be represented with sufficient accuracy with the equation

$$\frac{p_{t3}}{p_{t2}} = 1 - \left(\frac{\dot{m}_L \cdot T_{t2}}{p_{t2} \cdot A_2}\right)^2 \cdot R \cdot \left[\zeta_{hyd} + \zeta_{th} \cdot \left(\frac{T_{t3}}{T_{t2}} - 1\right)\right] \qquad (4.20)$$

where $\zeta_{hyd} = 0.33$ and $\zeta_{th} = 0.02$ are empirical loss coefficients [34]. /147

The hydraulic loss component can be determined with a similar formulation for finding total pressure loss in the afterburner chambers of the different types of engines. On the other hand, it is advisable to determine thermodynamic pressure drop exactly, due to the sometimes high Mach number level at the combustion chamber outlet.

A subroutine DPPC was written for this purpose which, starting with combustion chamber conditions known concretely -- i.e. not for the "equivalent combustion chamber" -- calculates the static and total state variables T_A, p_A and p_{tA} and flow Mach number M_A at the combustion chamber outlet. The required inlet data are provided by subprogram MISCH, which represented the reaction-free mixing of mass flows. Provisional total temperature T_{tA} at the combustion chamber outlet is determined with TCADI for the "equivalent combustion chamber." It must be improved by iteration with the results from DPPC.

The fact that specific heat and the isentropic exponent change between the combustion chamber inlet (plane E) and the combustion chamber outlet (plane A) was taken into consideration in calculating the thermodynamic total pressure drop. The gas constant and molar mass also vary with combustion gas composition, of course.

The equations for cylindrical combustion chamber calculations under these conditions are presented below.

-- Conservation of mass:

/148

$$A_E \cdot \frac{p_E}{R_E \cdot T_E} \cdot M_E \cdot \sqrt{\kappa_E \cdot R_E \cdot T_E} = A_A \cdot \frac{p_A}{R_A \cdot T_A} \cdot M_A \cdot \sqrt{\kappa_A \cdot R_A \cdot T_A}$$

yields the ratios of static temperatures and sonic velocities

$$\frac{T_A}{T_E} = \frac{\dot{m}_A}{\dot{m}_E} \cdot \frac{k_A \cdot p_A^2 \cdot M_A^2}{k_E \cdot p_E^2 \cdot M_E^2} \qquad (4.21)$$

$$\frac{a_A}{a_E} = \frac{k_A \cdot p_A \cdot M_A}{k_E \cdot p_E \cdot M_E} \qquad (4.22)$$

with $k_A = f(T_A)$ from CPBG.

-- Energy equation:

$$h_{tA} = h_A + \frac{(M_A \cdot a_A)^2}{2}$$

yields

$$\frac{T_{tA}}{T_A} = 1 + \frac{k_A - k_A/\bar{k}}{2} \cdot M_A^2 \qquad (4.23)$$

where $\bar{k}$ = mean between T_A and T_{tA}.

Equations (4.21) and (4.23), when substituted in

$$\frac{T_{tA}}{T_{tE}} = \frac{T_{tA}}{T_A} \cdot \frac{T_E}{T_{tE}} \cdot \frac{T_A}{T_E}$$

and solved for M_A, yield

$$M_A = \left(-\frac{1}{2 \cdot A} + \sqrt{\frac{1}{4 \cdot A^2} + \frac{C}{A \cdot B}}\right)^{1/2} \qquad (4.24)$$

where /149

$$A = \frac{k_A - k_A/\bar{k}}{2} \; ; \; B = \frac{T_E}{T_{tE}} \cdot \frac{\dot{m}_A}{\dot{m}_E} \cdot \frac{k_A \cdot p_A^2}{k_E \cdot p_E^2 \cdot \gamma_E^2} \; ; \; C = \frac{T_{tA}}{T_{tE}}$$

-- Conservation of momentum:

$$\dot{m} \cdot (c_A - c_E) + A \cdot (p_A - p_E) + F_R = 0$$

If we set $F_R = A \cdot \Delta p_{t\,hyd}$ and divide by A, we obtain

$$\frac{p_E}{R_E \cdot T_E} \cdot \kappa_E \cdot M_E^2 \cdot \left(\frac{c_A}{a_E} \cdot \frac{a_A}{a_E} - M_E\right) + p_A - p_E + \Delta p_{t,hyd} = 0$$

Substituting equation (4.22) and dividing by p_E yields

$$\frac{p_A}{p_E} = \frac{(1 - \Delta p_{t,hyd}/p_E) + \kappa_E \cdot M_E^2}{1 + \kappa_A \cdot M_A^2} \qquad (4$$

The mutually coupled equations (4.21) through (4.25) must be solved by iteration and $p_{tA} = f(T_A, T_{tA}, p_A)$ finally determined from ISENTB.

In conclusion, it should be noted that the cross sections which must be made available to the flow of gaseous hydrogen at the combustion chamber inlets remain within unproblematical limits in spite of the extremely low density of hydrogen. Due to the high sonic velocity, usable mass flow densities are feasible. Numerical values for the required cross section ratios A_{H_2}/A_{air} correspond approximately to the numerical values for β.

4.7. Nozzle

/150

Like the intake, the nozzle is an important structural component of air-breathing engines for high flight Mach numbers. This also applies with regard to its contribution to the weight of the entire engine system.

In contrast to the ramjet, in which the narrowest nozzle cross section A_5^* must be adjusted over a wide range (by a factor of about 15 or 20 between $M_0 = 2$ and $M_0 = 7$), it can remain almost unchanged in the turbojets under consideration. The expansion ratio for the supersonic portion of the nozzle and thus nozzle end cross section A_5, which preferably assumes the maximum available cross section in the upper flight Mach number range, must nevertheless be designed smaller for lower flight Mach numbers to adapt to the pressure ratio existing in each case. The admixture of bypass air in the nozzle reduces not only the added drag of the intake but also the external drag of the nozzle in this flight Mach number range by filling out the excess cross section and preventing the occurrence of "base pressure." A schematic of the plane nozzle with variable bypass contour is shown in Fig. 4.21.

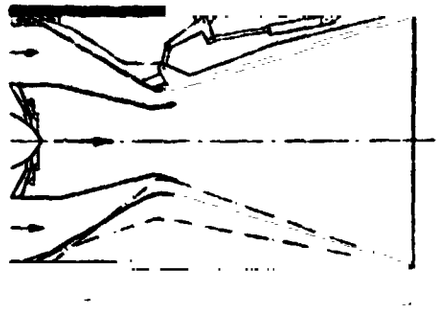

Fig. 4.21. Nozzle with variable bypass contour.

Program segment DUESE was written to calculate the thermodynamic state changes and geometric dimensions, making use of subroutine EXPAN, already mentioned. Throat cross section A_5^* for the convergent/divergent nozzle is first determined as the cross section of maximum mass flow density, and flow velocity c_5^* and the static state variables occurring within it are determined. In the subsequent calculation of expansion in the divergent section of the conical nozzle, losses due to wall friction and heterogeneity are covered with a nozzle efficiency; divergence losses at the nozzle outlet, with a corresponding divergence factor. /151

Since the problems of jet mixing are not a topic of these studies, multidimensional calculations for the divergent portion of the nozzle taking the effect of mixing on velocity and temperature profiles in the various nozzle planes into consideration have been dispensed with.

Complete mixing can in no case be assumed, due to the shortness of the mixing length available. For this reason, it was assumed for calculations for the other limiting case that the limiting flow area between the hot gas jet and the "admixed" bypass air can be considered completely adiabatic. The two gas flows expand side-by-side to the same final nozzle pressure p_5, at which they jointly fill out the available end cross section A_5. /152 This neglects the slight gain in thrust which results from the admixture of a low-energy bypass jet, which in the present case only occurs in the lower flight Mach number range anyway.

The program is set up in such a manner that nozzle end pressure p_5 and nozzle end cross section A_5 can be specified. It also allows total expansion to be calculated either with frozen combustion gas composition or with labile chemical equilibrium, as desired. It is possible, moreover, to represent the actual expansion curve between these conceivable limiting cases almost exactly by calculating expansion up to a selected cross section A_e with labile chemical equilibrium and assuming frozen combustion gas composition downstream from A_e.

During expansion, equilibrium composition shifts toward more complex components. According to Bray [31], we obtain results which agree well with reality if we assume that chemical equilibrium, e.g. in a reaction in which H_2O is produced, is maintained as long as the absolute rate r_b of H_2O formation is greater than the excess production r_{GG} of H_2O per second which must be achieved from all reversible sub-reactions in order to maintain equilibrium.

H_2O production is considered representative for determining the "freezing" cross section A_e, which under the conditions at hand lies in the divergent section of the nozzle. The rate of formation $(r_b)_{H_2O}$ and the rate of change of equilibrium production $(r_{GG})_{H_2O}$ are calculated stepwise for the different nozzle planes, starting from the throat cross section, and compared with one another. /155

Fig. 4.22 shows area ratio A_e/A_5^* for the combustion gas H_2/air as a function of fuel/air ratio β/β_{st} for an application in which total temperature and total pressure have constant values at the nozzle inlet. These are obtained with the different β values at the specified flight Mach numbers and associated altitudes.

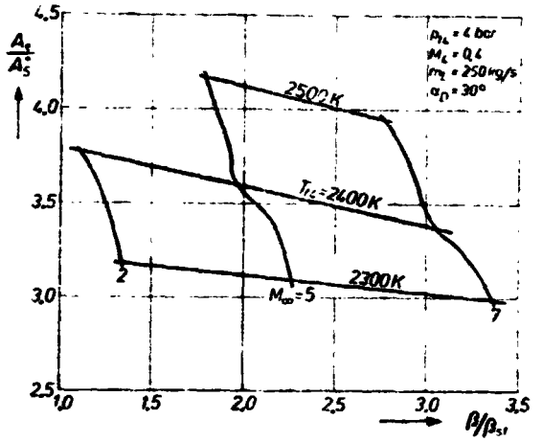

Fig. 4.22. Location of the "freezing" cross section.

It is found that a constant position can be assumed for the freezing cross section in these expansion calculations (T_{t4} = 2400 K) which lies near the nozzle end cross section, at about A_e/A_5^* = 3.5.

The unusually high value of A_e/A_5^* relative to the situation in an average rocket nozzle is explained by the size of the throat cross section -- and thus the large nozzle length for a given area ratio and aperture angle -- and the relatively low critical flow velocity. Thus the change in combustion gas composition with time which would be necessary for equilibrium flow is also relatively small, taking the low temperature level into consideration. /156

It should also be pointed out that the difference in thrust found between the two limiting cases of expansion under the conditions at hand averages about 3 to 4%.

5. Preliminary Design for a Turbojet with Air Precooling Prior to Compression for Propelling a Space Vehicle Carrier /157

The preliminary design for a turbojet with precooling that would serve as the power plant for the aerodynamic booster stage of a space vehicle carrier is presented below.

5.1. Requirements and Conditions

The goal of this project is an uncomplicated engine design. The power plant is supposed to be suitable for accelerating the booster stage from takeoff to a flight Mach number of $M_\infty = 7$ and for returning it economically. As far as possible, technological requirements should not exceed the norm achieved in present-day aviation engine construction. For this reason, for example, a drastic increase in temperature level in the combustion chambers is ruled out, and the possibility of also extending the flight Mach number range covered through direct cooling of the entire compressor blade system -- as well as the turbine blade system -- with the hydrogen used as fuel is intentionally dispensed with.

Performance calculations are based on the DIN standard atmosphere. The flight profile outlined in Fig. 5.1 has been assumed for the booster's flight path. The curve [3], relatively high for accelerated flight, does not cause maximum pressure in the afterburner chamber to rise beyond 6 bars. It also causes the wing angle of attack to assume the values given in Fig. 4.9 in the upper flight Mach number range, which cause the scoop cross section of the intake to increase by an appropriate degree (Fig. 4.10). The fact that the vehicle's drag does simultaneously increase here must be taken into consideration in optimization of the flight path, which will not be undertaken within the scope of these studies, however. /156

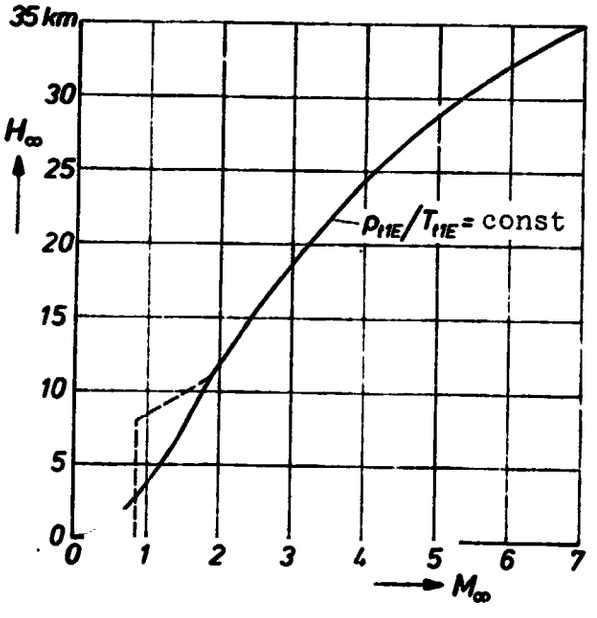

Fig. 5.1. Flight profile.

The flight profile was designed so that a constant value for the ratio p_{t1}/T_{t1} always exists at the intake outlet. Although the booster would preferably first follow something like the dashed curve in the flight profile after takeoff, all calculations are based on the solid flight profile curve even below $H_\infty = 11$ km, so that the curves calculated are more easily comprehended. /157

It is assumed that the four-shock intake shown in Fig. 4.8 is located behind the oblique shock wave propagating at the leading edge of the wing. Taking the variable angle of attack of the wing which

aerodynamic calculations for the propelled vehicle yield into consideration, the curve of total pressure ratio shown in Fig. 4.12 is obtained for the intake.

The heat exchanger is to be designed and regulated in such a manner that the flow of hydrogen is not heated to temperatures above $T_{H_2,max}$ = 1050 K even in the upper flight Mach number range. As a result, the hydrogen can still be used after it leaves the heat exchanger to effectively cool the afterburner chamber, the hot portion of the thrust nozzle and, at high flight Mach numbers, the adjustable nozzle also, without wall temperatures appreciably exceeding 1200 K in the process.

The inlet cross section of the compressor is always taken to be A_1 = 1 m^2 for calculations. The compressor pressure ratio has been limited to the ground value $(\pi_{tV})_{AP}$ = 7 so that the turbine can be designed with one stage. Numerical values for pressure ratio, relative mass flow and compressor efficiency, which vary continually during flight, are taken from the generalized performance graph shown in Fig. 4.16 and plotted over reduced rpm in Fig. 5.2.

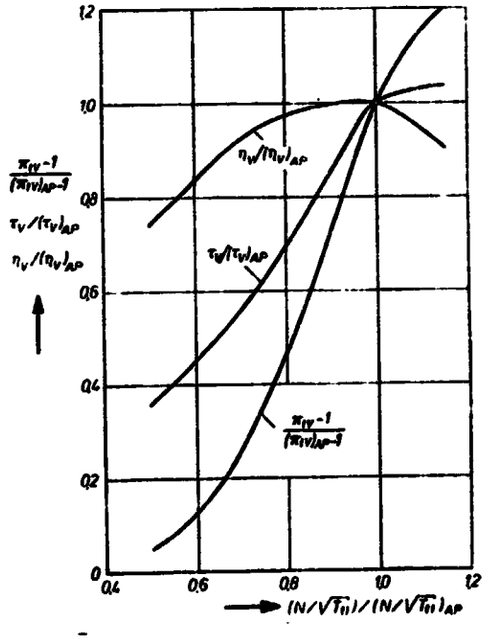

Fig. 5.2. Pressure ratio, relative mass flow and compressor efficiency for deviation from design starting point.

The calculations are based on standard averages for the design efficiencies of the compressor, turbine and thrust nozzle: /158

$$(\eta_V)_{AP} = 0.89; \quad \eta_T = 0.88;$$

$$\eta_D = 0.95$$

The efficiencies given describe the polytropic static changes of state. Their numerical values correspond approximately to total isentropic efficiencies η_{Vts} = 0.86 and η_{Tts} = 0.9.

Flow Mach numbers at the inlets and outlets of the different components were assumed to be the following for the design starting point: /159

	M_E	M_A
Compressor	$M_1 = 0.55$	$M_2 = 0.3$
Turbine	$M_3 = 0.3$	$M_4 = 0.4$
Afterburner	$M_{4a} = 0.25$	

Designations for engine planes can be found in Fig. 2.10.

Inlet temperature for the cooled turbine, $T_{t3} = 1800$ K, lies within the range of mean turbine inlet temperatures which are presently manageable in test stand operation. The cooling air required for turbine cooling is cooled intermediately to a constant value of $T_{KL} = 500$ K by heat exchange with the flow of fuel, so T_{t3} can be kept at the specified value regardless of the existent compressor outlet temperature T_{t2}, which increases with flight Mach number.

Maximum permissible heatup temperature in the afterburner chamber could be increased by about 300 K relative to the present standard, to $T_{tmax} = 2400$ K, for reasons mentioned above. While a combustion efficiency of $\eta_C = 0.98$ is expected for the main combustion chamber, it is assumed to be $\eta_{PC} = 0.95$ at the end of afterburning.

Calculation of the actual expansion curve in the thrust nozzle was approached with the Bray criterion.

In order to be able to determine the effect of precooling on the thrust/weight ratio, it is necessary to estimate required engine system weight. /160 While heat exchanger calculations yield the inherent weight of the heat exchanger, engine weight itself is determined roughly by a statistical method which appears suitably precise for comparison purposes. It is based on a reference engine and takes the way in which the inherent weight of individual components vary relative to the reference engine into consideration. Due to the different maximum flight Mach numbers of the engines compared, it is desirable not to consider the intake here. The higher thermal loads, particularly on the compressor, relative to present-day aircraft power plants are covered.

The reference engine is a turbojet in a single-shaft configuration with the following design data ($M_\infty = 0$; $H_\infty = 0$):

Reference Engines:

$$\pi_{tV,B} = 10; \quad T_{t3,B} = 1400\ K; \quad \dot{m}_{L,B} = 100\ kg/s$$

$$\Delta h_{tV,B} = \Delta h_{tT,B} = 320\ kJ/kg$$

On the basis of the statistical evaluation of turbojets which have been built, a value of

$$\left(\frac{\dot{m}_M}{\dot{m}_L}\right)_B = 18\ \frac{kg}{kg/s}$$

can be taken for the weight of the reference engine relative to airflow.

The following distribution of engine weight is assumed among the components of the reference engine:

$\mu_V = 0.50$	compressor	incl. housing, bearings, bearing flanges, shafts and coupling
$\mu_T = 0.33$	turbine	
$\mu_C = 0.07$	combustion chamber with injection system and lines	
$\mu_D = 0.05$	nozzle (adjustable)	
$\mu_R = 0.05$	regulators, auxiliary units (pumps, starters, oil ccolers, etc.)	
$\Sigma = 100\%$		

/161

An additional weight of

$$\mu_{PC} = 0.2 \cdot \left(\frac{A_{4_B}}{1.2 \cdot A_1}\right)^{3/2} \qquad (5.1)$$

is to be used for an afterburner; when H_2 is used for fuel, this is reduced to about 2/3 of the specified value.

The weights of the compressor and turbine naturally depend, via the numbers of stages, upon the pressure ratios or power conversions in these assemblies. This effect is covered by the factors

$$\nu_V = \frac{\Delta h_{tV}}{\Delta h_{tV,B}} \cdot \frac{T_{t1,B}}{T_{t1}}^{2/3} \qquad (5.2)$$

$$\nu_T = \frac{\Delta h_{tT}}{\Delta h_{tT,B}} \cdot \frac{T_{t3,B}}{T_{t3}}^{3/2} \cdot \left(\frac{\pi_{tV,B}^{-1}}{\pi_{tV}^{-1}}\right)^{1/3} \qquad (5.3)$$

wherein all thermodynamic quantities apply to the design starting point on the ground at a standstill.

From the relationship

$$\frac{\dot{m}_W}{\dot{m}_L} = (\mu_V \cdot \nu_V + \mu_T \cdot \nu_T + \mu_C + \mu_D + \mu_R + \mu_{PC}) \cdot \left(\frac{\dot{m}_M}{\dot{m}_L}\right)_B \cdot \frac{p_{t1,B}}{p_{t1}} \sqrt{\frac{T_{t1}}{T_{t1,B}}} \qquad (5.4)$$

we can now determine specific engine weight, whose value must also be supplemented with the weight contribution of the heat exchanger ($m_{WT}/\dot{m}_L = 4.5$) in the case of the turbojet with precooling. /162

5.2. Engine Configuration and Design of Components

Fig. 5.3 shows an overview drawing of the engine configuration.

Fig. 5.3. Overview of turbojet with precooling.

It is desirable to mount the engine under the wing. The plane four-shock intake is designed with a variable geometry and is dimensioned in such a manner that it is approximately matched to engine air requirements in the highest flight Mach number range. Since it thereby receives a larger flow of air at Mach numbers below $M_\infty \approx 4$ than the turbojet engine requires, a portion of the compacted air is led around the turbo section in a bypass in the lower flight Mach number range and is expanded along with the hot gas in the common thrust nozzle. The magnitude of the bypass flow is adjusted via the regulatable "cold" thrust nozzle so that the intake is always in critical operation.

Above $M_\infty \approx 4$, the turbojet's air requirements exceed the air supplied by the intake. The bypass is now closed by suitably positioning the nozzle and gates. In order to avoid "supercritical" operation of the intake, with the associated high pressure drops, rotor rpm must also be reduced continually beyond $M_\infty \approx 4$. The /163

intake is also cooled with hydrogen beyond this flight Mach number to counteract the high temperatures of the compacted air. Ablation cooling does not come under consideration here, due to the danger of fouling the heat exchanger and engine.

The heat exchanger, which operates by the countercurrent principle, is set up in such a way that the inflow of hydrogen can be distributed between two axial planes, as a result of which the exchanged heat and thus the maximum temperature to which the hydrogen is heated can be controlled and limited.

The scooped-in flow of air is fed to the six-stage compressor via an adapter with a convergent channel structure in which the transition takes place from a square to circular cross section. Its short structural length, in conjunction with the short combustion chamber and the single-stage turbine, permits very rigid construction and simple suspension of the undivided rotor.

Behind the short afterburner chamber, in the convergent portion of the "hot" thrust nozzle, a transition occurs from the rotationally symmetrical turbo section to the plane nozzle of variable geometry. Its end cross section corresponds to the maximum cross section of the overall engine $A_{max} = 1.2 \cdot A_e$, which exceeds the scoop cross section of the intake by 20%.

5.3. Effect of Precooling on the Thermodynamic Cycle

/164

The effect of precooling on temperatures T_{t1} at the compressor inlet is shown in Fig. 5.4.

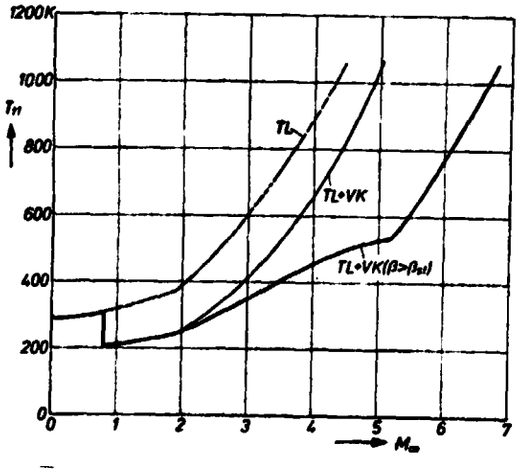

Fig. 5.4. Effect of precooling on temperatures at the compressor inlet.

During takeoff and initial climb, precooling of the air must be dispensed with because the danger of heat exchanger icing exists at low altitudes, below about H_∞ = = 8 or 10 km (depending upon weather conditions), due to the absolute humidity which occurs there. In accordance with the stylized flight profile in Fig. 5.1 (dashed), it is assumed that the carrier system climbs to about H_∞ = 8 km, for example, in high subsonic flight and accelerates through the transonic Mach number range to $M_\infty \approx 2$

at almost constant altitude after the initiation of precooling. /165
$M_\infty = 0.8$ can serve as the changeover point to operation with precooling for the calculations based, for the reason already mentioned, upon the solid curve for the flight profile.

In Fig. 5.4, the dashed curve indicates temperature T_{t1} at the compressor inlet in the turbojet without precooling. In practical terms, it corresponds to stagnation temperature $T_{t\infty}$. The break at $M_\infty \approx 2$ results from the fact that ambient temperature T_∞ has decreased with increasing altitude H_∞ up to this point. At $M_\infty \approx 2$, $H_\infty = 11$ km is reached and ambient temperature now remains approximately constant. The fact that T_∞ increases slightly again beyond $H_\infty = 20$ km and even somewhat more steeply beyond $H_\infty = 32$ km, according to the DIN standard atmosphere, is not visible in the curves.

The solid curves show the decrease in compressor inlet temperature due to precooling. The supply of fuel to the afterburner chamber and thus the values of fuel/air ratio β are regulated up to $M_\infty \approx 2$ in such a manner that under these conditions, the maximum combustion temperatures are obtained in each case at the end of the afterburner. Maximum permissible temperature $(T_{t4b})_{max} = 2400$ K is finally reached at $M_\infty \approx 2$. In order for this value not to be exceeded, either the fuel/air ratio must continually be further reduced as stagnation temperature $T_{t\infty}$ rises further (light solid curve), or final combustion temperature must be limited by combustion with a suitably high excess of fuel (heavy solid curve). Since different coolant flows exist in the different fuel flows, the outlined difference in the temperature drop, which becomes more and more distinct with increasing flight /166
Mach number, is obtained for the two types of operation.

The curve for $\beta > \beta_{st}$ has an upward break at about $M_\infty \approx 5$, since the flow of hydrogen heated in the heat exchanger has reached its upper temperature limit here. Nevertheless, the drop in compressor inlet temperature and thus the possibility of extending the flight Mach number range are particularly conspicuous for this case.

Fig. 5.5 shows how the fuel/air ratios must vary with flight Mach number in order that the maximum permissible value for final combustion temperature $(T_{t4b})_{max}$ is not exceeded.

The effect of precooling on temperature T_{t2} at the compressor outlet is shown in Fig. 5.6. The upper temperature limit /167
$(T_{t2})_{max} = 1200$ K, which was determined as a criterion for the feasible limiting flight Mach number, is first reached at about $M_\infty \approx 7$, rather than at $M_\infty \approx 4.5$.

Due to the drop in compressor inlet temperature (Fig. 5.4), reduced rpm $N/\sqrt{T_{t1}}$ and thus relative mass flow density τ_V at the compressor inlet assume higher values (Fig. 5.7).

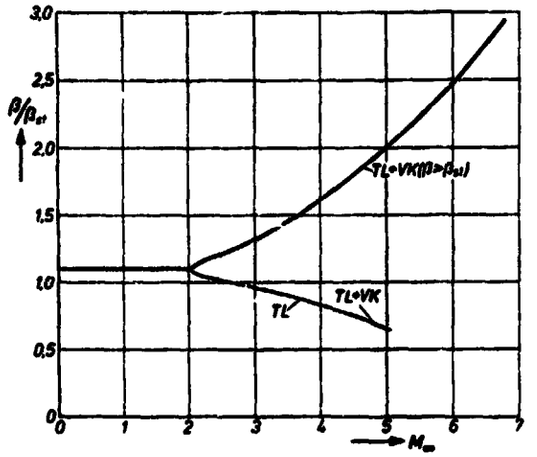

Fig. 5.5. Curves of fuel/air ratios.

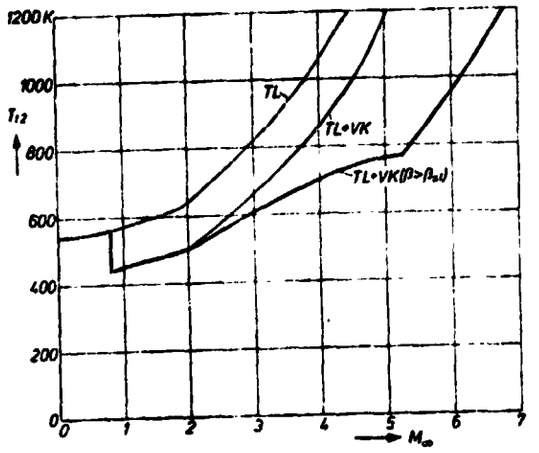

Fig. 5.6. Effect of precooling upon temperatures at compressor outlet.

The appreciable increase in the air mass flow received by the engine, which makes up the major portion of the increase in thrust due to precooling, is shown in Fig. 5.8. As a first approximation, natural air mass flow $\dot{m}_L$ is inversely proportional to compressor inlet temperature.

Since the flow of air in the turbojet with precooling is already flowing through the heat exchanger even while no heat is yet being exchanged with the flow of hydrogen, it is still subject to the heat exchanger pressure drops. Thus mass flow density at the compressor inlet in the turbojet with precooling below $M_\infty = 0.8$ is lower than is the case in the same turbojet engine without the heat exchanger upstream from it, i.e. without precooling. /169

The curves of total pressure drop in the air passing through the heat exchanger are plotted over flight Mach number in Fig. 5.9.

The fact that not only the flow of air received but also specific thrusts are increased by air precooling is a direct result of the increase in compressor pressure ratio without a corresponding increase in pressure drop in the turbine -- the specific power required by the compressor remains approximately constant. This becomes apparent in an increase in pressure ratio p_{t4}/p_{t1E} which the overall turbo section builds up (Fig. 5.10). /170

Here, p_{t4} is total pressure downstream from the turbine, and p_{t1E} is total pressure at end of intake, i.e. upstream from the

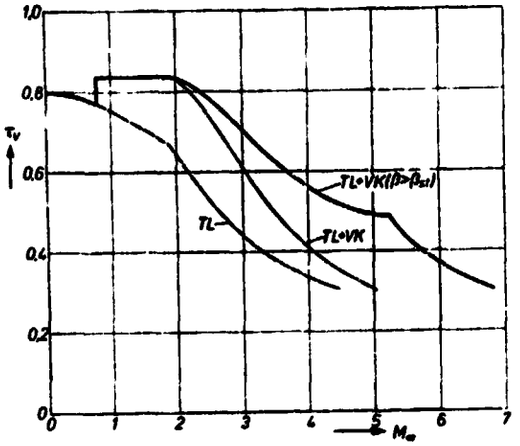

Fig. 5.7. Effect of precooling upon relative mass flow density at compressor inlet.

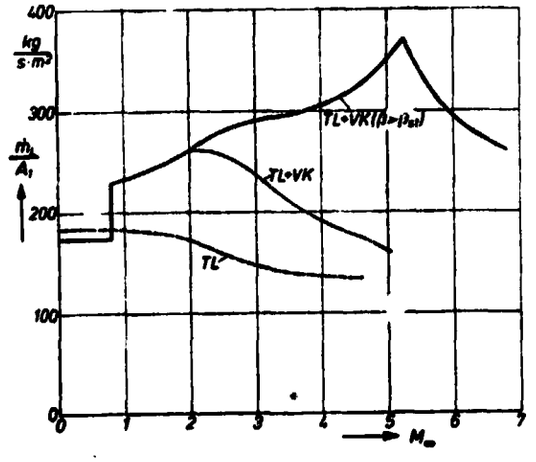

Fig. 5.8. Effect of precooling on mass flow density at compressor inlet.

heat exchanger. For reasons described above, the curve for the turbojet with precooling is initially below that for the turbojet engine without precooling.

The effect of precooling on the curves for compressor pressure ratio π_{tV} is shown in Fig. 5.11. The unusually high values for the compressor pressure ratio in the medium and high flight Mach number range correspond to the temperature ratio T_{t3}/T_{t1} for the turbo section. This can be seen from Fig. 5.12. The effect of the compressor pressure ratio on the magnitude of turbo section pressure ratio p_{t4}/p_{t1E}, which in addition to heatup temperature T_{t4b} and inlet pressure ratio p_{t1E}/p_o is of decisive importance for the magnitude of specific thrusts σ_L and σ_B (cf. pp. 7 ff), is shown here. /171

The pressure ratio selected, $(\pi_{tV})_{AP} = 7$, proves to be a suitable compromise value, particularly when we consider the simple design and the weight of the turbo section (e.g. single-stage turbine). The ratio of thrust to engine weight exhibits distinctly poorer values for $(\pi_{tV})_{AP} = 10$ over the entire range of flight Mach numbers. The slight advantage in the lower pressure ratio $(\pi_{tV})_{AP} = 5$ at the upper flight Mach numbers does not counterbalance the disadvantage in the lower Mach number range (Fig. 5.12).

5.4. Analysis of the Engine's Performance /172

In this section, the performance of the turbojet with precooling will be determined and the effects of precooling will be

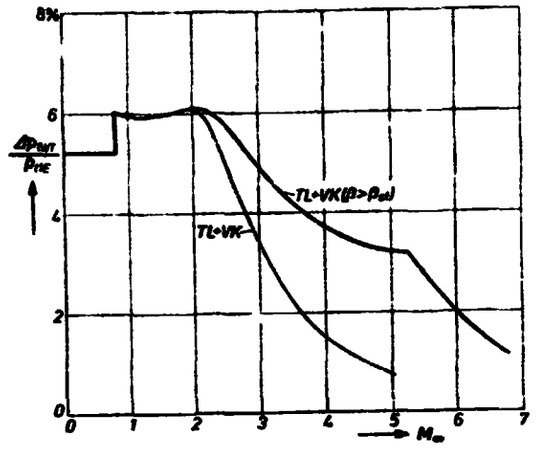

Fig. 5.9. Total pressure drop in heat exchanger.

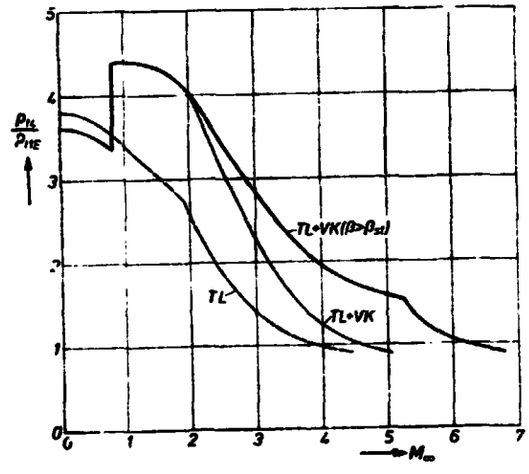

Fig. 5.10. Effect of precooling on the total pressure ratio built up by the turbo section.

shown by a comparison with performance data obtained with the same engine without heat exchanger. Specific thrusts $\sigma_L = F/\dot{m}_L$, $\sigma_B = F/\dot{m}_B$ and $c_G = f/(m_M \cdot g_c)$ are studied as characteristic values for assessment.

In order to eliminate the effect which the type of engine installation has on the magnitude of thrust, the engine is considered here as removed from the airframe or pod. Thrust is determined as gross thrust, without considering external drags. Since wing precompression is absent, the calculation of total pressure ratio $\pi_{tE} = p_{t1}/p_{t\infty}$ is based on the ideal plane four-shock intake (cf. Fig. 4.12). Otherwise, it is assumed that the intake covers the air requirements of the engine in each case and that a maximum nozzle end cross section of $A_{5max} = 4 \cdot A_1$ is available for expansion in the thrust nozzle. /173

Figs. 5.4 through 5.12 in the preceding section were also computed under the above conditions.

The curves for thrust relative to airflow, $\sigma_L = F/\dot{m}_L$, is shown in Fig. 5.13 for the engine with and without precooling.

This figure makes it apparent that more than a considerable extension of the flight Mach number range covered is made possible by a superstoichiometric supply of fuel to the afterburner chamber; the pronounced rise in specific thrust σ_L at high flight Mach numbers also eliminates the necessity of having to receive an undesirably high airflow in order to deliver the required thrust. This would cause the size of the intake, which determines the magnitude of airflow in the upper flight Mach number range, to /174

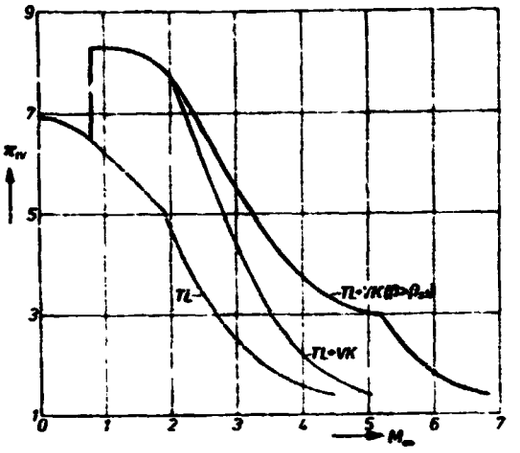

Fig. 5.11. Effect of precooling on the curve of compressor pressure ratio.

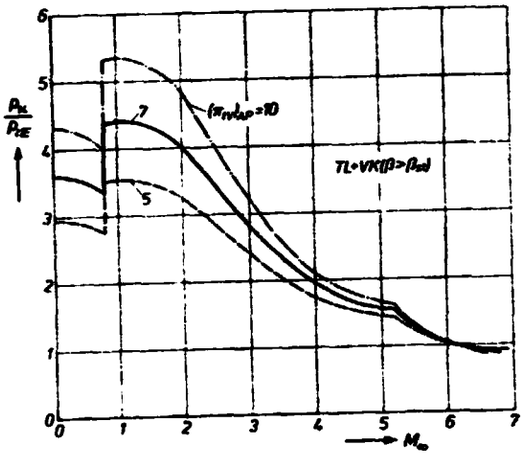

Fig. 5.12. Effect of compressor pressure ratio on the total pressure ratio built up by the turbo section.

be increased undesirably with regard to engine weight and drag in the transonic range (cf. p. 4).

Fig. 5.14 shows the curves for thrust relative to fuel flow, $\sigma_B = F/\dot{m}_B$, versus flight Mach number M_∞. While σ_B can be increased by almost 10% on the average by precooling with substoichiometric combustion, it drops to considerably lower values with superstoichiometric fuel feed. The advantage of greater thrust and the extended flight Mach number range must be bought with higher specific fuel consumption. This need not have negative effects on the total outlay required to satisfy the mission, however, as already mentioned (p. 20). /175

In addition to the precooler's effect on the total weight of fuel required for the propulsion phase, its effect on the engine's thrust/weight ratio is of decisive importance. Thrust relative to engine weight ($\sigma_G = F/m_M \cdot g_0$) is plotted over flight Mach number M_∞ in Fig. 5.15.

Engine mass m_M for the turbojet with precooling, which aside from the additional heat exchanger is identical to the reference turbojet without precooling, is indeed greater by the weight of the heat exchanger. Due to the higher thrusts above $M_\infty = 0.8$, however, this extra equipment weight is far more than compensated for. /176

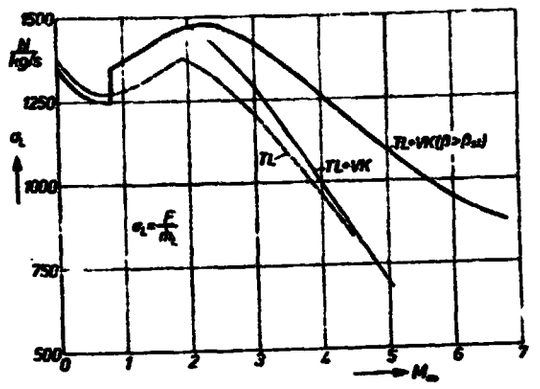

Fig. 5.13. Curves of thrust relative to airflow versus flight Mach number.

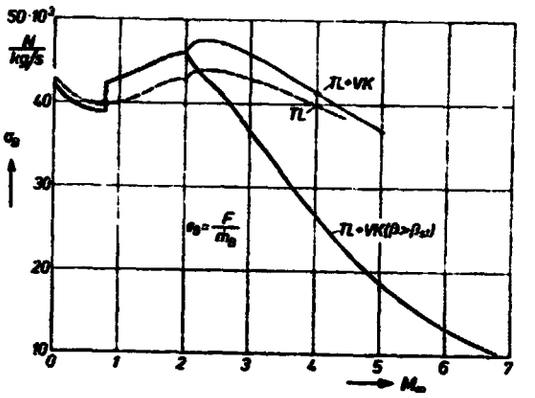

Fig. 5.14. Curves of thrust relative to fuel flow versus flight Mach number.

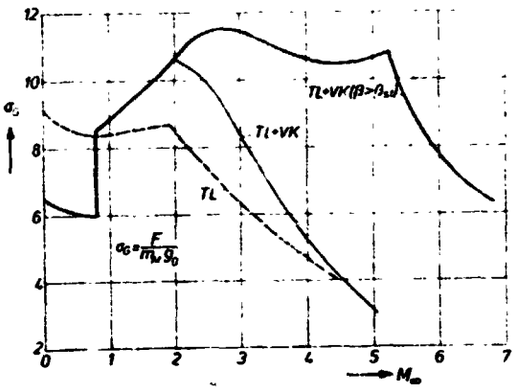

Fig. 5.15. Curves of thrust relative to engine weight versus flight Mach number

6. Comparison between the Turbojet with Precooling and Competing Engine Designs

/177

In the following, performance data for the turbojet with precooling will be compared with the corresponding data on comparable engine designs.

The engines compared are the turbojet with precooling, the turborocket with precooling and the ramjet combined with the turbojet, the turborocket, or the rocket. Schematics of the different engines are shown in Fig. 6.1.

/178

The goal of this comparison is to pick out the propulsion systems best suited to practical application in an aerodynamic space vehicle carrier and to determine the total outlay in fuel weight and engine weight for it, integrated over a given flight path. In order to allow a fair comparison, equivalent or corresponding values are assumed for component efficiencies, maximum heatup temperature and maximum intake scoop cross section for all engines. In addition, compressor inlet area is assumed to be the same for the turbo engines. In other respects, all comparable engines, which are best thought of as being mounted under the

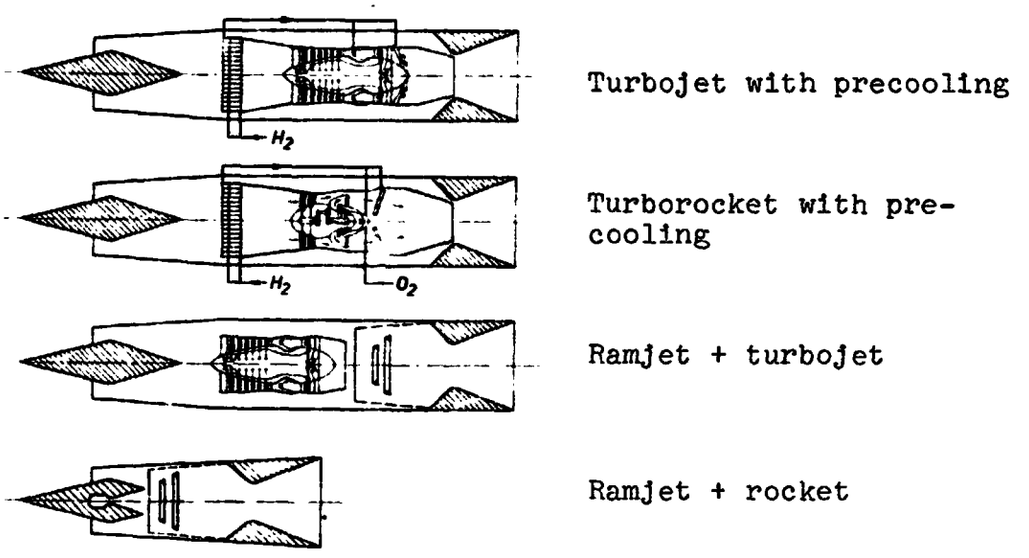

Fig. 6.1. Schematics of comparable engine designs.

vehicle's wing, have been analyzed on the basis of the same systematics and with the same computer program, in which only the portion used for gas generator calculations has had to be altered accordingly.

6.1. Performance Data for Turbojet with Precooling, Taking Installation Effects into Consideration

For the sake of clarity, installation effects have initially been neglected in determining the performance of the turbojet with precooling in Section 5.4. At this point, the performance parameters will now be presented taking the finite size of the intake scoop cross section, wing mounting and engine drags in external flow into consideration. In view of the enlargement ratio of the freestream scoop cross section due to wing precompression (cf. Fig. 4.10), the geometric scoop cross section A_E of the intake is dimensioned so that it can fully satisfy the air requirements of the turbojet with precooling up to about $M_\infty = 4$. Above this flight Mach number, the engine's air requirements are /179
are matched to the air supplied by the intake in each case by suitably reducing natural rotor rpm -- as the result of a drop in turbine inlet temperature. This drop in rpm is desirable anyway for strength reasons, since the temperature level of the compressor ultimately comes close to its technological limit with increasing flight Mach number.

A further reduction in rotor rpm through the corresponding limitation of heat fed to the main combustion chamber prevents reduced rpm $N/\sqrt{T_{t1}}$ from exceeding the design value by more than 15% if precooling becomes operant at $M_\infty = 0.8$. This reduction in rpm is also desirable for technical reasons, due to the extremely low compressor inlet temperatures.

The effect of wing precompression on inlet oncoming-flow Mach number M_0 and on total pressure ratio $p_{t1}/p_{t\infty}$ (cf. Figs. 4.11 and 4.12) is likewise taken into consideration in the graphs which follow.

Only flow-mechanics parameters in the pressure field under the wing are of interest in the calculation of engine thrust, but not vehicle speed c_∞ and ambient pressure p_∞. According to Fig. 6.2, the resultant force acting upon the control area in the direction of throughflow can be given as

$$F_{Rx} = \dot{m}_5 \cdot c_5 + A_5 \cdot p_5 - \dot{m}_0 \cdot c_0 - A_0 \cdot c_0 - (A_E - A_0) \cdot p_{1a} - (A_5 - A_E) \cdot p_h$$

The thrust acting against throughflow thus becomes /180

$$F = \dot{m}_L \cdot \left[(1+\beta) \cdot c_5 - c_0 \right] + A_5 \cdot (p_5 - p_0) - \left[\underbrace{(A_E - A_0) \cdot (p_{1a} - p_0)}_{D_z} + \underbrace{(A_5 - A_E) \cdot (p_h - p_0)}_{D_h} \right] \qquad (6.1)$$

where p_{1a} is static pressure downstream from the first oblique shock wave of the supersonic intake and p_h is static pressure on the intake cowling; p_h can be considered constant over the entire length of the cowling, with its non-zero angle of attack.

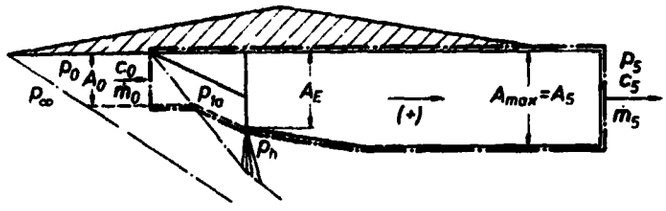

Fig. 6.2. Schematic for thrust calculations.

The external drag of the intake and engine pod are described with sufficient accuracy by added drag D_z and cowling pressure drag D_h. Since the underside of the pod can be looked upon as a lower-lying portion of the wing, the friction drags of the intake cowling and the pod need /181

not be attributed to the power plant. The friction contributions of the two side walls of the four to six engine pods, thought of as being combined in one unit, are neglected in this discussion.

Thrust equation (6.1) also applies to the case in which the engines project beyond the trailing edge of the wing, since p_0 is static pressure in the oncoming flow to the intake and not expansion backpressure at the downstream end. In other respects, internal bypass drag D_b is already included in equation (6.1); it is expressed in a reduction in the values of c_5 and p_5.

In Figs. 6.3 and 6.4, specific thrusts σ_L and σ_B are plotted over flight Mach number M_∞ for the turbojet with precooling as determined under the above conditions. Maximum heatup temperature in the afterburner chamber is again limited to T_{t4b} = 2400 K. Since the engine can be operated only up to about M_∞ = 5 in the case of substoichiometric combustion (thin curves), a superstoichiometric fuel supply to the afterburner chamber (heavy curves) is necessary if we intend to accelerate an aerodynamic space vehicle carrier to about M_∞ = 7 with this propulsion system. Due to the deterioration of fuel consumption, however, a transition to superstoichiometric operation is suitable only at flight Mach numbers which are rather far above those at which permissible combustion temperature is just reached. The most favorable transition Mach number can be obtained only from optimization of the entire flight program.

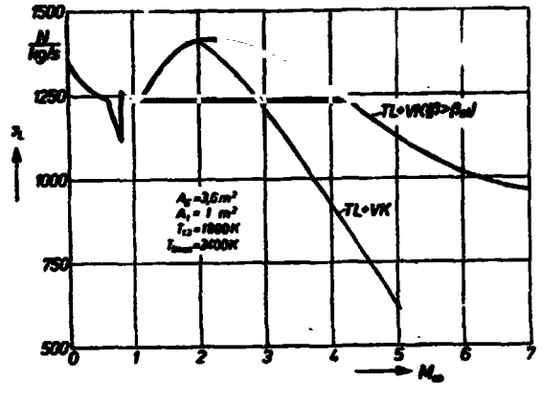

Fig. 6.3. Thrust of turbojet with precooling relative to airflow.

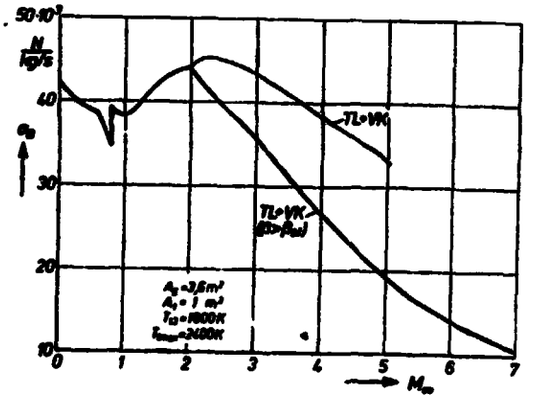

Fig. 6.4. Thrust of turbojet with precooling relative to fuel flow.

The fact that the stream of air fed to the engine is limited by the geometric scoop cross section A_E of the intake beyond about

$M_\infty = 4$ is of course hardly apparent in the curves for specific thrusts σ_L and σ_B. On the other hand, the curve of thrust (Fig. 6.5) exhibits a pronounced break at this point. From this flight Mach number on, the engine's air requirements must be matched to the air supplied by the intake by a drop in rotor rpm via a reduction in the fuel supply to the main combustion chamber. The decrease in T_{t3}, π_{tV} and η_V has negative effects on the useful pressure ratio p_{t4}/p_{t1E} of the turbo section. In order to keep this effect within limits, it is therefore desirable to intentionally reduce the quantity of heat which can be transferred in the heat exchanger somewhat via suitable regulation of the flow of hydrogen (cf. pp. 93, 97) without reaching the permitted maximum heatup temperature for hydrogen. A higher reduced rotor rpm can be achieved with the same airflow in this way. /183 /184

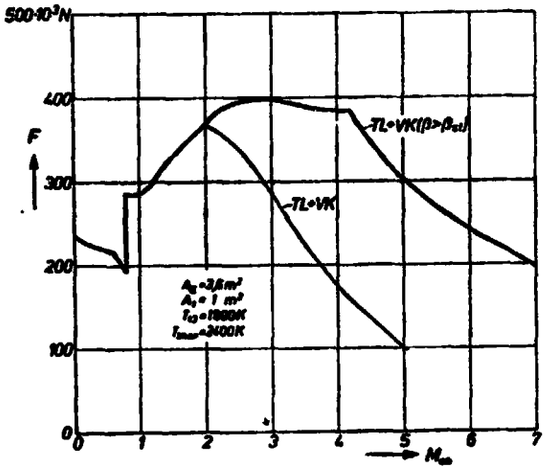

Fig. 6.5. Thrust curve for turbojet with precooling.

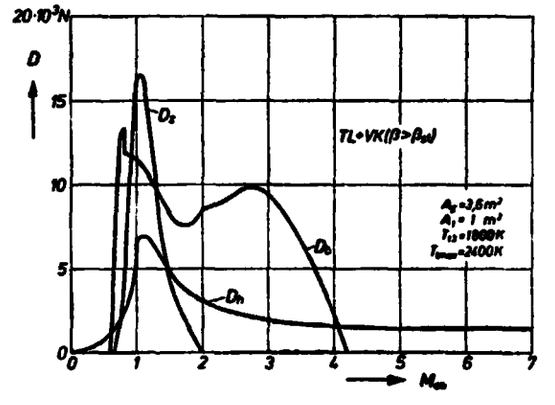

Fig. 6.6. Drag curve for turbojet with precooling ($\beta > \beta_{st}$).

The curves shown in Fig. 6.5 indicate net thrust; drags D_Z, D_h and D_b have already been subtracted. Their magnitude is plotted over flight Mach number in Fig. 6.6. Bypass drag D_b is made up of two parts here:

-- the direct portion, which consists of the bypass airflow momentum loss and can be attributed to losses in the intake, bypass duct and thrust nozzle (including losses due to incomplete expansion);

-- an indirect component, arising from the fact that thrust nozzle mismatch losses also increase in the flow of hot gases, since only a reduced area ratio is /185

available for expansion due to bypass mass flow. A portion of nozzle end cross section is required by the bypass mass flow, which expands with the hot gas to a common final nozzle pressure p_5.

Fig. 6.7 shows cross section curves for A_0, A_{omax}, A_5^* and A_5 versus flight Mach number. Cross section A_0 corresponds here to the airflow received by the compressor; bypass mass flow fills out the difference in area to A_{omax}.

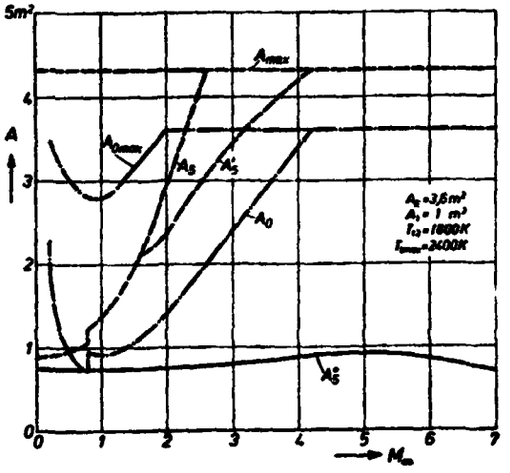

Fig. 6.7. Cross section curves for turbojet with precooling ($\beta > \beta_{st}$).

The narrowest cross section A_5^* in the hot thrust nozzle need vary only slightly with M_∞. Variation of control and design parameters would make it possible for it to be designed with a fixed geometry. /186

The flow of hot gas would fill out nozzle end cross section A_5 during expansion to backpressure p_0. Due to the limitation of A_5 to $A_{max} = 1.2 \cdot A_E$, complete expansion would be possible only up to about $M_\infty = 2.5$. In addition, only component nozzle end cross section A_5' remains available, due to the bypass airflow.

6.2. Performance Data for Engine Combinations Involving the Ramjet /187

An important disadvantage of the ramjet to be mentioned is the fact that it does not deliver adequate thrust in the subsonic range. It must be combined with a gas generator, which might be a turbojet, a turborocket or a rocket, for example. This combination is best accomplished in integrated form.

6.21. Ramjet

The performance of the ramjet will be discussed in this section, as obtained under the same, largely realistic assumptions which were made in analyzing the turbojet with precooling.

Although it is common practice, it does not appear very meaningful to use a ramjet in which combustion at a constant

stoichoimetric fuel/air ratio is provided for as a reference for evaluating the performance of air-breathing high-speed engines. Under this assumption, usable performance data can be calculated up to flight Mach numbers $M_\infty \approx 9$. To be sure, combustion chamber temperatures occur here which extend far beyond the levels occurring in rocket combustion chambers.

The specific thrusts σ_L and σ_B which the ramjet achieves with a substoichiometric and superstoichiometric fuel supply, respectively, under the given conditions are plotted against flight Mach number in Fig. 6.8 and 6.9. The curves break downward in the region of low flight Mach numbers, since high total pressure drops occur in the combustion chamber due to thermal blockage. For the same reason, it is also necessary to dispense with receiving and heating up the entire stream of air which approaches the intake in this range. /190

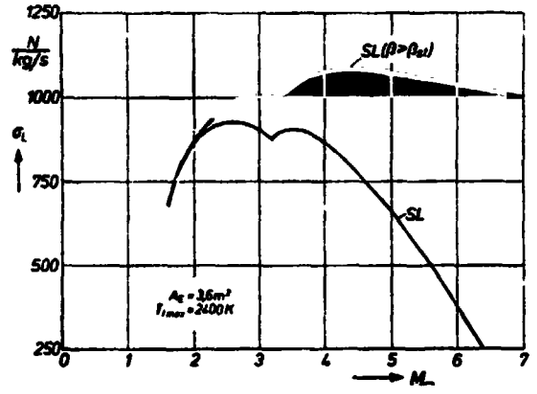

Fig. 6.8. Ramjet thrust relative to airflow.

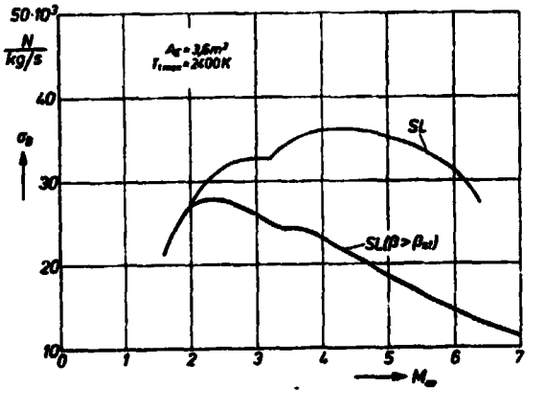

Fig. 6.9. Ramjet thrust relative to fuel flow.

With a substoichiometric fuel supply, specific thrust σ_L drops off so markedly above $M_\infty \approx 5.5$ that the flow of air and thus the size and weight of the engine must be increased to an undesirable extent in order to supply the required thrust. The increase in σ_L produced by combustion at a superstoichiometric fuel/air ratio is again obtained at the cost of a corresponding deterioration in specific consumption (Fig. 6.9).

The associated thrust and drag curves are shown in Figs. 6.10 and 6.11. As for the turbojet with precooling, a value of $A_E = 3.6\ m^2$ has been taken as the basis for intake geometric scoop cross section.

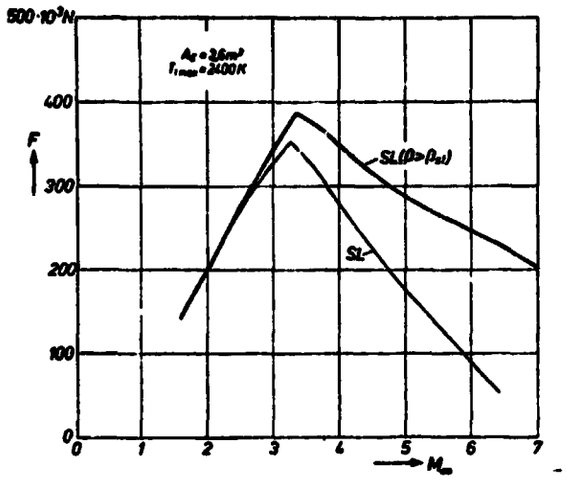

Fig. 6.10. Thrust curves for ramjet.

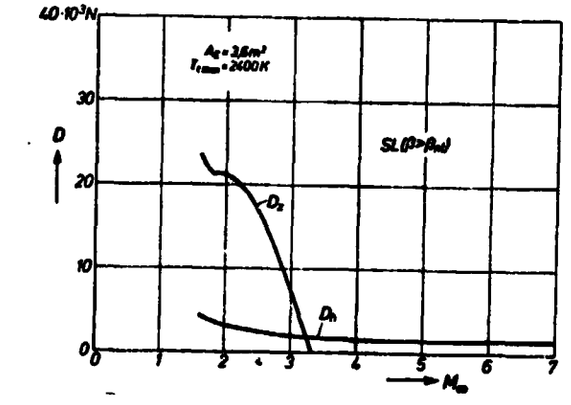

Fig. 6.11. Drag curves for ramjet.

6.22. Turbojet and Turborocket as Gas Generators

Of the turbo engines, the single-shaft turbojet and the turborocket in designs without afterburner chambers are available as characteristic gas generators suitable for combinations with the ramjet (cf. Fig. 6.1 c). Exhaust gases from the turbo engines are used along with the drawn-in flow of bypass air for secondary combustion in the combustion chamber of the ramjet.

So that these engines can be studied with regard to their suitability for combination with the ramjet, specific thrusts σ_L and σ_B as obtainable with the turbojet and the turborocket, with afterburner operation in each case, are compared in Figs. 6.12 and 6.13. While the turbojet has the same design data as the turbojet with supercooling for this comparison, the turborocket is designed for a pressure ratio of $(\pi_{tV})_{AP} = 2.2$. Inlet temperature for the superstoichiometric H_2/O_2 combustion gas entering the turbine is $(T_{t3})_{TR} = 1000$ K. An extensive analysis of the turborocket -- alternatively, kerosene is also used as fuel -- taking the different engine weights into consideration has indicated that the two-stage design for the fan can be considered the optimum compromise. For comparison, the σ curves for a single-stage fan design have been plotted in the graphs (dashed curves). /191

If the turborocket to be combined with the ramjet is designed so that the entire flow of air received is compressed in the fan in the lower flight Mach number range, the bypass airflow and the transfer of energy through mixing, involving relatively high losses, are absent. In this case, approximately the same nozzle pressure ratio is obtained with just a single-stage fan, which now comes

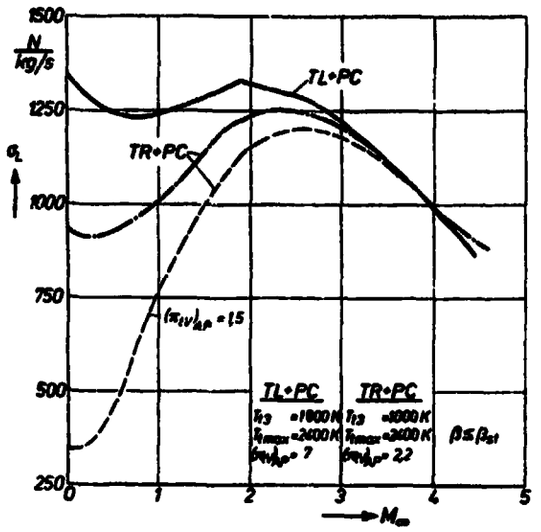

Fig. 6.12. Comparison of specific thrusts σ_L of turbojet and turborocket.

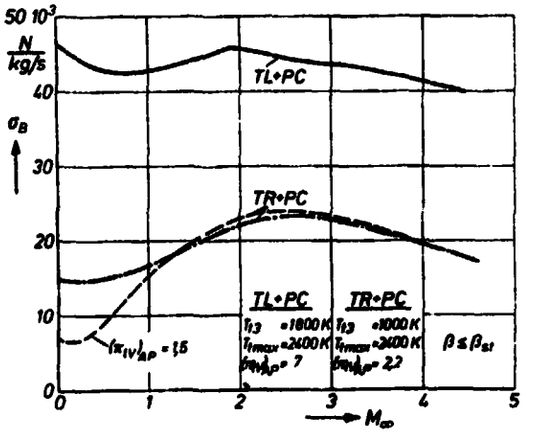

Fig. 6.13. Comparison of specific thrust σ_B of turbojet and turborocket.

out much larger, however. Combined with a heavy gear system, this can ultimately result in greater engine weight than for the smaller two-stage design.

A similar consideration also applies if we discuss the use of a turbofan in place of the turbojet. The advantage of its more flexible adaptability to various requirements is opposed by an increased equipment outlay.

In both cases, moreover, the design with a single-stage fan is opposed by the fact that a higher system pumping sensitivity must be expected even with low turbulence in the afterburner chamber, due to the small fan pressure ratio. /193

The comparison has indicated that the turbojet is more suitable for combination with a ramjet than is the turborocket. In a design which is oriented toward this special application, the turborocket provides only a minor advantage with regard to the engine weight required. The thrust/engine weight ratio has practically the same values in the flight Mach number range up to $M_\infty \approx 2$, which is of primary interest for the utilization of engines being discussed. Only at higher flight Mach numbers does this ratio become more favorable, a fact which is based primarily on the different throughflow behavior of the two-stage fan in the turborocket and the multistage compressor in the turbojet. The decisive disadvantage of the turborocket is its considerably higher on-vehicle weight consumption (Fig. 6.13).

6.23. Selected Combination Engines

For the above reasons, it is desirable to compare the combination of ramjet plus turbojet and the turbojet with precooling. In addition, the combination of ramjet plus rocket, which offers a considerable savings in engine weight relative to the ramjet plus turbojet -- though obtained at the cost of a very high on-vehicle mass flow -- will be included in the comparison.

The curves of specific thrusts σ_L and σ_B are plotted in Figs. 6.14 and 6.15 for the ramjet plus turbojet and ramjet plus rocket combination engines as obtained in each case with substoichiometric and superstoichiometric combustion in the ramjet combustion chamber.

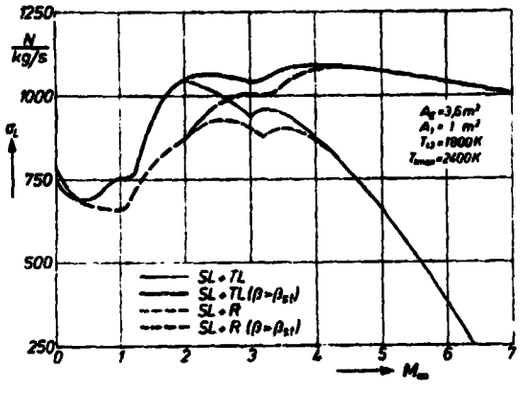

Fig. 6.14. Thrust relative to airflow for the ramjet + turbojet and ramjet + rocket combination engines.

The curves are determined in the lower flight Mach number range, up to about $M_\infty = 2.5$, by thermal blockage of the engines. The necessity of leading a portion of the oncoming airflow over the intake cowling and past the engine is clearly manifested in the magnitude of added drag (Fig. 6.17). /195

An effective reduction of losses from jet mixing could be achieved by drawing in the bypass duct upstream from the mixing chamber inlet and thereby reducing the velocity difference between the jets to be mixed. The mixing and combustion chamber itself is best designed with a divergent duct configuration. The magnitude of the airstream received by the intake and heated in the engine is limited in the lower flight Mach number range by the size of the thrust nozzle throat cross section, which can be set at maximum for design reasons. It has been assumed to be 75% of the largest engine cross section (maximum thrust nozzle end cross section) for the calculations.

It proved to be of advantage to operate the turbojet up to about $M_\infty \approx 4$ and only then change over to pure ramjet operation. For the upper flight Mach number range, finally, it must be completely encapsulated and protected from the high stagnation temperatures of the compacted airflow. The entire outer skin of

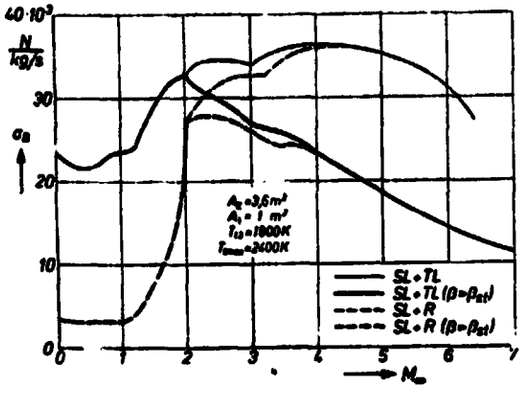

Fig. 6.15. Thrust relative to on-vehicle mass flow for the ramjet + turbojet and ramjet + rocket combination engines.

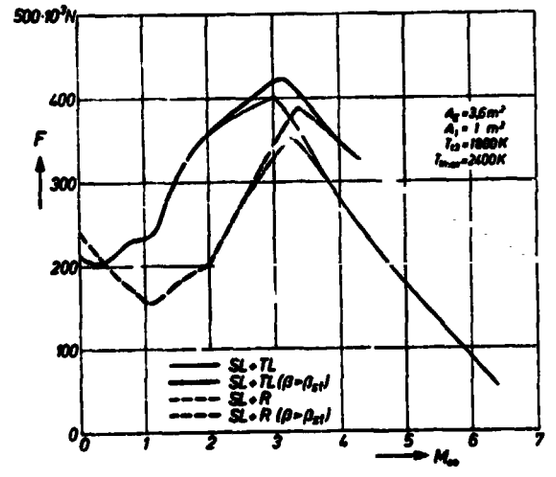

Fig. 6.16. Thrust curves for ramjet + turbojet and ramjet + rocket combination engines.

the turbojet can be cooled for this purpose, for example, with the hydrogen needed for combustion in the combustion chamber of the turbojet.

Due to its high on-vehicle mass consumption, the H_2/O_2 rocket in the combination ramjet-rocket engine is operated only during the initial phase of flight. The flow of oxygen to the rocket combustion chamber is set up so that takeoff thrust and initial thrust is available at the necessary level (Fig. 6.16). The flow of oxygen is reduced continuously with increasing flight Mach number here so that beyond $M_\infty = 2$, only the flow of hydrogen needed for combustion with the air continues to be fed to the ramjet through the rocket combustion chamber. /197

The upper temperature limit for the ramjet combustion chamber, $T_{tmax} = 2400$ K, was maintained during rocket operation for both curves by substoichiometric combustion with the total oxidizer (air + oxygen). In the case at hand, a superstoichiometric fuel supply would produce not only an increase in specific thrust σ_L but also an improvement in σ_B. The thrust curve would not change significantly, however, due to earlier thermal blockage. Because of the even higher H_2/O_2 ratio in this case, moreover, the stabilization of combustion in the rocket combustion chamber would be made more difficult.

6.3. Performance Data for Turborocket with Precooling

Due to the limit on fan outlet temperature, the flight Mach number range of the turborocket with afterburning extends only slightly beyond $M_\infty = 4.5$ even if it ultimately operates with

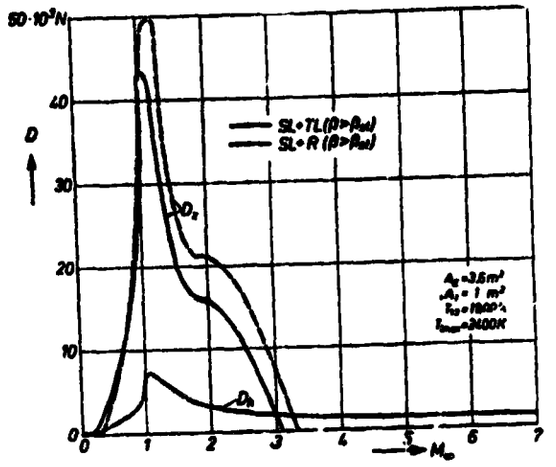

Fig. 6.17. Drag curves for ramjet + turbojet and ramjet + rocket combination engines.

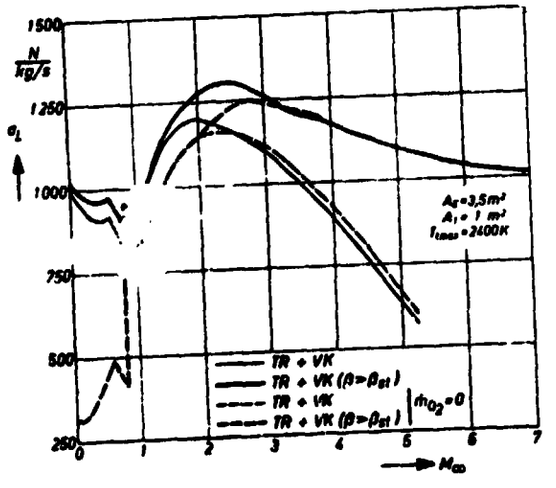

Fig. 6.18. Thrust with respect to airflow for turborocket with precooling.

autorotation in ramjet operation -- in this form, it represents a combination engine with a fully integrated design. However, it can be extended to about $M_\infty \approx 7$ by precooling the air prior to compression. Figs. 6.18 and 6.19 show the curves of specific thrusts σ_L and σ_B achieved, respectively.

Beyond $M_\infty \approx 1.5$, it is sufficient merely to expand the hydrogen heated in the heat exchanger and in cooling the afterburner chamber in order to cover the compressor's power requirements. In order to allow the necessary thrust also to be delivered during takeoff and in the transonic range, however, it is necessary to feed the turbine here with an H_2/O_2 combustion gas as in the turborocket without precooling. The O_2 supply is adjusted so that the fan can always be operated at full-load rpm. The additional flow of oxygen causes on-vehicle mass consumption to increase undesirably. For comparison, dashed curves are plotted in the graphs for the limiting case of the turborocket with precooling fed exclusively with hydrogen. The deviation even for operation without additional oxygen ($M_\infty > 3.4$) can be attributed to the differences in turbine and heat exchanger design. The thrust and drag curves for the turborocket with precooling are shown in Figs. 6.20 and 6.21.

/200

6.4. Comparison of Performance

6.41. Comparison of Performance Data

The performance data on the four engine concepts, turbojet with precooling, turborocket with precooling, ramjet plus

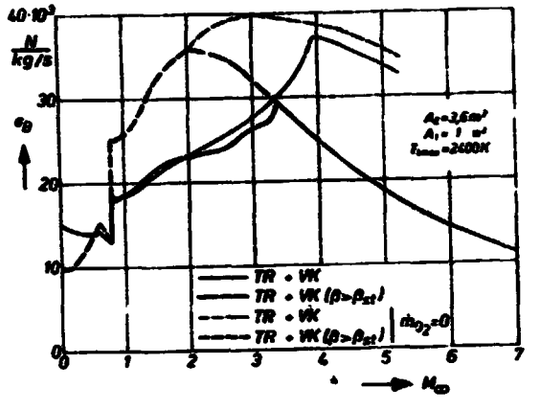

Fig. 6.19. Thrust with respect to on-vehicle mass flow for turborocket with precooling.

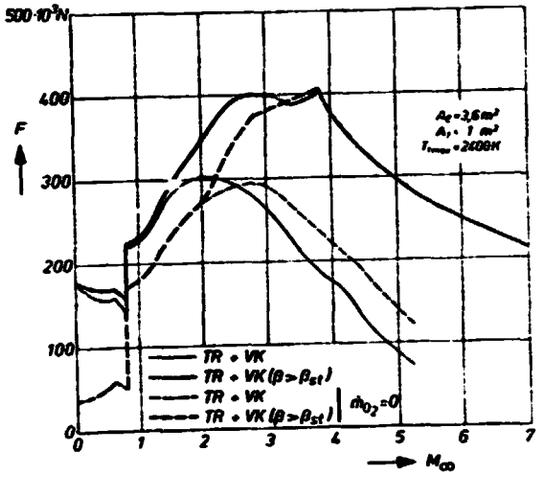

Fig. 6.20. Thrust curves for turborocket with precooling.

turbojet and ramjet plus rocket, will be considered together once more for direct comparison. Since all four engines are suitable for accelerating a space vehilce carrier in the intended flight Mach number range only if excess fuel is burned, just the curves corresponding to this will be shown. Since it is also desirable, for reasons already given, to provide an additional oxygen supply upstream from the turbine in the turborocket with precooling in the subsonic and transonic region, the curves for pure hydrogen operation need not be considered.

Figs. 6.22 and 6.23 show the curves of specific thrusts σ_L and σ_B over flight Mach number. The fact that for the turborocket /202
with precooling they are above the values for the turbojet with precooling at the highest flight Mach numbers was to be expected, since expansion of the heated airflow in a turbine does not occur in the turborocket with precooling. In this range, the curves coincide approximately with those for the combination engines, which operate as pure ramjets here. The small pressure ratio built up in the fan just compensates for the pressure drop which occurs in the heat exchanger.

The pronounced decrease in the thrusts σ_B, relative to on-vehicle mass flow, in the turborocket with precooling and the ramjet + rocket in the lowest flight Mach number rangeis a consequence of the oxygen supply required here. For comparison, specific thrust σ_B is plotted in Fig. 6.23 for an O_2/H_2 rocket that is operated with a combustion chamber pressure of 100 bars with an optimum mixture ratio.

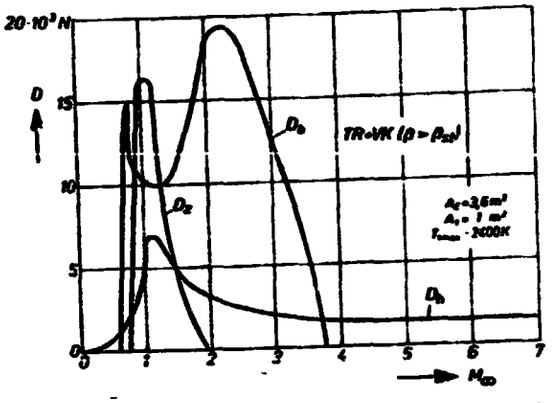

Fig. 6.21. Drag curves for turborocket with precooling.

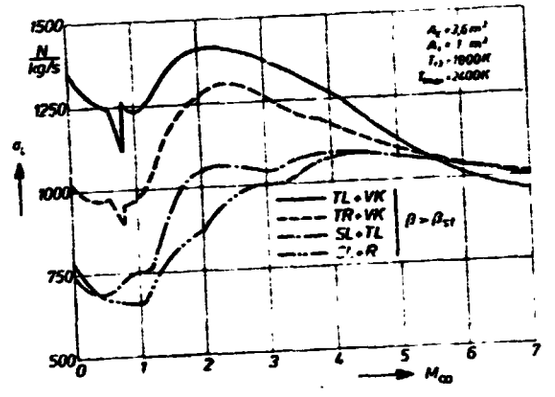

Fig. 6.22. Thrust relative to airflow for high Mach number engines.

The four engines compared have the same intake with a geometric scoop cross section of $A_E = 3.6\ m^2$, the same compressor inlet cross section of $A_1 = 1\ m^2$, the same nozzle end cross section (maximum engine cross section) of $A_5 = 1.2 \cdot A_E$ and same maximum heatup temperature, $T_{tmax} = 2400$ K. Turbine inlet temperature in the turbojets is $T_{t3} = 1800$ K in full-load operation; turbine inlet temperature in the turborocket with precooling varies within the approximate range $600\ K < T_{t3} < 1200\ K$.

The thrust curves for the different engines are combined in Fig. 6.24. The curves represent the net thrusts which are effectively available, after subtraction of the power plant drags, for propulsion of the vehicle. Its drag curve is likewise plotted in the graph. D_{F1}/n_M is the fraction of drag allotted to each engine (net drag of missile D_{F1} divided by number of engines n_M). /203

Net drag (without engine pods) was determined for the quasi-steady case of unaccelerated horizontal flight for an aerodynamic space vehicle carrier which, with a takeoff weight of $m_A \approx 230{,}000$ kg, is designed to operate in conjunction with a two-stage rocket to put a payload $m_N = 12{,}000$ kg in a 200 km orbit. The excess thrust, whose differences among the different types of engine can be seen from the graph, is available for climbing and accelerating. The drag curve given as an example was calculated assuming $n_M = 4$. The optimum size of the overall propulsion system is of course different for each of the engine designs shown, just as the required takeoff weight and decrease in vehicle weight differ, as determined by the engine's on-vehicle mass consumption. This has a slight effect on the shape of each drag curve.

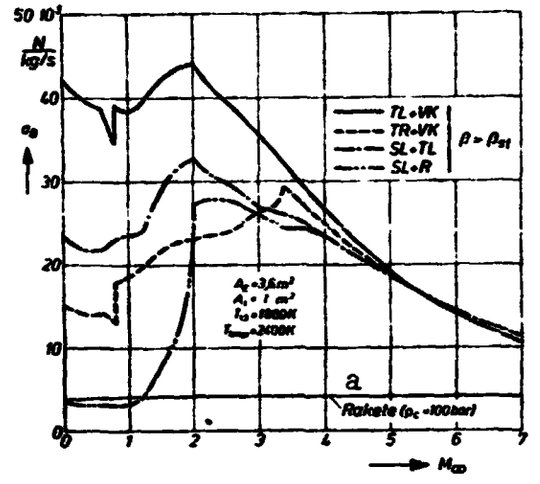

Fig. 6.23. Thrust relative to on-vehicle mass flow for high Mach number engines.

Key: a. Rocket

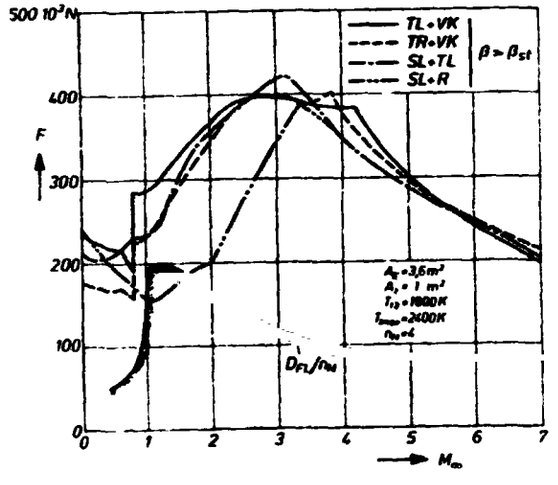

Fig. 6.24. Thrust curves for high Mach number engines.

The high excess in thrust between $M_\infty \approx 2$ and $M_\infty \approx 4$ offers all four engine designs the possibility of achieving somewhat more favorable values for total weight with economic substoichiometric combustion in this flight Mach number range. For reasons already mentioned, however, this applies only to a very limited degree, as will be shown quantitatively in Section 6.42, below.

Fig. 6.25 shows the drag curves for the engines being compared. The high added drag for the combination engines at relatively low flight Mach numbers is due to thermal blockage in this region. /205

The second rise in the drag curve for the turborocket with precooling in the vicinity of $M_\infty \approx 2$ is due to a pronounced increase in bypass drag in this range (see Fig. 6.21). Although the bypass airflow in the turborocket with precooling is lower than the corresponding values for the turbojet with precooling, due to the different throughflow behavior of the compressor, the turborocket with precooling exhibits a higher bypass drag here (cf. Figs. 6.6 and 6.21). This can be attributed to a sharp increase in the indirect component of D_b (see pp. 107-108). Mismatch losses increase sensitively as the result of the admixture of bypass air in the thrust nozzle.

This effect is less pronounced in the turbojet with precooling, as almost all the matching area ratio is still available for the expansion of combustion gas in the flight Mach number range under

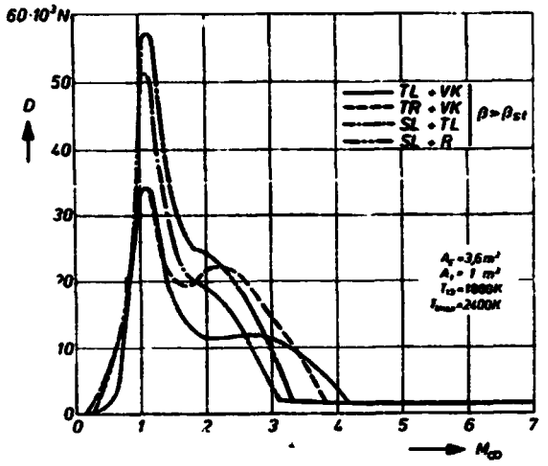

Fig. 6.25. Drag curves for high Mach number engines.

consideration, for which reason the slope of the decrease in thrust accompanying an additional reduction of area ratio is small. For the same nozzle end cross section, the throat cross section A_5^* in the turbojet with precooling is only about half as large as that in the turborocket with precooling.

The drag curves of the engine designs being compared coincide in the upper flight Mach number range. The cowling drag D_h remains here, of the same magnitude for all engines.

6.42. Total Weight Comparison for an Example of Application in a Space Vehicle Carrier /206

The total weight required to satisfy the mission will be estimated and compared now for the two engine designs, turbojet with precooling and ramjet + turbojet, which have been found from the comparison of performance data to be best suited, for application in the booster stage of a space vehicle carrier system. It is assumed to consist of installed engine weight and the total weight of fuel which is needed during acceleration of the booster stage along the specified flight profile up to the point of stage separation. The weight of fuel which is required for returning the booster stage to the takeoff point will be neglected or assumed to be equal in both cases for comparison.

Due to the mutual interaction of flight Mach number M_∞, altitude H_∞, instantaneous vehicle weight m_{Fl}, wing angle of attack α, total intake pressure ratio $p_{t1E}/p_{t\infty}$ and the total thrust of all engines F_{ges}, the flight profile outlined in Fig. 5.1 could be determined only by iteration. The same naturally also applies to the values for wing angle of attack α, freestream area ratio A_∞/A_0, oncoming flow Mach number M_0 for the intake, and intake pressure ratio $p_{t1E}/p_{t\infty}$ itself as shown in Figs. 4.9 through 4.12.

Due to the uncertainty in calculating engine weights, a comparison of engine design will first provide relative information concerning the equipment weight required for the turbojet with precooling and the combined ramjet-turbojet engine. /207

Sectional views of the turbojet with precooling and the ramjet + turbojet are compared in Fig. 6.26. While the intake and turbo section in the two engines can be considered identical, the additional equipment required by the heat exchanger in the turbojet with precooling is counterbalanced in the combination engine by an additional outlay due to the significantly larger afterburner chamber and the gate system for hermetically sealing the turbo section at the aft end. The gate system for sealing the forward end of the turbo section (e.g. with cooled lid gates) correspo to the regulating gates servin as flow dividers in the turboj with precooling.

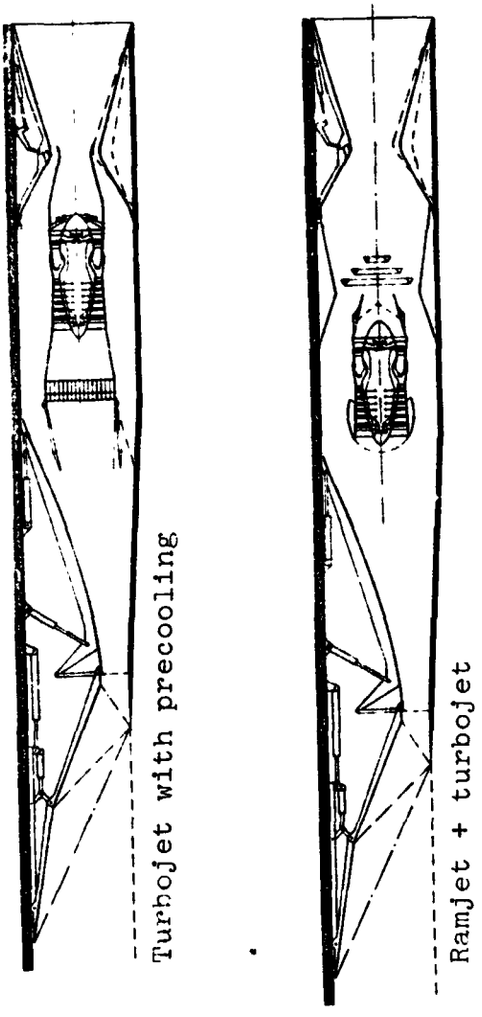

Fig. 6.26. Overall configurations of the turbojet with precooling and the ramjet + turbojet.

Sinc e the bypass duct in the turbojet with precooling is completely closed above $M_\infty \approx 4$, it is subjected neither to the high pressure loads (pressure can be equalized with the outside air by ventilation) nor the high thermal stresses which occur in the upper flight Mach number range. Thus in comparison to the combination engine, it can have a less sturdy design and also does not need to be cooled. In the combination engine, moreover, cooling must be provided for the outer skin of the turbo section. The adjustable thrust nozzle, also fed with combustion gas in the convergent section, should likewise be slightly heavier.

The total additional equipment weight for the combination engines will considerably exceed the additional weight for the turbojet with precooling required by the weight of the heat exchanger. An attempt to reduce the weight contribution of the turbo section in the combination engine by further reducing compressor pressure ratio is likely to produce the opposite effect. An effective reduction in the overall turbo section through a reduction in the flow of air must likewise be dispensed with because of the effects on thrust during takeoff and in the transonic range. /209

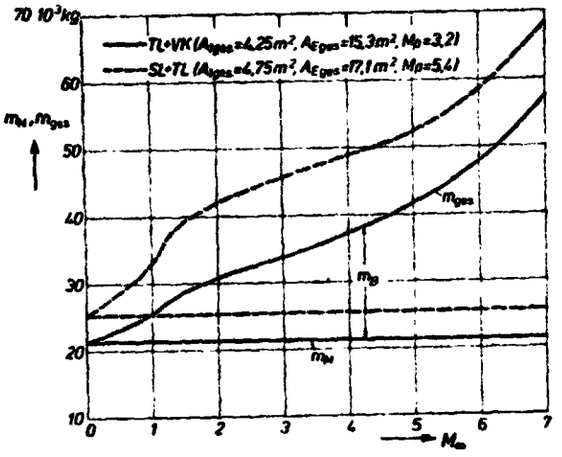

Fig. 6.27. Comparison of total propulsion system weights.

Total weight m_{ges}, consisting of installed engine weight m_M and consumed fuel weight m_B, required for the alternative use of the turbojet with precooling versus the ramjet + turbojet for acceleration to a particular flight Mach number M_∞ is shown in Fig. 6.27. The aerodynamic booster stage required for the given mission has dimensions and takeoff weight only slightly greater than those for the Concorde SST. Flight time until the limiting flight Mach number $M_\infty = 7$ is reached amounts to about $t = 770$ sec for the turbojet with precooling and /210 $t = 860$ sec for the ramjet + turbojet. The distance covered over the ground here is $s = 740$ km (turbojet with precooling) and $s = 850$ km (ramjet + turbojet).

Determination of the curves shown in Fig. 6.27 for the engine designs being compared was based on the differing optimum values for the number of engines and for total installed engine size. In addition, consideration was given to the different optimum changeover Mach numbers at which the transition was to be made from substoichiometric combustion to a superstoichiometric fuel supply to the afterburner chamber.

Figs. 6.28 and 6.29, using the example of the turbojet with precooling, show how total weight is effected by installed engine size, which is determined by total installed compressor inlet area A_{1ges}, and how it is affected by changeover Mach number M_B.

In closing, it should also be pointed out with regard to the comparison presented between the turbojet with precooling and the ramjet + turbojet that slightly better values are obtained for the combination engine if the ramjet is combined with a turbojet + afterburner. The primary mass flow precompressed in the turbo section and the bypass mass flow can be heated to different temperatures in separate combustion chambers corresponding to the existent expansion pressure ratios, and the high mixing losses at lower flight Mach numbers avoided. Comparative calculations show that in the lower flight Mach number range, considerably better consumption values can be obtained with approximately the same thrust curve. This advantage ultimately has a more pronounced effect on the total weight required than the slight reduction in thrust and deterioration in consumption in the range of intermediate flight Mach numbers.

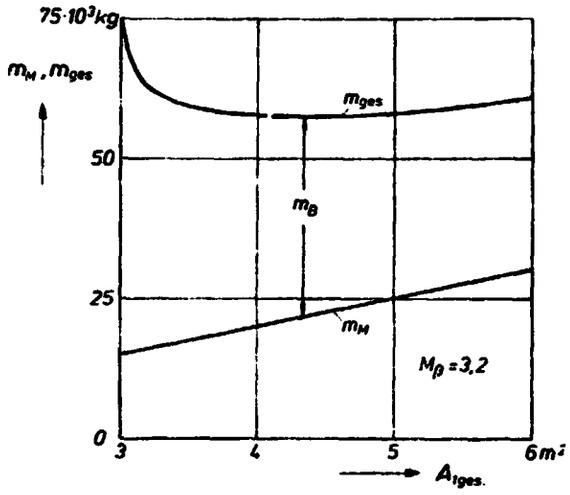

Fig. 6.28. Effect of engine size on total weight (turbojet with precooling).

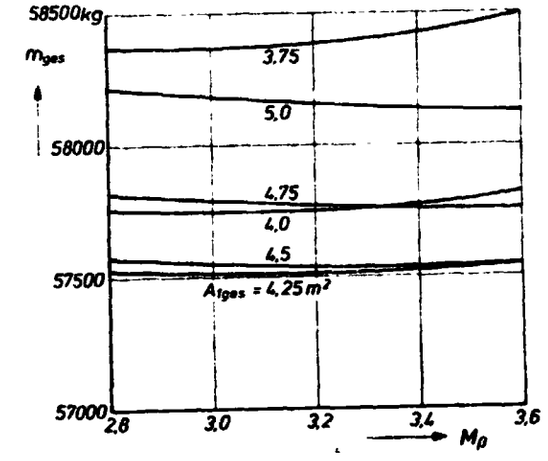

Fig. 6.29. Effect of change-over Mach number on total weight (turbojet with precooling.

7. Concluding Remarks /212

It has been shown that air precooling prior to compression is a suitable way to considerably extend the flight Mach number range of turbojet engines. Thus they become attractive as air-breathing propulsion units for an aerodynamic booster stage for the takeoff and initial acceleration of space vehicles if a combination employing a ramjet is not used. An additional advantage of turbo-jets with precooling with regard to development time is that these propulsion systems just require test facilities which are designed for oncoming flow Mach numbers of M_0 = 4 to 4.5, in spite of their suitability for flight Mach numbers up to about $M_\infty \approx 7$.

For reasons mentioned above, more or less approximate methods of calculation are completely unusable even for purely comparative purposes in these considerations. For this reason, the analysis of different engine designs has been conducted with the required care wherever necessary to obtain sufficiently precise quantitative results and still justifiable within the scope of this work and with regard to the intended goal. The author is aware of the short-comings to be found primarily in the sometimes wholesale treatment of the operating behavior of individual components, particularly since the multidimensionality of flow could be covered only with correction factors.

Performance with respect to the intended mission was deter-mined for the engine designs studied, and the main problems to be expected in their development were shown and possible solutions to them outlined.

The turbojet engine with precooling presented as a preliminary design is particularly worth considering for the intended application in a space vehicle carrier. Compared to the turborocket with precooling, it exhibits a considerably lower on-vehicle mass consumption rate and greater utilization flexibility in the lower half of the flight Mach number range covered. Advantages in consumption and weight over the combined ramjet + turbojet engine lead us to expect the total weight required for the propulsion system in order to satisfy the planned mission with accelerated flight to $M_\infty = 7$ to assume the more favorable values shown in Fig. 6.27 for the turbojet with precooling. During return flight of the booster stage, the engine operates economically without afterburning, with precooling reduced to correspond to the smaller flow of fuel. /213

A special advantage of this engine design which might be mentioned, moreover, is that it fully utilizes the high level of development achieved in the building of aircraft engines, with its almost conventional design, but hardly exceeds it. The problems involving the heat exchanger have largely been eliminated upon the development of suitable types of matrices and on the basis of experience gained with them. But the heat exchanger, along with the variable intake, will still represent a point of emphasis in development, due to the high temperature gradients applied to it. The high thermal stresses, which in this case occur in heat exchangers of conventional design, will remain within manageable limits, however, due to the relatively elastic matrix.

The intake cooling required in the upper flight Mach number range can be accomplished without additional coolant flow and without an appreciable impairment of precooling, since the heat which the flow of H_2 absorbs in the intake need no longer be led away in the heat exchanger. The remainder of the power plant is cooled, as it were, by the heat exchanger, which reduces the overall temperature level to a value which corresponds to a lower flight Mach number. /214

In addition to the turbojet with precooling, other possibilities have been outlined for making air-breathing turbo propulsion systems suitable for the acceleration of an aerodynamic space vehicle carrier through the precooling of air prior to compression. However, it was not possible to go into an analysis of these systems in detail within the scope of this work. Reference is made here particularly to the high-pressure power plant in which the already compressed air is also employed to precool the flow of air compacted in the intake, as well as to the two-stage project in which some of the air flow is liquefied prior to stage separation and later fed to the rocket engine of the second stage as oxidizer.

The turbofan with precooling may represent an attractive alternative to the turbojet with precooling if all of the fuel

required in the afterburner is fed to the primary-circuit airflow upstream from the turbine. Turbine inlet temperature in this case is limited by superstoichiometric combustion in the main combustion chamber. For a given fan power requirement, the primary circuit airflow can now be reduced or, for a given bypass ratio, the pressure ratio available for expansion in the thrust nozzle can be increased. Enhancement of the performance data and the ratio of thrust to power plant weight can be expected to result. This effect can of course basically also be achived in turbofans /215
with afterburning and without precooling if the bypass ratio has values of $\lambda > 2$.

All considerations which have been raised in this study with regard to the flight path curves were based on the consistent assumption that the aerodynamic space vehicle carrier takes off and lands horizontally like a conventional supersonic aircraft. The horizontal takeoff is favored primarily by the fact that a considerably smaller equipment weight is required for propulsion than for vertical launch. While an optimum ratio of takeoff thrust to takeoff weight $F/(m_A \cdot g_o) \approx 0.45$ was calculated in Section 6, more than three times the engine weight would have to be installed in a corresponding practical case involving vertical launch. To this are added the lower on-vehicle mass consumption rate required to satisfy the overall mission in the case of the aerodynamic space vehicle carrier which takes off horizontally, and the fact that the necessary large scoop cross section of the engine intakes, which makes the required high engine thrust feasible even in the upper flight Mach number range, can be achieved without problems via wing precompression. This much more than compensates for the disadvantage of the heavier structure relative to the vertically launched ballistic missile.

In this regard, the desirability of a catapult launch should also be pointed out, by means of which transport costs can be further reduced to an appreciable degree if the space vehicle carrier is accelerated to a lift-off speed of about 200 or 250 m/s.

It should also be noted in closing that the turbojet with /216
precooling is to be preferred as the propulsion system for an SST with flight Mach numbers between $M_\infty = 3$ and $M_\infty = 5$ using liquid methane as fuel with substoichiometric combustion.

REFERENCES

1. Noblitt, G., NASA, "Space vehicle logistics," UTSI-VKI Lecture Series on Technology of Space Shuttle Vehicles, November, 1970. /217

2. Dettmering, W., "Lines of development of air-breathing jet engines," Arbeitsgemeinsch. Forsch. Landes Nordrhein-Westfalen (182) (1967).

3. Lane, R.J., "Recoverable air-breathing boosters for space vehicles," J. Roy. Aeronaut. Soc. (June 1962).

4. Lombard, A.A. and Keenan, J.G., "A turborocket engine for air-breathing high-speed aircraft," Interavia (Jan. 1965).

5. Luidens, R.W. and Weber, R.J., "An analysis of air-turbo-rocket engine performance including effects of component changes," NACA Research Memorandum, August 1962.

6. Anonymous, "Trio proposes inverted turbojet," Air Space Technol. (October 1961).

7. Dettmering, W. and Becker, B., "A new concept of the inlet design and of the thermodynamic cycle of the turbojet engine at high flight Mach numbers," AGARD Conference "Inlets and Nozzles," Sandefjord, 1971.

8. Beller, W., "Engine may oust big booster," Missiles Rockets (April 1963).

9. Anderton, D.A., "LACE concept feasibility proof sought," Aviat. Week Space Technol. (November 1961).

10. Jeffs, R.A. and Beeton, A.B.P., "Liquid air cycle engines," Flight International (December 1963). /218

11. Bedel, J., "The space shuttle," Rev. Fr. Astronaut. (March/April 1966).

12. Hilsenrath, Josef, Tables of Thermodynamic and Transport Properties of Air, Argon, Carbon Dioxide, Carbon Monoxide, Hydrogen, Nitrogen, Oxygen and Steam, Pergamon Press, 1960.

13. Steward, R.B., Hust, H.G. and McCarty, R.D., "Interim thermodynamic properties for gaseous and liquid oxygen at temperatures from 55 to 300°K and pressures to 300 atm," NBS Report 7922, 1963.

14. Strobridge, Thomas R., "The thermodynamic properties of nitrogen from 64 to 300 K between 0.1 and 200 atmospheres," NBS Technical Note 129, 1962.

15. Roder, Hans M. and Godwin, Robert D., "Provisional thermodynamic functions for parahydrogen," NBS Technical Note 130, 1961.

16. Din, F., Thermodynamic Functions of Gases, Vol. 2, Butterworths, London, 1962.

17. Hust, J.G. and Gosman, A.L., "Functions for the calculation of entropy, enthalpy and internal energy for real fluids using equations of state and specific heat," Advances in Cryogenic Engineering, Vol. 9, Plenum Press, New York, 1964.

18. Beattie, J. and Bridgeman, O.C., "A new equation of state for fluids (II. Application to helium, neon, argon, hydrogen, nitrogen, oxygen, air and methane)," J. Am. Chem. Soc. 50 (1928).

19. Plank, R., Handbuch der Kältetechnik [Handbook of Cryogenics] /2:9
Thermodynamische Grundlagen [Thermodynamic Principles], Vol. 2, Springer-Verlag, 1953.

20. Baehr, H.D. and Schwier, K., Die thermodynamischen Eigenschaften der Luft [The Thermodynamic Properties of Air], Springer-Verlag, 1961.

21. Morsy, T.E., Zum thermischen und kalorischen Verhalten realer Stoffe [The Thermal and Caloric Behavior of Real Materials], Dissertation, Karlsruhe Engineering College, 1963.

22. Penner, S.S., Chemistry Problems in Jet Propulsion, Pergamon Press, New York, 1957.

23. McBride, B.J., Heimel, S., Ehlers, J. and Gordon, S., "Thermodynamic properties to 6000 K for 210 substances involving the first 18 elements," NASA-SP-3001, 1963.

24. Oswatitsch, K., "Pressure recovery for projectiles with reactive propulsion at high supersonic velocities," DVL Report No. 49, Westdeutscher Verlag, Cologne and Opladen, 1957.

25. Söffker, E., "Matching between air-breathing engine and supersonic intake," ERNO-Raumfahrttechnik GmbH, Bremen, 1970.

26. Du Pont, A.A., "Jet propulsion," Space Aeronaut. 50 (1968).

27. Connors, J.F. and Meyer, R.C., "Design criteria for axisymmetric and two-dimensional supersonic inlets and exits," NACA TN 3589, 1956.

28. Tjonneland, E., "The design, development and testing of a supersonic transport intake system," AGARD-CP-91, 1971.

29. Kays, W.M. and London, A.L., Compact Heat Exchangers, McGraw-Hill Book Company, New York, 1964.

30. Grieb, H., "Effect of individual components and their mechanical arrangement on the steady operating behavior of turbofans," DLR Report 73-05, Deutsche Gesellschaft für Luft- und Raumfahrt, May 1972. /220

31. Bray, N.N.C., "Atomic recombination in a hypersonic wind tunnel nozzle," J. Fluid Mech. 6(1) (1959).

32. Gaballah, I.F., Theoretische Untersuchungen der Relaxationsvorgänge bei hohen Temperaturen im Hinblick auf die Berechnung und Optimierung von Schubdüsen [Theoretical Studies on Relaxation Processes at High Temperatures with Regard to Thrust Nozzle Calculations and Optimization], Dissertation, Rhine/Westphalian Technical College, Aachen, 1969.

33. Schaffrath, M., Zustandsänderungen hochenergetischer Treibstoff-Oxydator-Systeme im Bereich hoher Temperaturen unter Berücksichtigung der chemischen Relaxation [Changes of State of High-Energy Fuel/Oxidizer Systems in the High Temperature Range, Taking Chemical Relaxation into Consideration], Dissertation, Rhine/Westphalian Technical College, Aachen, 1970.

34. Scholz, N., "Remarks concerning the practical determination of combustion chamber pressure drops," DLR Report 64-09, 1964.

35. Lenke, G., Untersuchungen zur Frage der Anwendbarkeit luftatmender Triebwerke als Antrieb der ersten Stufe eines Raumtransporters [Studies on the Question of the Usability of Air-Breathing Engines to Propel the First Stage of a Shuttle], Dissertation, Darmstadt Engineering College, 1970.

36. Monsler, K., Zerlegung verflüssigter Luft während des Fluges eines wiedergewinnbaren Raumfahrzeugträgers, der durch luftansaugende Triebwerke angetrieben wird [Separation of Liquified Air during Flight in a Recoverable Space Vehicle Carrier Propelled by Air-Breathing Engines], Dissertation, Rhine/Westphalian Technical College, Aachen, 1971.

37. Trevina, C., "Analysis of the performance of a turborocket for propelling a high-speed aircraft," unpublished study, Institute for Jet Engines, Rhine/Westphalian Technical College, Aachen, 1973.

38. Künkler, H., "The problem of matching an intake to a turbo engine for extremely high flight Mach numbers," DGLR Technical Committee on "Air-Breathing Engines," Darmstadt, May 1972.

39. Künkler, H., "The effect of precooling prior to compression in air-breathing engines for a space vehicle carrier," 5th annual meeting of the DGLR, Berlin, October 1972.